İSTANBUL TECHNICAL UNIVERSITY ★ INSTITUTE OF SCIENCE AND TECHNOLOGY

MODELING AND FORCED VIBRATIONS FOR A UNIVERSAL ELECTRIC MOTOR

M.Sc. Thesis by
Cihan ORHAN

Department : Mechanical Engineering

Programme : Machine Dynamics, Vibration & Acoustics

JUNE 2011

İSTANBUL TECHNICAL UNIVERSITY ★ INSTITUTE OF SCIENCE AND TECHNOLOGY

MODELING AND FORCED VIBRATIONS FOR A UNIVERSAL ELECTRIC MOTOR

M.Sc. Thesis by
Cihan ORHAN
(503081402)

Date of submission : 06 May 2011
Date of defence examination: 10 June 2011

Supervisor (Chairman) : Prof. Dr. Kenan Yüce ŞANLITÜRK
Members of the Examining Committee : Prof. Dr. Halit Temel BELEK
Prof. Dr. Zahit MECİTOĞLU

JUNE 2011

İSTANBUL TEKNİK ÜNİVERSİTESİ ★ FEN BİLİMLERİ ENSTİTÜSÜ

ÜNİVERSAL ELEKTRİK MOTORUNUN ZORLANMIŞ TİTREŞİMLERİNİN SAYISAL MODELİNİN KURULMASI

YÜKSEK LİSANS TEZİ
Cihan ORHAN
(503081402)

Tezin Enstitüye Verildiği Tarih : 06 Mayıs 2011
Tezin Savunulduğu Tarih : 10 Haziran 2011

Tez Danışmanı : Prof. Dr. Kenan Yüce ŞANLITÜRK
Diğer Jüri Üyeleri : Prof. Dr. Halit Temel BELEK
Prof. Dr. Zahit MECİTOĞLU

HAZİRAN 2011

FOREWORD

First, I give my special thanks to The Scientific and Technological Research Council of Turkey (TÜBİTAK) for scholarship during my M.Sc. It was possible that I could not have found any opportunity to start MSc without this scholarship. I am very grateful to our people who pay taxes and I hope we can pay our dept throughout our lives.

Second, I would like to express my sincere thanks to my advisor, Prof. Dr. Kenan Yüce ŞANLITÜRK, for his general supervision, continual encouragement and valuable support throughout my research. I could not imagine an adviser more caring, encouraging, supportive and willing to help in all aspects of my work.

This project would not have studied without funding of ARÇELİK A.Ş. I would also like to thank to Mr. Metin Gül, Leader of Vibrtation and Acoustics Technology Family at R&D Department of ARÇELİK A.Ş., because of his infinite encouragement and faith to me and my studies.

I have many skillful collegues who have valuable contributions to my thesis in terms of various aspects. Ball Bearing Model used in this thesis is a results of guidance of Mr. Onur ÇAKMAK. He also helped me about both measurements and interpretations of Order and Campbell diagrams during my tests. I want to thank him for all of his advices and helps. I always ask for advice from Deniz YAZGAÇ for interpreting analytical expressions of electromagnetic vibrations. I want to thank him for his helps during this study. Mr. Ahmet Ali USLU is a very helpful person who has serious contributions during my MSC. ADAMS studies. I also want to express my sincere thanks to Mr. Erkan TARAKÇI and Mr. Çetin AYDINTUĞ for their patience while studying with I-DEAS. I always ask Mr. Kenan ATAÇ's advices and ideas about generally testing issues. So I owe his thanks a lot. And I would like to thank my work friends Mr. Selçuk ÇELİKEL, Mr. Erdem SÖZER, Mr. Burak UKUŞER, Mr. Mete ÖĞÜÇ , Mr. Volkan KAZANCI and Fatih ÖZBAKIŞ for their support.

Finally, my specail thanks go to my family Vildan ORHAN, Ali ORHAN and Canan ORHAN. I am nothing without their supports and loves.

Cihan ORHAN

(Mechanical Engineer)

May 2011

TABLE OF CONTENTS

Page

ABBREVIATIONS

AC	**:** Alternating Current
BPFO	**:** Ball Passing Frequency of the Outer Race
BPFT	**:** Ball Passing Frequency of the Inner Race
BSF	**:** Ball Spin Frequency
DC	**:** Direct Current
DSA	**:** Dynamic Signal Analyzer
EMF	**:** Electromotive Force
FEM	**:** Finite Element Method
FFT	: Fast Fourier Transform
FRF	: Frequency Response Function
FTF	**:** Fundamental Train Frequency
ISO	**:** International Standards Organization
MMF	**:** Magnetomotive Force
MSM	**:** Multi-Slice-Method
PMDC	**:** Permanent Magnet Direct Current
RPM	**:** Round per Minute
SCR	: Silicon Controlled Rectifier
UMP	**:** Unbalanced Magnetic Pull
2D/3D	**:** Two/Three Dimensional

LIST OF TABLES

Page

LIST OF FIGURES

Page

MODELING AND FORCED VIBRATIONS FOR A UNIVERSAL ELECTRIC MOTOR

SUMMARY

Nowadays, electric motors are the most common machines which are used almost all machine in order to provide mechanical power. So, quality, reliability and life span of electric motors directly influence machines where the electric motors are used. As a result, vibration and acoustic properties of electric motors take over in order to decrease total noise and vibration problems in the machines.

The aim of this study is modelling a reliable numerical model of a universal electric motor in order to investigate the effects of the mechanical and electrical forces on the dynamics of the electric motor.

In this context, every parts of the electric motor are modelled as a FE model and these models are validated by experimental modal analysis. After this study, all of these models are assembled in the MSC ADAMS. So, free vibration numerical model of the electric motor is created. One step further of free vibration model is to compose a forced vibration model which contains dynamic forces created by both electrical and mechanical manner.

A test rig is designed in order to validate this numerical model. Effects of dynamic forces are investigated and forced vibration numerical model is improved on the basis of experimental data.

ÜNİVERSAL ELEKTRİK MOTORUNUN ZORLANMIŞ TİTREŞİMLERİNİN SAYISAL MODELİNİN KURULMASI

ÖZET

Elektrik motorları günümüzde neredeyse her türlü cihaz ve makinalarda vazgeçilmez olarak kullanılan mekanik güç sağlayıcı elemanlardır. Dolayısı ile elektrik motorlarının kalitesi, güvenirliği ve ömrü bu motorları kullanan makinelerin kalitesini doğrudan etkilemektedir. Bu bağlamda elektrik motorlarının titreşim ve gürültü anlamındaki özellikleri ön plana çıkmaktadır.

Bu çalışmanın temel amacı, elektrik motoru dinamiğinde etkili olan mekanik ve elektriksel kaynaklı zorlanmış titreşimleri tahmin edebilecek güvenilir bir model ortaya koymaktır.

Bu kapsamda motorun herbir parçasının ayrı ayrı sonlu eleman modeli oluşturulmuş ve bunlar deneysel modal analiz ile güncellenmiştir. Daha sonra motor elemanların güncellenmiş bu esnek modelleri MSC ADAMS programında monte edilmiştir. Herbir aşamada yine deneysel modal analiz ile modelin doğruluğu hem kontrol edilmiş hem de gerekli güncellemeler yapılmıştır. Motorun serbest titreşim modeli elde edildikten sonra, motor üzerinde kuvvet üreten etkilerin modelleri elde edilmiştir. Bunlar kabaca mekanik ve elektriksel olarak sistemi uyaran bileşenlerdir. Bu etkilerin modele eklenerek zorlanmış titreşim modeli elde edimiş, incelenmiş ve tasarlanan test düzeneği baz alınarak gerekli düzenleme ve düzeltmeler yapılmıştır.

1. INTRODUCTION

1.1 Problem

Electric motors are essential components in many applications as they provide mechanical power to many machines. Also, it is easy to observe that dynamic properties of the electric motors have major effects on the dynamic behavior of machines.The sources of forces in the electric motor are generally classified as mechanical and electrical. Although the effects of dynamic forces in electric motors can easily be observed and measured, it is difficult to establish precise locations where these forces emerge and to quantify these dynamic forces causing the vibrations and noise. As a result, there are some problems at this stage to answer this type of questions. These questions are especially focused on observation of vibrations caused by electromagnetic effects and also modeling of electromagnetic forces that lead to these vibrations.

1.2 Literature Survey

Generally, the vibration and noise investigations of an electric motor are coupled physic problems (Figure 1.1), starting from the electromagnetic force excitation, computing the mechanical deformation and concluding in the estimation of the radiated audible noise [1]. The central part of the computational chain is the electromagnetic field computation. These excite the stator of the machine resulting in vibrations. The periodical oscillations of the machines surface is decoupled and radiated as disturbing audible noise [2]. There are several studies in the literature associated with modeling of electric motors in terms of vibration and noise perspectives. These can be classified as analytical, numerical and experimental studies. Due to the complex nature of the problem, the number of analytical studies are quite limited compared to to those of numerical and experimental studies. However, there are extensive literature on the applications of the finite element method to the analyses of electrical machines [3].

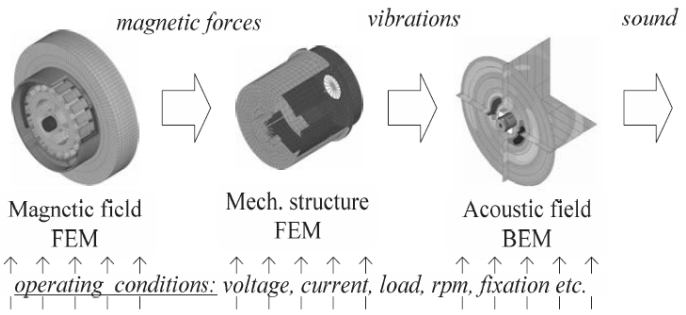

Figure 1. 1 : Prediction of the magnetic noise in a DC electrical motor [1].

In reference [4], both numerical and analytical approaches are used to describe the electromagnetic problems. In this manner, it is aimed to take advantage of inherent of using analytical expressions and the versatility and attributes of the Finte Elemet (FE) method. F. Ishibashi et. al. [5] calculated the flux distribution of a motor by finite element method (FEM), and from the results of this study, they analysed flux density over the motor's radial direction in space and time domains. The vibration behavior of the motor caused by electromagnetic forces is simulated using FEM for structural analysis. The modes and amplitudes of vibration provided by these calculations are then compared with experimental results.

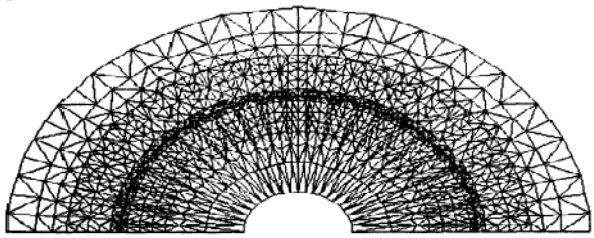

Figure 1. 2 : The electromagnetic FE model [5].

Most of the studies [5,6,7] in this field are performed in two dimensional space because of its simplicity with respect to 3 dimensional analyses. Martin et al [6] built-up 3D FEM models for the magnetic force calculation. But they indicated that most authors who deal with the structural dynamics use 2D models of induction machines in the magnetic field calculation (Ishibashi et al, 1998) and they also added that the reason for the limited use of three-dimensional (3D) models is probably due to the structural complexity of the real electric machines and the fact that the results obtained via 2D analysis (Jang and Lieu,1991) give fairly good vibration predictions. Nevertheless, some researchers (Wang and Lai,1999) presented good examples of

3D dynamic models validity of which were also tested using experimental results.They also extended their research to acoustic modeling (Lai and Wang, 1999).

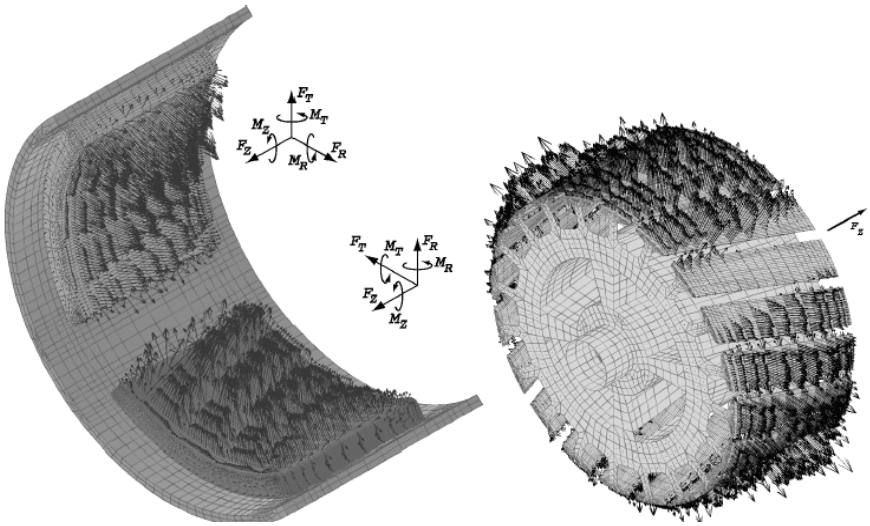

Figure 1. 3 : The system types in modelling field. 3D FE electromagnetic model, stator (on the left) and rotor (on the right) [1].

Whenever possible, it is desirable to use 2D techniques as they allow reducing the analyst effort and CPU time numerical effort and including more physical aspects in the model. On the other hand, the results that can be obtained from a 2D structural dynamic simulation of electrical machines may be limited, due to 3D effects that cannot be captured in 2D analyses. A detailed evaluation of both appraoches, a comparison of their strength and weaknesses as well as a numerical comparison of accuracy and computational effort are given in reference [8]. Reference [8], compares 2D and 3D coupled electromagnetic and dynamic simulations of various types of machines. In [8], it is stated that numerically weak or strong coupling are two types of approaches (Figure 1.4) generally adopted. But each of these approaches has its own advantages and disadvantages. Numerically weak coupling allows for using different grids, on which the different problems are solved. On the other hand, a strong coupling allows for an efficient implementation of reaction and close interaction between the solution quantities. Using this technique, additional aspects, such as magnetostriction[1] and the influence of the deformation on the electromagnetic forces, can be taken into account [8].

[1] Magnetositriction is a property of ferromagnetic materials that causes them to change their shape or dimensions during the process of magnetization.

Table 3.1: Comparison 2D/3D simulation.

Structural-Dynamic-Simulation	
2D	3D
fast	slow
easy mesh generation (quads)	complicated mesh generation
frequency band	selected frequencies
no 3D mode shapes	full 3D mode shapes
no consideration of rotor	consider rotor vibration
no coupling to acoustics	coupling to acoustic simulation
strong coupling and magnetostriction possible	only weak coupling implemented so far

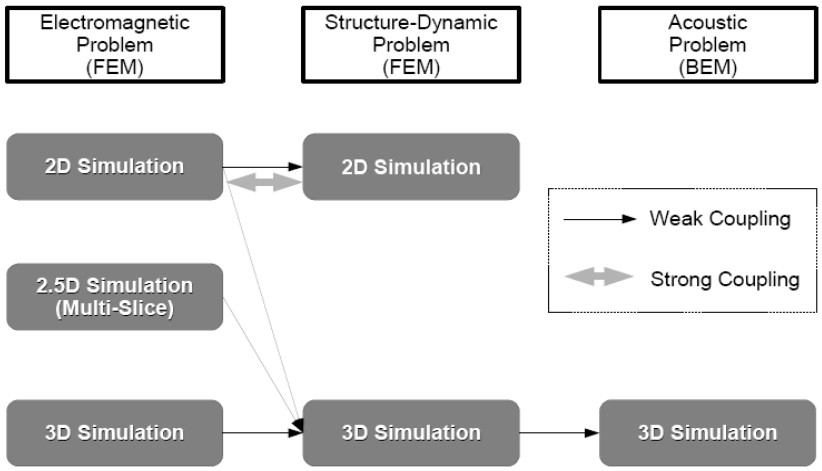

Figure 1. 4 : Overview of simulation methods [8].

If an electrical machine, is homogenous in the axial direction and if its axial dimension is sufficiently small compared to its diameter, it is then possible to use 2D electromagnetic FEM to obtain the field distribution. For machines, of which the cross section is only varying slightly with respect to the axial direction, the Multi-Slice-Method (MSM) can be applied [9]. Due to a high ratio between accuracy and computational effort, the 2D or 2D MSM has become a standard for the electromagnetic simulation of electrical machines. SAKAMOTO, et. al. [10] described a method to calculate vibrations due to electromagnetic forces for rotating electric machines. This method has an ability of calculating the vibration spectrum due to higher harmonics of electromagnetic forces and it is verified by comparing the

calculated and the measured results. Using this analysis method, complicated dynamic behavior due to eccentricity is calculated.

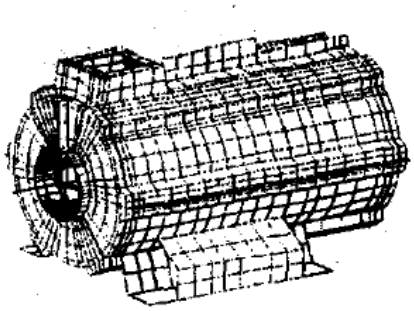

Figure 1. 5 : The system types in modelling field. Analysis model of induction motor(This model has about 3000 node points)[10].

The frame, stator core are divided into shell elements and rotor is modelled by beam elements that have the equivalent mass and stiffness real structures (Figure 1.5). The main concept of analysis method used in this study[10] is the combination of 2D magnetic field analysis and 3D vibration analysis. 2D magnetic field analysis shows electromagnetic forces in the radial direction of a stator core (Figure 1.6).

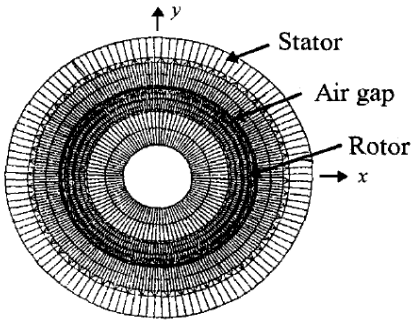

Figure 1. 6 : The system types in modelling field. Mesh division for magnetic field analysis. (This model has about 6000 node points) [10].

In many studies [11,12] simulations are implemented in the MATLAB/SIMULINK software package. Liang et al [11] aimed to investigate whether induction motor operational simulations with general equations could be used for monitoring and fault diagnosis of such motors. They showed that a generalized motor model can be used to simulate induction motor faults to a high degree of accuracy (Figure 1.7).

In reference [12], based on the design data, a dynamic model of universal motors, was developed. After the development of the mathematical model, a simulation model based on the Matlab-Simulink was derived (Figure 1.8). This allowed for the

determination of the waveforms of the speed, current and torque of the machine for different operating conditions.

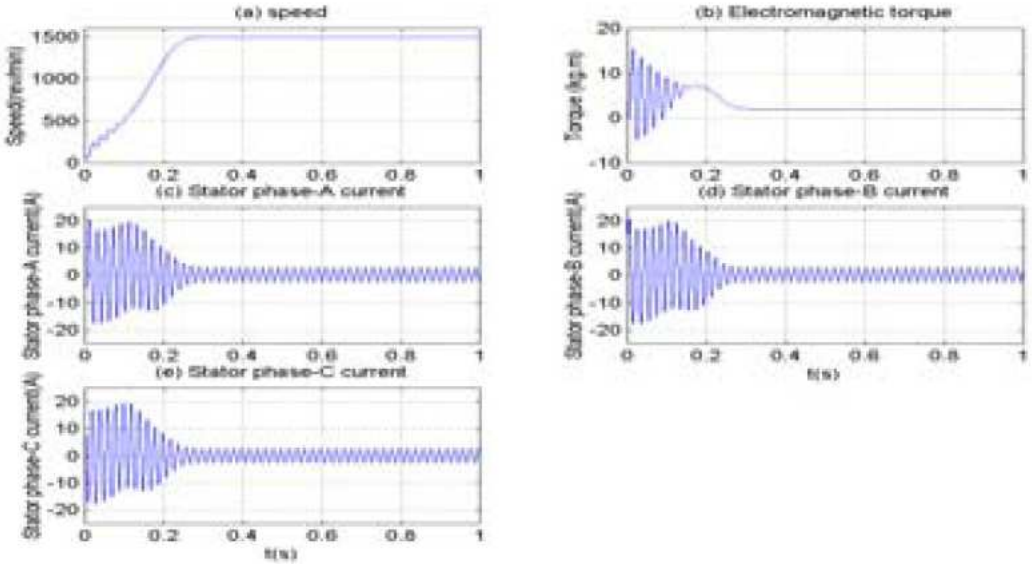

Figure 1. 7 : The sytem types in modelling field. Simulation of a healty motor during start-up [11].

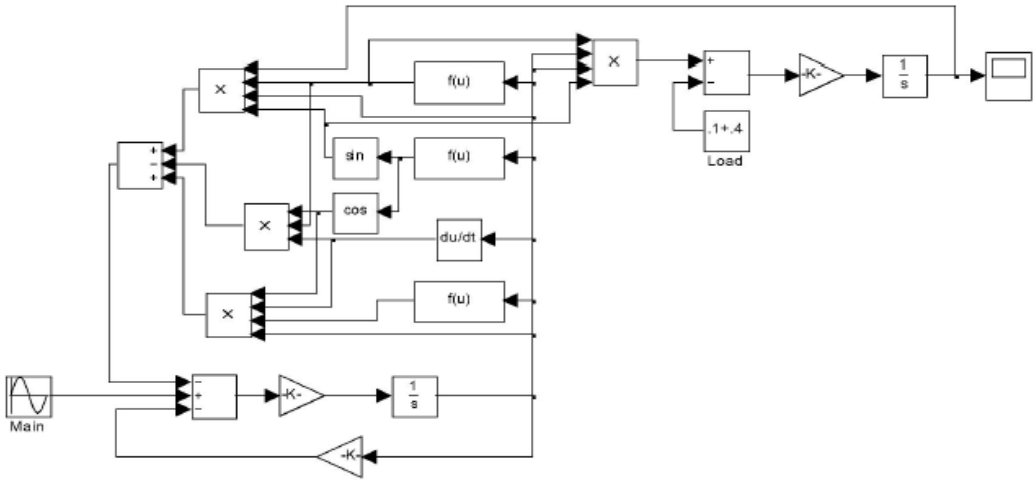

Figure 1. 8 : Block diagram of a universal motor [12].

In addition to the modelling studies of electric motors described in previous section, there are also studies focussing on mechanical/electromagnetic vibration and noise. In reference [13], an analytical model has been proposed for predicting the vibration frequencies of rolling bearings and the amplitudes of significant frequency components due to a localized defect on outer race/inner race or on one of the rolling elements under radial and axial loads. Çakmak, and Şanlıtürk [14] developed a dynamic model of a rotor-ball bearing system in Msc. ADAMS commercial

software. It is aimed to create a new model for a rotor-bearing system, which can demonstrate not only the vibrations generated by a ball bearing itself, but also the effect of the flexible shaft and rigid disc structure on the resonance characteristics of the system. A numerical model of a ball bearing which is capable of representing the effects of bearing defects and internal clearances is represented (Figure 1.9).

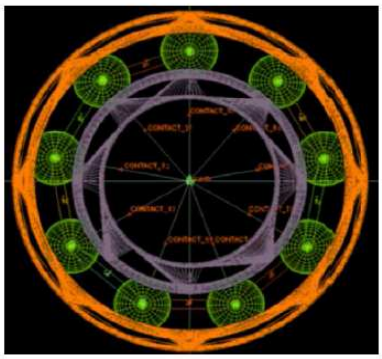

Figure 1. 9 : Model of ball bearing created on MSC ADAMS [14].

In reference [15], a numerical model of 2-hp permanent magnet motor is presented by taking into account of magnetostriction effect in addition to other electromechanical forces. Magnetostriction forces are calculated by expension of the free body due to magnetostriction based upon the magnetic flux density. Figure 1.10 (a) shows stator deformation from the coupled transient magneto-mechanical solution at six rotor positions without the magnetostriction effect. Figure 1.10 (b) shows the stator deformations with the magnetostriction effect added at the same rotor positions of Figure 1.10 (a). The results in [15] indicate that magnetostrictive forces are significant and mut be accounted for in the electromagnetic system's design stage. Don-Ha Hwang, et. al. [16] presents results of a finite element (FE) analysis and experiment of airgap flux variation in induction motor under conditions of rotor eccentricity.

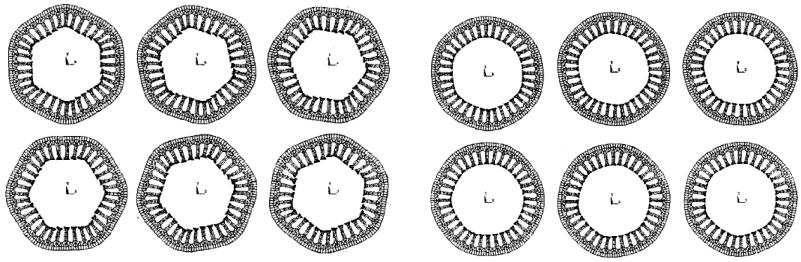

a) b)

Figure 1. 10 : Stator deformation from the coupled transient solution (a) with and (b) without magnetostriction [15].

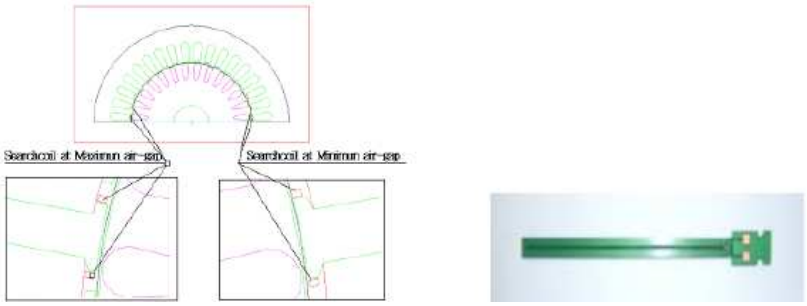

a) b)

Figure 1. 11 : a) Vibration analysis model with inserted search coils, b) search coil-typed flux sensor [16].

On the modelling side an accurate modelling and analysis of rotor vibration in the motor are made using air-gap flux simulation (Figure 1.12). On the experimental side, search coils are used for measuring the actual magnetic flux (Figure 1.11). Induction motor vibration is simulated and search coils are designed and inserted under the stator wedge of the motor. FE analysis results are compared with experimental test results [16]. Reference [17], presents the analytical characterization of Maxwell radial vibrations due to saturation effects in induction machines. Effects of some parameters such as stator and rotor slot numbers and stator natural frequencies on magnetic noise are investigated especially during starting and braking period. In order to avoid saturation magnetic noise, a formulation is proposed and applied to an industrial motor. Applied formulation propose that a numerical relation between number of rotor and stator slots and pole pairs for a succesfully design in terms of noise in induction machines. Results are shown in Figure 1.13. Approximately a 5dB improvement is achieved in magnetic noise.

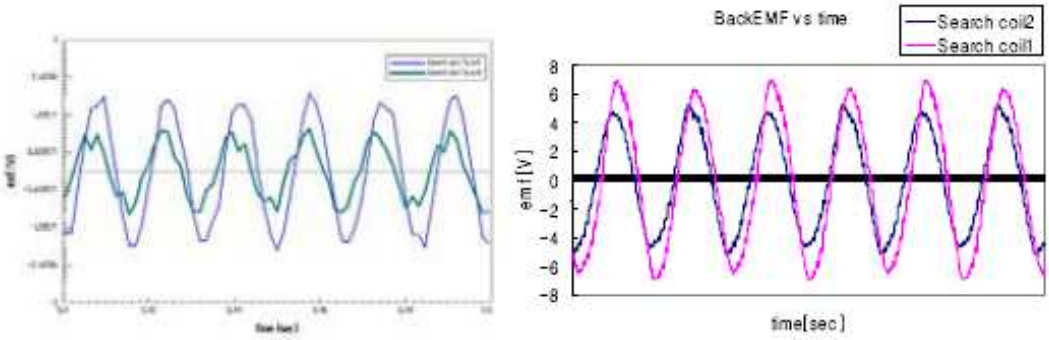

(a) FE analysis (b) Test result

Figure 1. 12 : Induced voltages from search coils under eccentricity conditions [16].

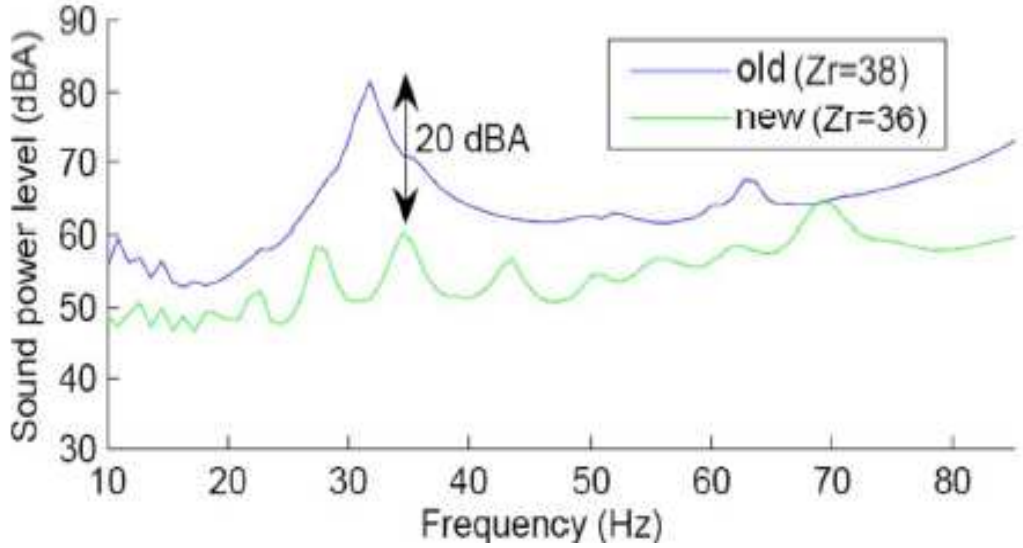

Figure 1. 13 : Sound power level comparison between different rotor slots [17].

Curiac, and Singhal [18] discusses the theoretical foundations for various causes of electromagnetic noise generation and practical reduction techniques for new or existing motors. Numerical results are given for various stator-rotor slot combinations and slot geometries. Theoretical predictions are also compared with measured data.

Besnerais and Brochet [19] proposed that two methods can be used to avoid high levels of magnetic noise: the first one requires avoiding resonances by properly choosing the slot combinations that have an influence on both the exciting force frequencies and spatial order. A second method consists of reducing the exciting forces magnitude by choosing the slot geometry properly. The effects of the slot combination on the acoustic noise is calculated by an accurate computational method in reference [20]. The moving of the rotor and eddy currents are also taken into account in the FE method.

Reference [21], aims to eliminate squeaking noise in a permanent-magnet DC motor. Analysis on noise spectra of motor is performed. Based on noise spectral analysis, the authors found that apart from some mechanical issues, such as the shaft strength and bearing system, the main reason for the production of this squeaky noise is attributed to the presence of unbalanced magnetic radial force, which is caused by the asymmetrical air-gap field distribution in the motor being studied.

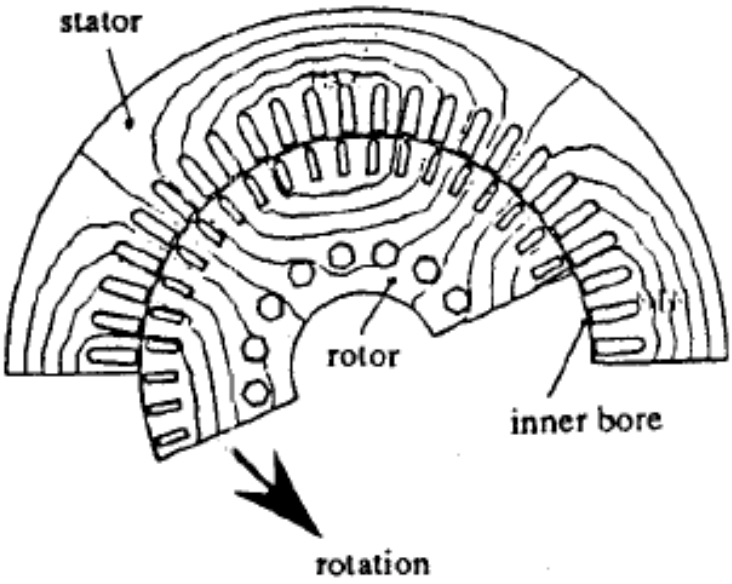

Figure 1. 14 : Magnetic vector potential contours [20].

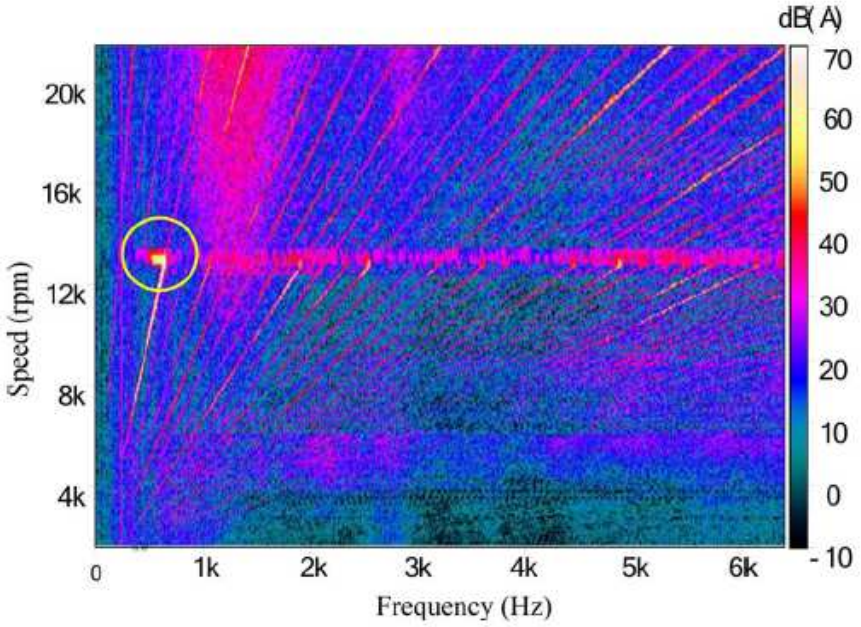

Figure 1. 15 : Noise spectrum during running up [21].

From the magnetic field analysis, it is found that for this kind of motor, its magnetic field distribution in the air gap is asymmetrical. Figure 1.16 (a) shows the field flux line distributions at no-load, and Figure 1.16 (b) shows its field distribution in the air gap. Consequently, an alternative design with one dummy slot or punching hole in the center of the rotor tooth is proposed, as shown in Figure 1.16 (a). The improved method is validated by test results [21].

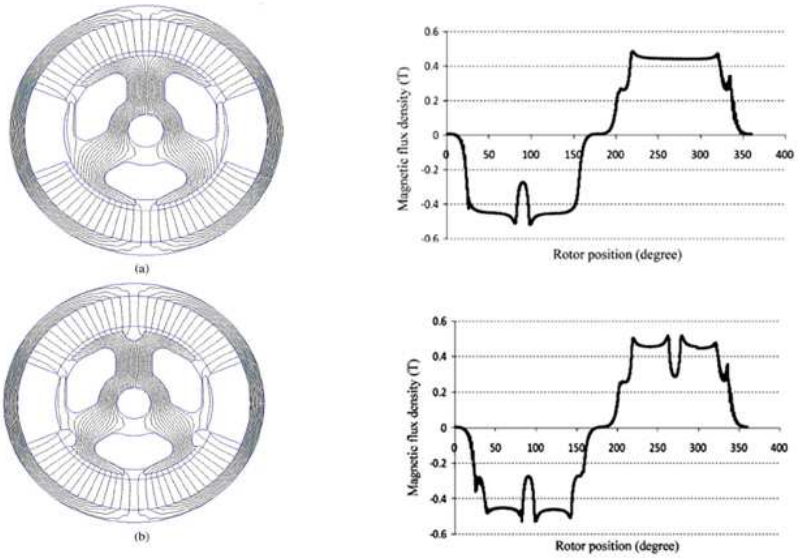

a) b)

Figure 1. 16 : No-load field distribution, a) traditional PMDC geometry, b) proposed design [21].

Another study [22] describes a simple analytical model for calculating the unbalanced magnetic pull generated in a three phase cage induction motor. It is observed that skewing the rotor increases the Unbalanced Magnetic Pull (UMP)[2] and, in addition, it is necessary to include higher space harmonics stator Magnetomotive Force (MMF)[3] waves to obtain accurate UMP calculation. Akgül, E. Orhon and H.T. Belek [23] investigated the sources of vibrations of a chimney gas fan. They performed vibration measurements during run up and run down in order to separate magnetical-based vibrations from that of mechanical-based.

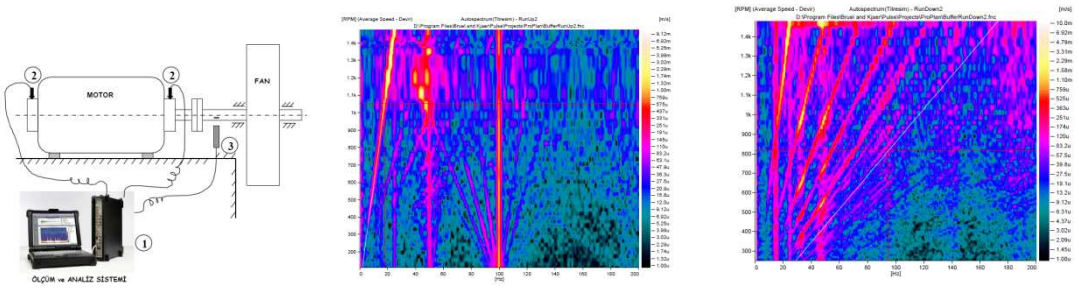

a) b) c)

Figure 1. 17 : Measurement set-up of electric motor of chimney gas fan, b) ru-up measurement of system, b) run-down measurement of system [23].

[2] Non-uniform air gap flux density occurs due to the eccentric rotor which causes a radial force in the direction of greatest flux density(smallest air gap). This radial force has been referred to in the literature as unbalanced magnetic pull (UMP).
[3] Magnetomotive Force (MMF) is any physical driving (motive) force that produces magnetic flux.

1.3 Objectives And Scope Of The Thesis

The main purpose of this thesis is to develop a reliable numerical model of a universal electric motor in order to understand the dynamic behaviour of electric motors under the actions of the mechanical and electrical forces. The effects of any design changes to the dynamics of the electric motor can be easily observed with such numerical models. Consequently, reliable numerical models of electric motors can be used to for designing better electric motors and can help to reduce the number of prototypes during the development stage. In this context, the works that need to be carried out in this thesis are summarized below as;

1) To build finite element models of individual parts of an electric motor and validate these finite element models by means of experimental data.
2) To assemble these finite element models by using appropriate software and obtain dynamic model by adding the effects of dynamic forces.
3) To simulate operating conditions of electric motor and determine the vibration characteristics.
4) To validate the forced response model.
5) To investigate some parameters which affect the vibration characteristics of the electric motor.

This study is consisting of six steps. First, objectives and scope of the thesis are discussed and literature survey is presented. Theoretical background of the thesis is investigated as a second step. In the third and fourth step results of experimantal and numerical studies are reported separately. Comparisons of these results are discussed in the fifth step. In the last step of the thesis, conclusions and suggestions are criticized.

In the first chapter of the thesis, problem aimed to be solved, purpose and also scope of the thesis are described. Literature survey about the topic is presented. Studies available in the lierature that are about modelling electric motors and sources of mechanical/electromagnetic vibration/noise are investigated.

In chapter 2, thoretical background of this study is summarised. First, the principles of the electromagnetism is investigated as it is necessary to understand the basic design principles of electric motors. After that, the operating principles of electric motors are briefly described and vibration and noise sources mostly encountered

in electric motors are presented. Last part of this chapter presents basic theory behind order and modal analyses.

In chapter 3, experimental studies are presented. It consist of FRF analysis, Campbell and order diagrams of current and acceleration measurements. A test rig used for measurements of electrical motor and set-ups of this measurements are explained and results are discussed.

In chapter 4, the steps of numerical modelling process is discribed in detail. The finite elements (FE) models of individual components of motor and the results of numerical modal analyses of them are shown. The assembled model of the electrical model is introduced. A simple model which explain mechanisms of electromagnetic vibrations of electric motor. Results obtained from simple model are discussed and presented simple model is applied to the motor model. Forced vibration model and analysis results in terms of campbell diagrams are presented finally.

In chapter 5, the data obtained from the measurements are assessed and the numerical model is improved in the light of this experimental information. The validated model is subjected to modal analyses and the modal results obtained from both experimental and numerical models are compared in terms of frequency response functions.

After the model is validated for the non-rotating case, the dynamic simulations are performed. The simulation results are processed with Short Time Fourier Transform (STFT) technique. Campbell diagrams obtained form both the numerical and the experimental models are compared.

In the last chapter of the thesis, assessment of the study and suggestions for further studies are introduced.

2. THEORY

2.1 Principles of Electromagnetism

2.1.1 Electricity and electromagnets

Materials that can be magnetized are called ferromagnetic (Figure 2.1). These include iron, nickel, cobalt, some rare earth metals and some of their alloys.

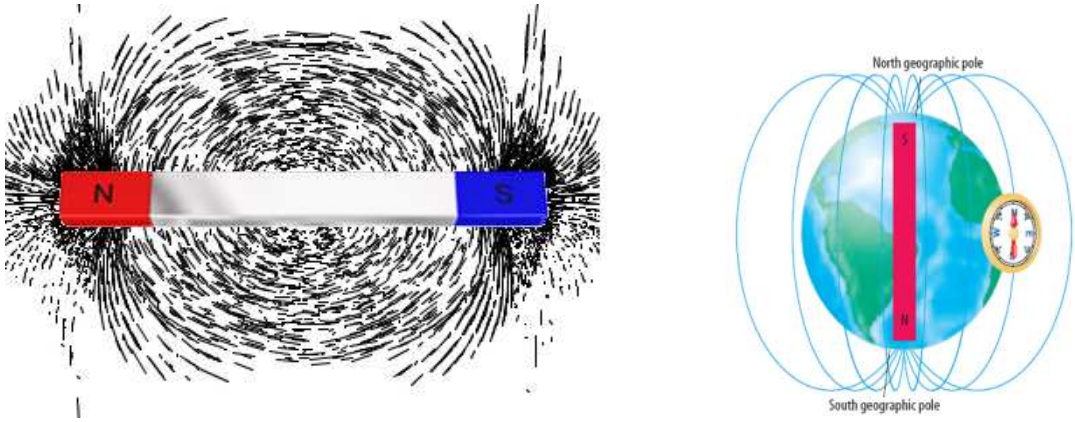

a) b)

Figure 2. 1 : a) Permanent magnet and its magnetic field, b) earth's magnetic field.

When electricity is applied to an electrical conductor, magnetic field is created around the conductor (Ampere's Law). Here, the magnetic field fluxes are constructed as a circumferential ring around the electrical conductor (Figure 2.2). The direction of this magnetic field is dependent on the direction of the electricity. An electromagnet (Figure 2.3) is made from a coil of wire which acts as a magnet when an electric current passes through it, but it stops being a magnet when the current is cut-off. Often an electromagnet is wrapped around a core of ferromagnetic material like steel, which enhances the magnetic field produced by the coil.

When the wire is wound into a coil, all the flux lines produced by each turn of wire join up and form a single magnetic field around the coil. The greater the number of turns of the coil, the greater the strength of the magnetic field (Figure 2.4).

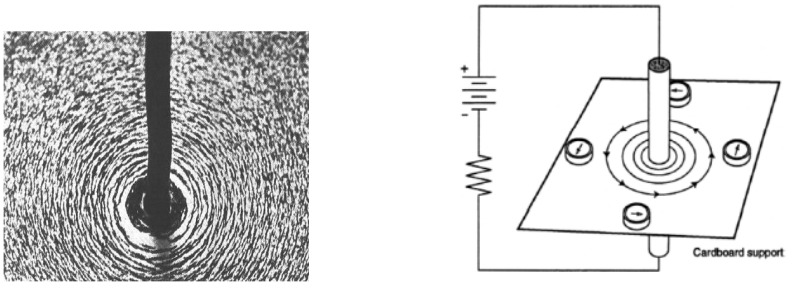

a) b)

Figure 2. 2 : a) Concentric magnetic flux around a current-carrying conductor, b) distribution of the metal particles around a current-carrying conductor [41].

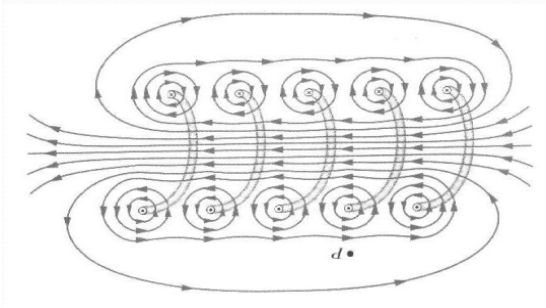

Figure 2. 3 : Electromagnet without core.

Quite apart from strength, the advantage of having a magnetic field created by a current-carrying coil is that it makes it possible to reverse the poles of the magnet by reversing the direction of the current (Figure 2.5). This ability to reverse the poles is precisely the method used to create mechanical energy in electric machines.

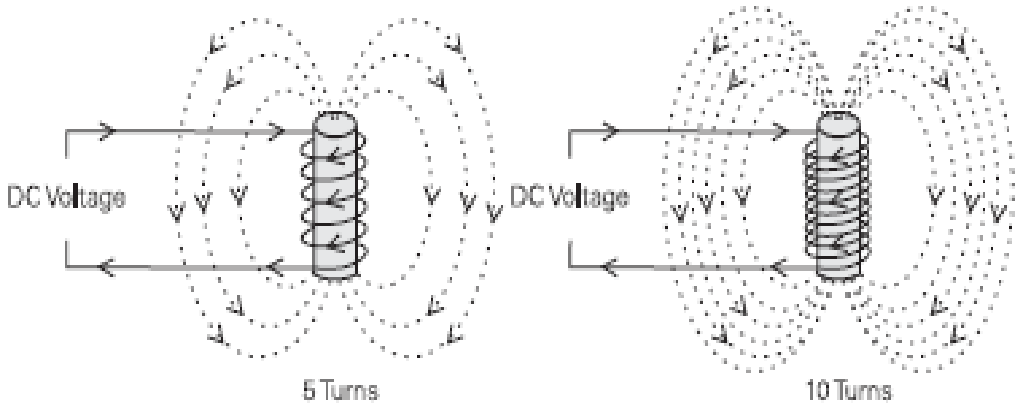

Figure 2. 4 : Electromagnet with iron core and relation between number of turns and magnetic flux [42].

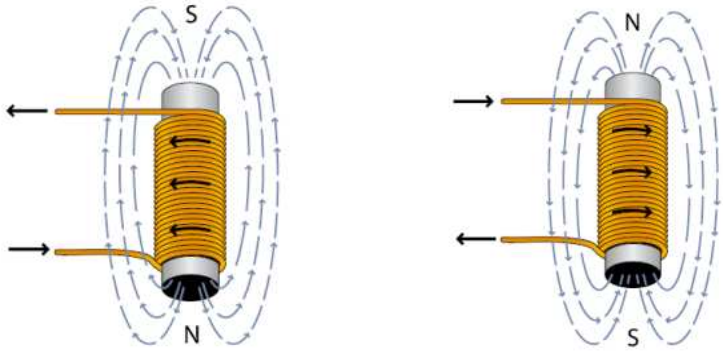

Figure 2. 5 : Relation betwenn direction of electrical current and electromagnet poles[44]

2.1.2 Interaction between electric current, magnetic field and movement

It is shown in Figure 2.6 that there is a definite relationship between the directions of the magnetic field, the current-flow, and the resultant force. The main parameter is the direction of the current flow. Two viewpoints are available in the technical literature. The modern viewpoint is that current flow consists of negatively-charged electrons that leave the negative terminal of the source and complete the circuit by returning to the positive terminal. This is known as an electron current. However, many electrical phenomena have been dealt with for many years in terms of the older concept in which current is assumed to flow from the positive terminal of the source and returned to the negative terminal. Current flow described in this way is known as a conventional current.

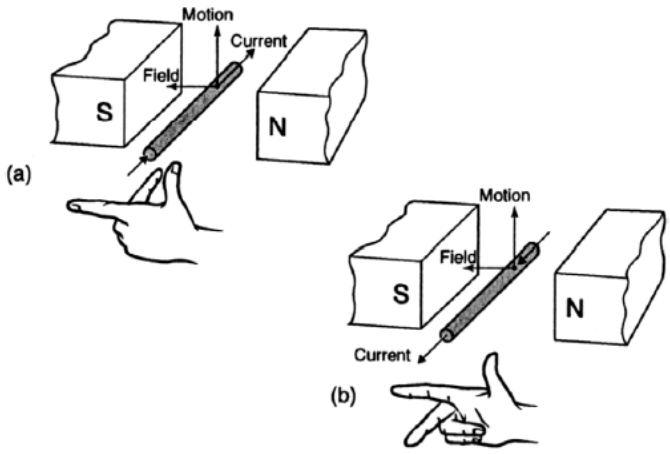

Figure 2. 6 : a) The left hannd rule for conventional current-flow (from ‘plus’ to ‘minus’), b) the right hand rule for electron vurrent-flow (from ‘minus to ‘plus’) [41].

Besides indicating a third operational feature of motors when two of them are known, another characteristic is revealed by the hand rules. Maximum motor action occurs with the magnetic and the current-carrying conductor perpendicular to both, the field and the current. This is known as the orthogonal relationship.

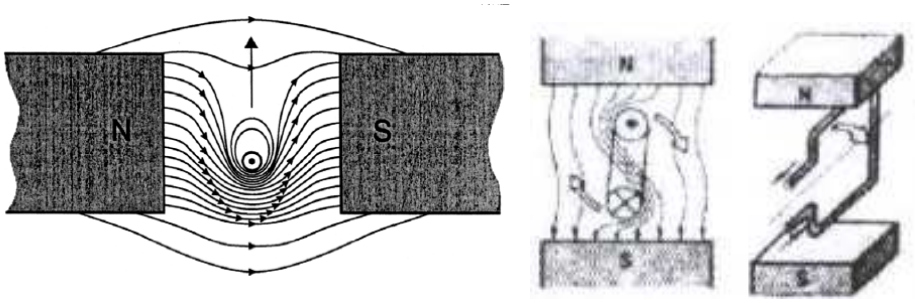

Figure 2. 7 : Motor action exerted on current-carrying conductor in a magnetic field [41].

In addition to the physical motion of the current-carrying conductor in Figure 2.7, a voltage is also induced in the conductor. This simultaneous behavior as a generator is the practical manifestation of Lenz's Law. In a general, it tells us *"an induced current is always in such a direction as to oppose the motion or change causing it"*.

2.1.3 Faraday's Law and Lenz's Law

Faraday's Law explains the electromotive force which is obtained by induction. Any change in the magnetic environment of a coil of wire will cause a voltage (emf) to be "induced" in the coil. No matter how the change is produced, the voltage will be generated. The change could be produced by changing the magnetic field strength, moving a magnet toward or away from the coil, moving the coil into or out of the magnetic field, rotating the coil relative to the magnet, etc.
According to the Induction Law, the induced voltage in a coil is expressed as;

$$e = -N\frac{d\varphi}{dt} \qquad \textbf{(2.1)}$$

e: induced voltage
N: number of turns
$\boldsymbol{\varphi}$: magnetic flux
t: time

Negative sign at the beginning of the equation 3.1 was placed by Lenz. This addition is known as Lenz's Law. When an emf is generated by a change in magnetic flux, the polarity of the induced emf is such that it produces a current whose magnetic field opposes the change which produces it. The induced magnetic field inside any loop of wire always acts to keep the magnetic flux in the loop constant. In the examples below (Figure 2.8), if the B field is increasing, the induced field acts in opposition to it. If it is decreasing, the induced field acts in the direction of the applied field to try to keep it constant.

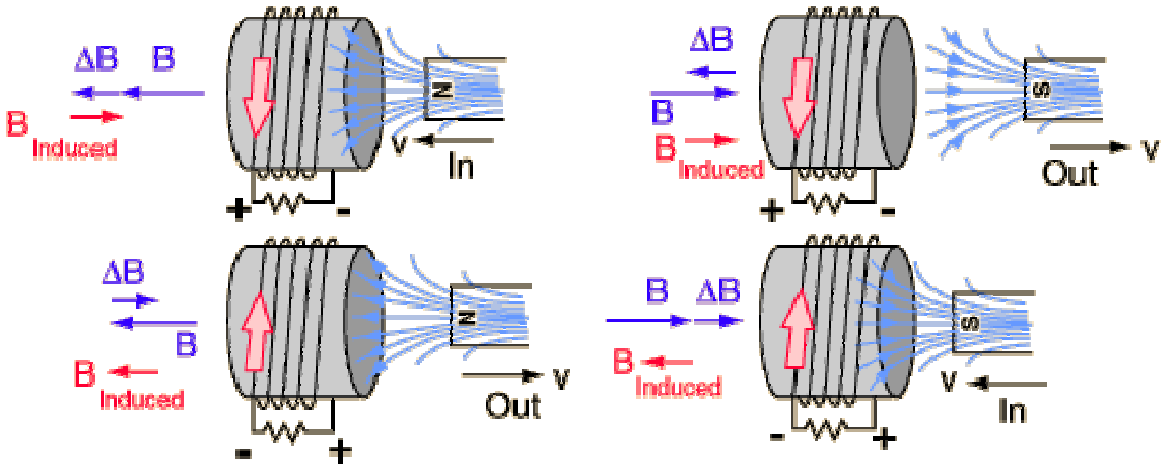

Figure 2. 8 : An induced electromotive force generate a current that a counter magnetic field that opposes the magnetic field generating the current [48].

2.1.4 Electromagnets and ac source

When the direction of current flow through the electromagnet changes, the polarity of the electromagnet also changes. The polarity of an electromagnet connected to an AC source will change at the same frequency as the frequency of the AC source. This can be demonstrated in the following illustration (Figure 2.9).

When a conductor is moved through a magnetic field, a voltage is induced into it. This electrical principle is used in the operation of AC induction motors. In the following illustration (Figure 2.10) an electromagnet is connected to an AC power source. Second electromagnet which is in a separate circuit is placed above it. There is no physical connection between the two circuits.

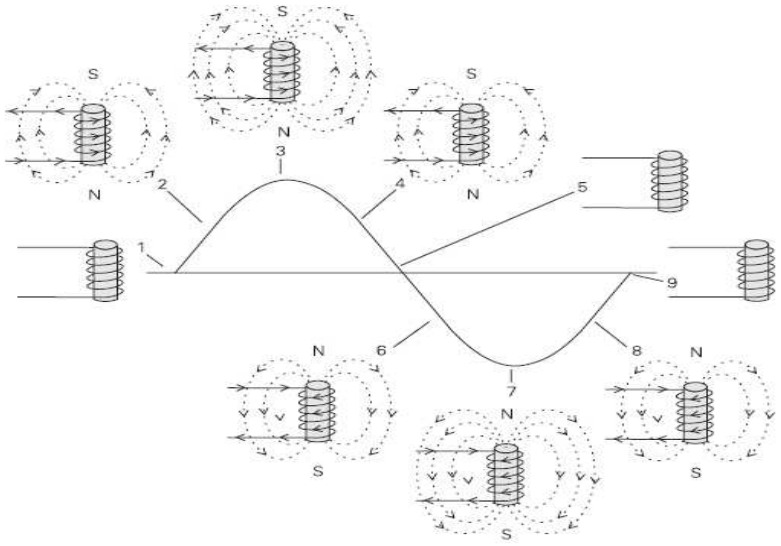

Figure 2. 9 : Condition of the polarity of an electromagnet connected to an AC source. [42]

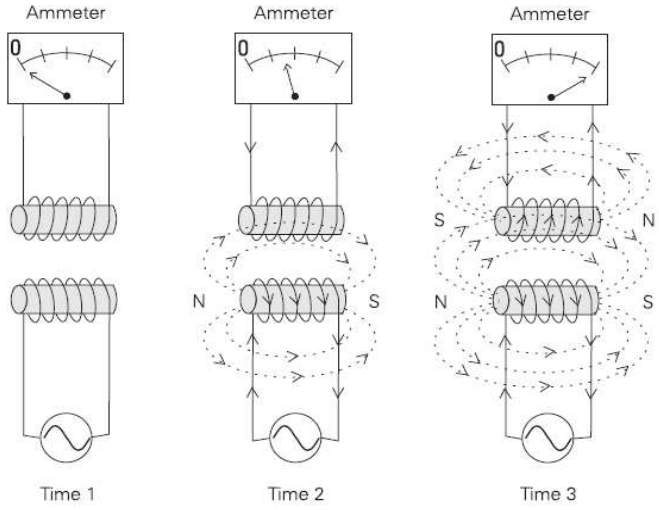

Figure 2. 10 : Voltage induction on the electromagnet by means of AC source [42].

At Time 1 voltage and current are both zero in the circuits (Figure 2.10). At Time 2 voltage and current are increasing in the bottom circuit. A magnetic field builds up in the bottom electromagnet. Lines of flux from the magnetic field building up in the bottom electromagnet affects the top electromagnet. A voltage is induced in the top electromagnet and current flows through it. At Time 3 current flow reached its peak. The maximum current is flowing in both circuits. The magnetic field around the coil continues to increase and decrease as the alternating current continues to increase and decrease.

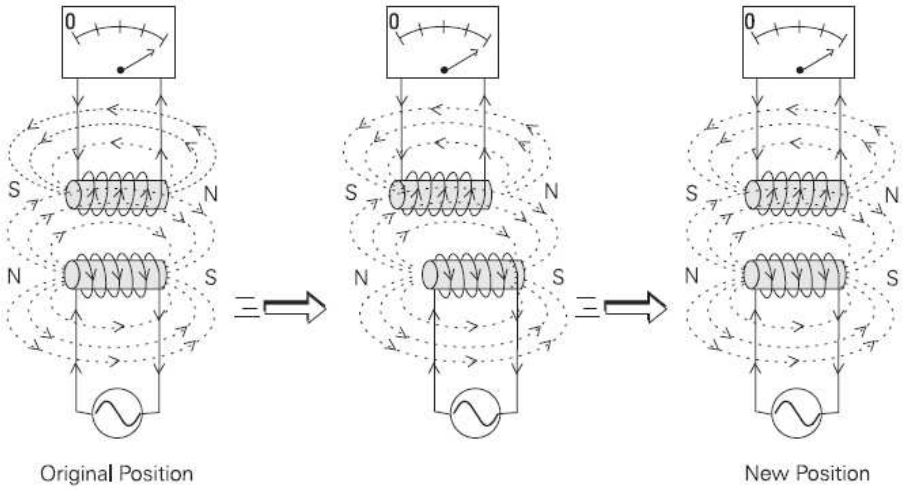

Figure 2. 11 : Voltage induction and motion [42].

As current flows in the top electromagnet it creates its own magnetic field. The polarity of the magnetic field induced in the top electromagnet is opposite to the polarity of the magnetic field in the bottom electromagnet (Figure 2.11). Since opposite poles attract, the top electromagnet will follow the bottom electromagnet when it is moved.

2.2 Principles of Electric Motors

2.2.1 Direct current (DC) electric motors

DC machines are the first practical devices which convert electrical power into mechanical power. Inherently straightforward operating characteristics, flexible performance and high efficiency have encouraged the widespread use of DC motors in many types of industrial drive applications [24].

Advantages of a brushed DC motor include low initial cost, high reliability, and simple control of motor speed. Disadvantages are high maintenance cost and low life-span for high intensity uses. DC motor has two fundamental parts: stator and rotor (Figure 2.12). Stator is a stationary part of motors which has two main function: one of them is to support poles and the other one is to provide a path for electromagnetic field circuit which is produced by poles of motors. Poles are used to create required constant magnetic field. This magnetic field completes its circuit along the stator shown in Figure 2.13.

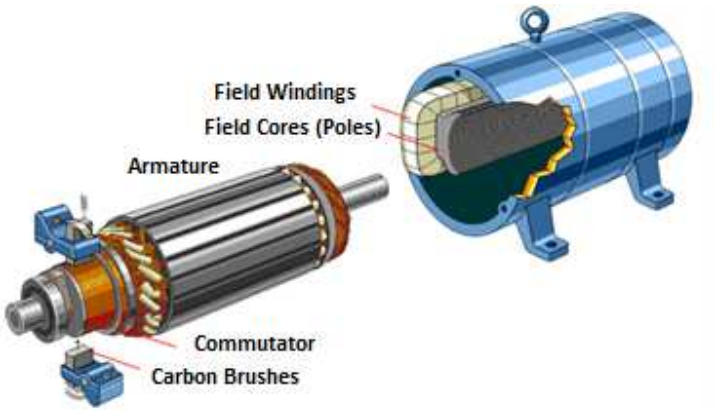

Figure 2. 12 : Construction of a DC motor [43].

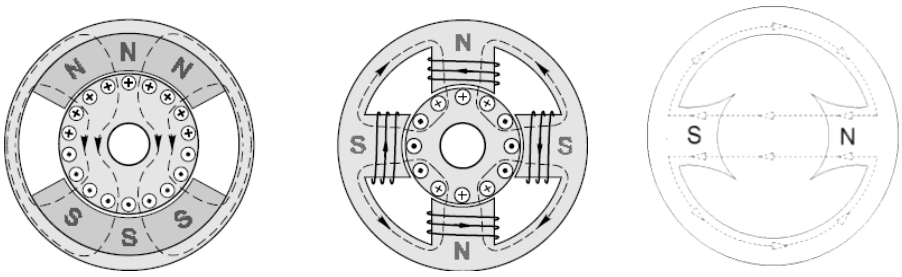

a) b) c)

Figure 2. 13 : Excitation (field) systems for DC motors a) 2-pole permanent magnet; b) 4-pole wound field; c) circuit of a magnetic flux [47].

As the name implies, rotor is the rotating part of an electric motor. Generally, required magnetic field is provided by conductors which are wrapped around the rotor as shown in Figure 2.14.

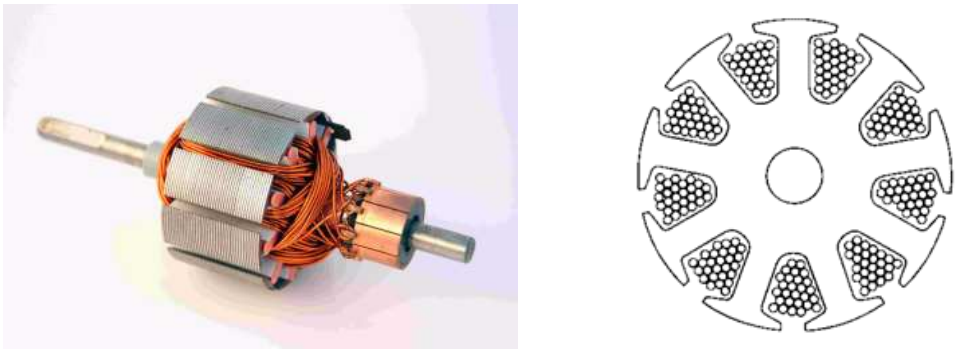

a) b)

Figure 2. 14 : a) Rotor and b) windings of a DC motor.

Commutator (Figure 2.15) is placed at one end of the rotor and, as mentioned before, it is used for changing the direction of the electric current applied on the rotor

windings. Each section of commutator is connected with one winding circuit wrapped around the rotor. Current applied on the rotor windings is first pass along brushes (Figure 2.16). These components are used for providing electric current to the rotor windings via commutator. Brushes are generally made of carbon based materials. Main reason of using carbon based materials in brushes is to prevent commutator from wearing. The reason for this is that the brushes can be replaced more easier than commutator.

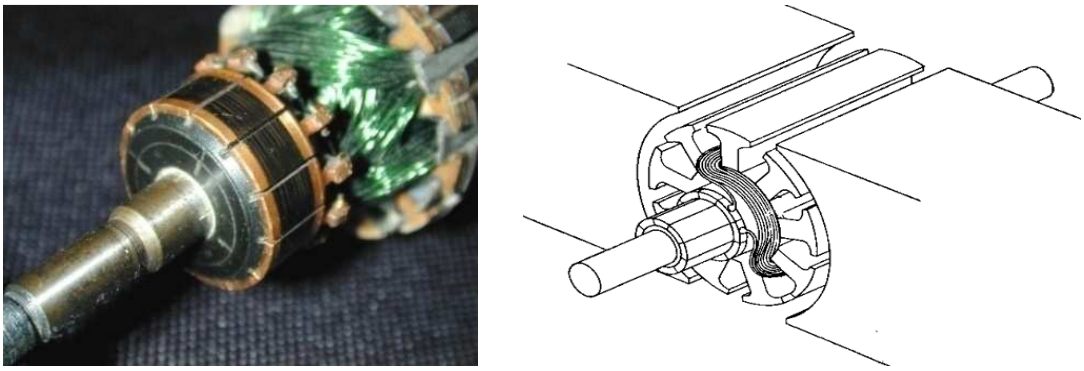

Figure 2. 15 : Commutator construction of a DC motor.

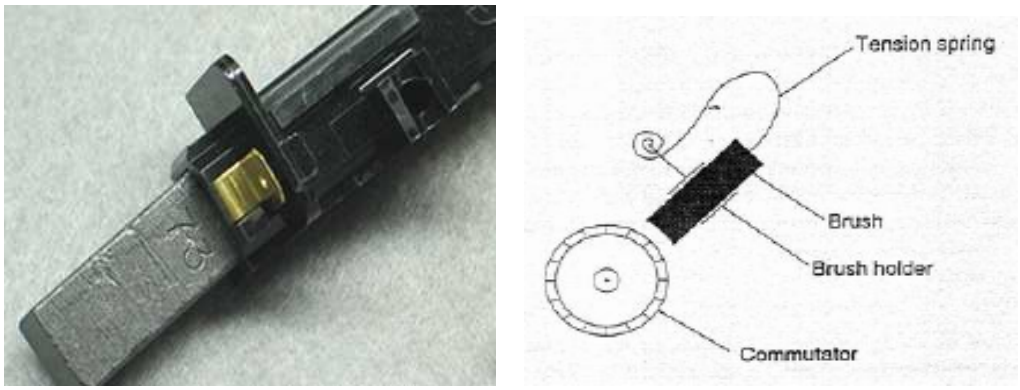

Figure 2. 16 : Brush construction of a DC motor

Brush pressure is an important parameter in motors. Figure 2.17 shows relative brush and commutator wear versus brush pressure. At low pressures, the wear is mostly electrical in nature because the poor contact results in high-resistance spots with localized heating and arcing. At high pressures, the wear is mostly mechanical and is due to the parts in effect grinding themselves away because of friction losses. [25]. DC motor generates torque directly from DC power supplied to the motor by using internal commutation, stationary permanent magnets and rotating electrical magnets. It works on the principle of Lorentz force , which states that any current carrying conductor placed within an external magnetic field experiences a torque or force.

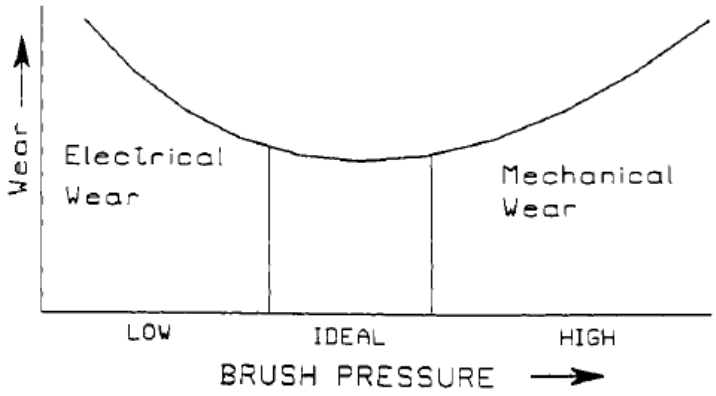

Figure 2. 17 : Brush pressure versus wear [25].

In DC electric motors, torque is produced by the interaction between the axial current-carrying conductors on the rotor and the radial magnetic flux produced by the stator. The flux can be furnished by permanent magnets or by means of field windings. It can be seen in Figure 2.18 that forces created on the windings are proportional to the magnitude of the magnetic field, electric current applied in the rotor windings and also length of the rotor windings.

It should be noted that, in order to obtain continuous rotational motion, the direction of the torque created on the rotor has to be in the same direction of rotation during one cycle of motion. To provide this condition, commutator is used (Figure 2.15). Main function of commutator is to change the direction of electric current in the rotor windings. So, as a result of changing electric current at required positions, force directions don't vary and continuous rotational motion is obtained.

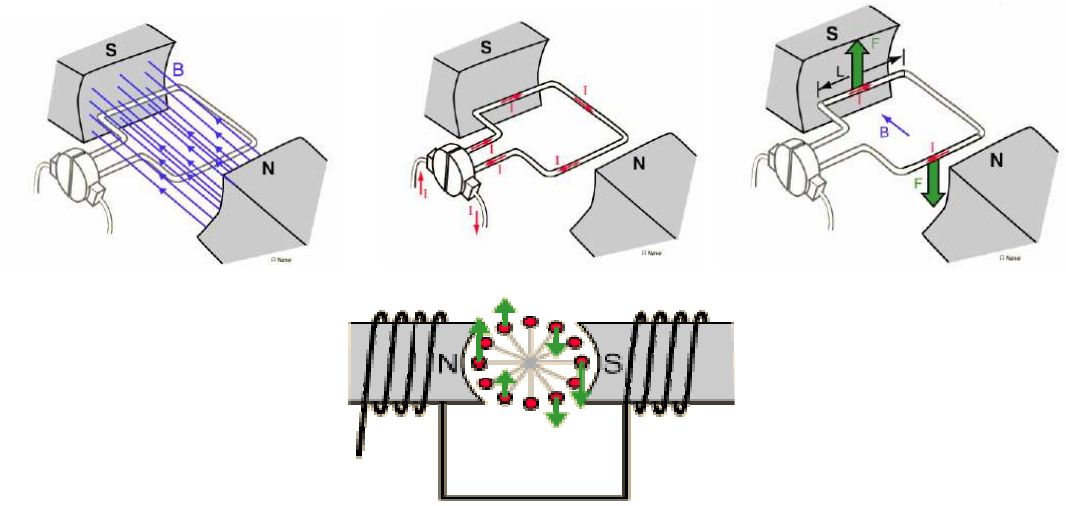

Figure 2. 18 : Schematic view of operation of a DC motor.

2.2.2 Alternating current (AC) electric motors

AC induction motors are the most common motors used in industry motion, as well as in main powered home appliances. Simple and rugged design, low-cost, low maintenance and direct connection to an AC power source are the main advantages of AC induction motors. Various types of AC induction motors are available in the market. Different motors are suitable for different applications. Although AC induction motors are easier to design than DC motors, the speed and the torque control in various types of AC induction motors require greater understanding of the design and the characteristics of these motors.

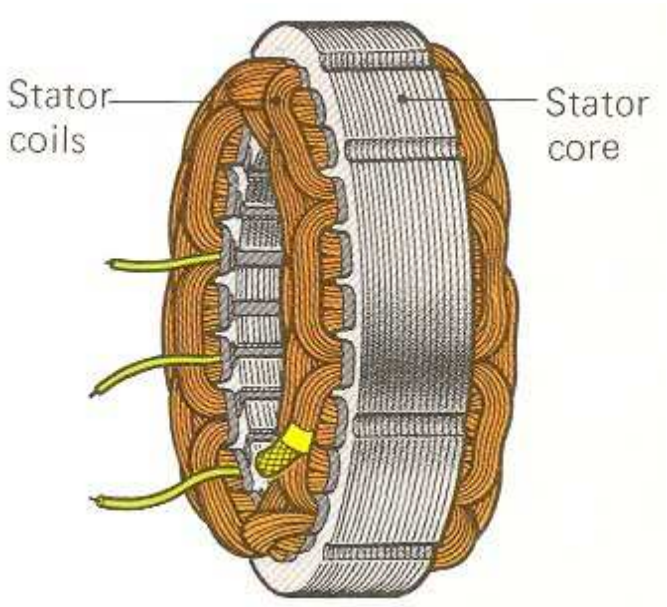

Figure 2. 19 : Stator core and coils of an AC motor.

In AC electric motors, electric current is only applied to the stator colis (Figure 2.19). Electromagnetic field created in the stator is not a stationary field as in the stator of DC motors. It has a constant rotational speed which is called 'synchronous speed' and it is calculated by formula;

$$N_s = \frac{2F_L}{P} \qquad \textbf{(2.2)}$$

$\mathbf{N_S}$ = Synchronous speed

$\mathbf{F_L}$ = Electrical Line Frequency

$\mathbf{P}$ = Number of poles

The most important difference between DC and AC motors is seen in the rotor in terms of both construction and the way magnetic field is created. The rotor is made up of several thin steel laminations with evenly spaced bars, which are made up of aluminum or copper, along the periphery. In the most popular type of rotor (squirrel cage rotor), these bars are connected at the ends mechanically and electrically by the use of rings. Almost 90% of induction motors have squirrel cage rotors. This is because the squirrel cage rotor has a simple and rugged construction. The rotor consists of a cylindrical laminated core with axially placed parallel slots for carrying the conductors. Each slot carries a copper, aluminum, or alloy bar. These rotor bars are permanently short-circuited at both ends by means of the end rings, as shown in Figure 2.20. This total assembly resembles the look of a squirrel cage, which gives the rotor its name.

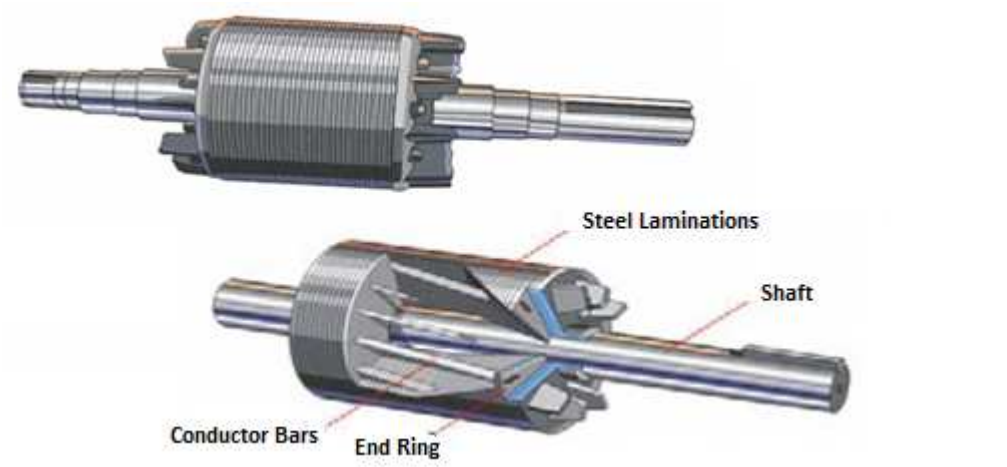

Figure 2. 20 : Rotor construction of an AC-motor [44].

While the magnetic field of the stator is rotating around the rotor, it cuts alloy bars which are short circuited by end rings and this cutting process is naturally induced a current in the rotor bars which give rise to the rotor own magnetic field. Two sets of electromagnets are formed inside any motor. In an AC induction motor, one set of electromagnets is formed in the stator because of the AC supply connected to the stator windings. The alternating nature of the supply voltage induces an electromotive force (emf) in the rotor (just like the voltage is induced in the transformer secondary) as per Lenz's law, thus generating another set of electromagnets (Figure 2.21). Interaction between the magnetic field of these

electromagnets generates twisting force, or torque. As a result, the motor rotates in the direction of the resultant torque.

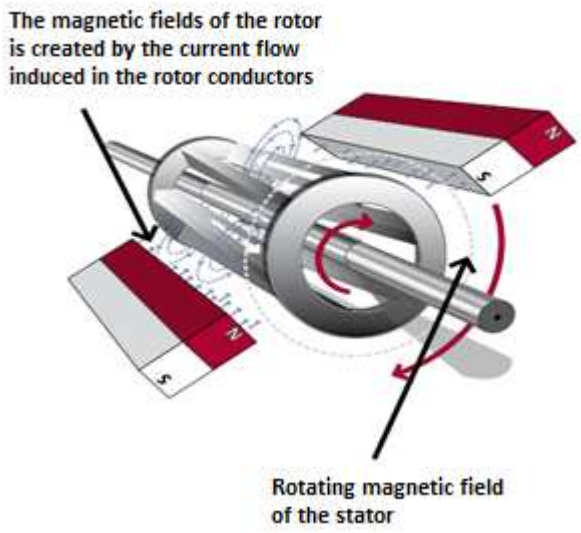

Figure 2. 21 : Schematic view of operation of AC motor [44].

The magnetic field produced in the rotor naturally tries to catch up with rotating magnetic field of stator. However in practice, because of the loads the rotor never reaches 'catching up' position. The rotor rotates slower than the speed of the stator field. Differences between magnetic field rotational speed of stator and rotor is called as 'slip' which is proportional to the load. While load is increasing, slip increases too. The slip is expressed as a percentage and can be determined using the following formula:

$$\%slip = \frac{N_s - N_R}{N_S} \times 100 \qquad \textbf{(2.3)}$$

$\mathbf{N_S}$ = the synchronous speed in RPM

$\mathbf{N_R}$ = the rotor speed in RPM

2.2.3 Universal electric motors

The universal motor is a rotating machine similar to a DC motor but designed to operate either from DC or single-phase AC. A DC motor cannot tolerate AC power because its rotational direction will reverse with every half cycle of the power line and it will simply vibrate in place. An AC motor can't tolerate DC power because,

as it depends on the power line's reversing current to keep the rotor moving. The stator and rotor windings of the motor are connected in series through the rotor commutator (Figure 2.22). Therefore the universal motor is also known as an AC series motor or an AC commutator motor.

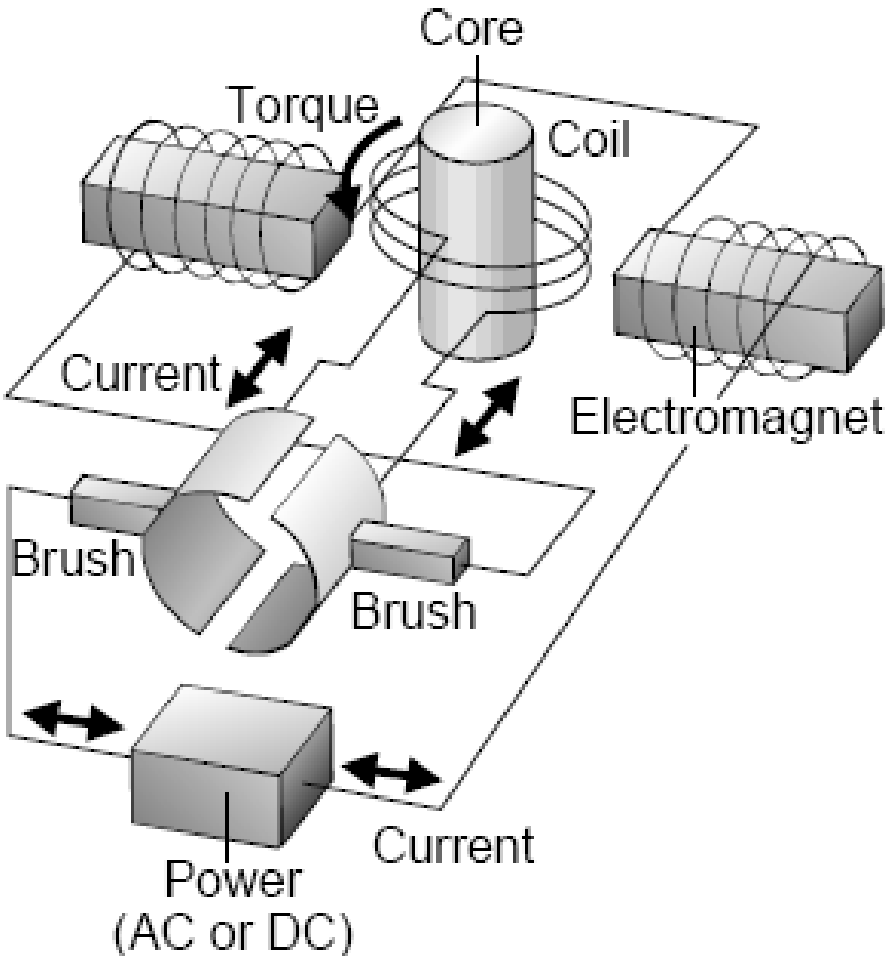

Figure 2. 22 : Schematic view of opretation of universal motor.

When DC power is connected to a universal motor, the stationary electromagnets will behave as if they were permanent magnets and the universal motor will operate just like a DC motor. It will continue turning in the same direction because reversing the current through the rotor also reverses the current through the electromagnets. Since the universal motor contains no permanent magnets, every pole in the entire motor changes from north to south or from south to north. Since the universal motor always turns in the same direction, regardless of which way current flows through it, it works just fine with AC electric power. There are moments during the current

reversals when the rotor experiences no torque, but the average torque is still high and the rotor spins as though it were connected to DC electric power.

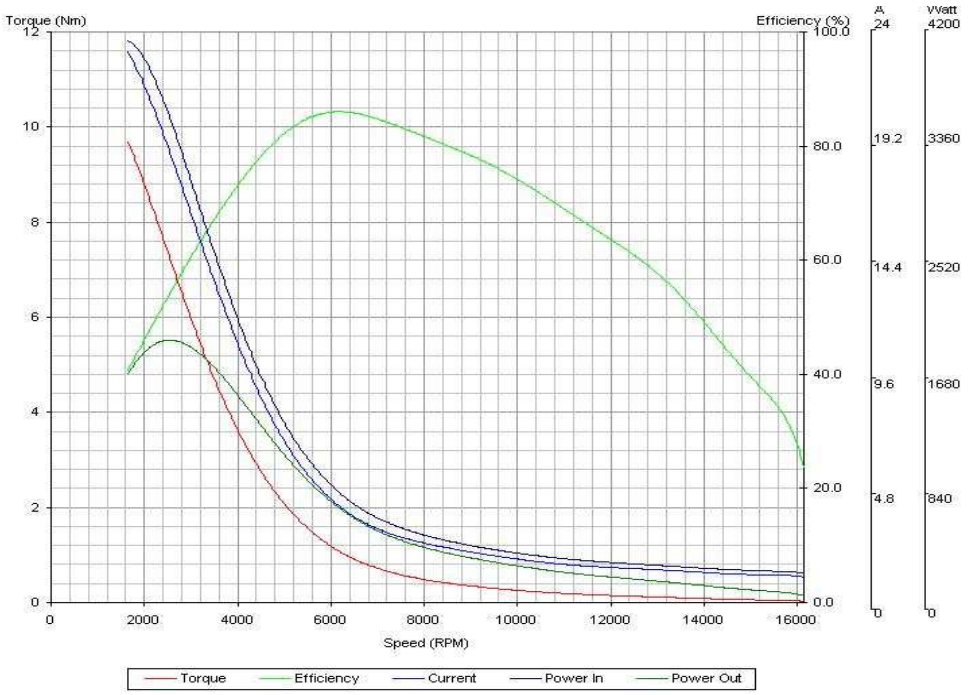

Figure 2. 23 : Speed-torque chacteristics of universal motor.

Speed-torque diagram of a typical universal motor is given in Figure 2.23. This feature is similar to the DC series motors. Universal motor generates high torque and uses high current in low speeds. Generally it is used in speed range of 6000-16000 RPM. The universal motor works equally well on DC or AC electric power. But Eddy current and Hysteresis losses are seen while it is working on AC electric power. Besides, it produces less torque and speed in AC. Universal motors has high power/cost rate with respect to the single phase motors. For this reason the usage of universal motor is wide in home appliances. When a universal motor is connected to a 50 Hz supply for example, the (sinusoidal) current will change direction every 10 msec, and there will be a peak in the torque 100 times per second (i.e.,100 Hz) (Figure 2.24). But the torque will always remain unidirectional, and the speed fluctuations will not be noticeable because of the smoothing effect of the armature inertia. Series motors for use on a.c. supplies are always designed with fully laminated construction (to limit eddy current losses produced by the pulsating flux in the magnetic circuit). Commutation and sparking are worse than when operating from DC. Universal motor is perhaps the best everyday example which demonstrates

how a high power can be obtained with small size by designing for a high speed. Other small AC machines, such as induction motors and synchronous motors, were limited to maximum speeds of 3000 rev/min at 50 Hz (or 3600 rev/min at 60 Hz), and therefore could not compete in terms of power per unit volume. The availability of high-frequency inverters has opened up the prospect of higher specific outputs from induction motors, but currently the universal motor remains the dominant force in small low-cost applications, because of the huge investment that has been made over many years to produce them in vast numbers. The universal motor can be controlled by a phase-angle drive, a chopper drive or a triac. The voltage applied to the motor can be varied to provide speed control. This approach is widely used for electric drills, fans etc. If torque control is required (as in hand power tools, for example), the current is controlled rather than the voltage, and the speed is determined by the load [1].

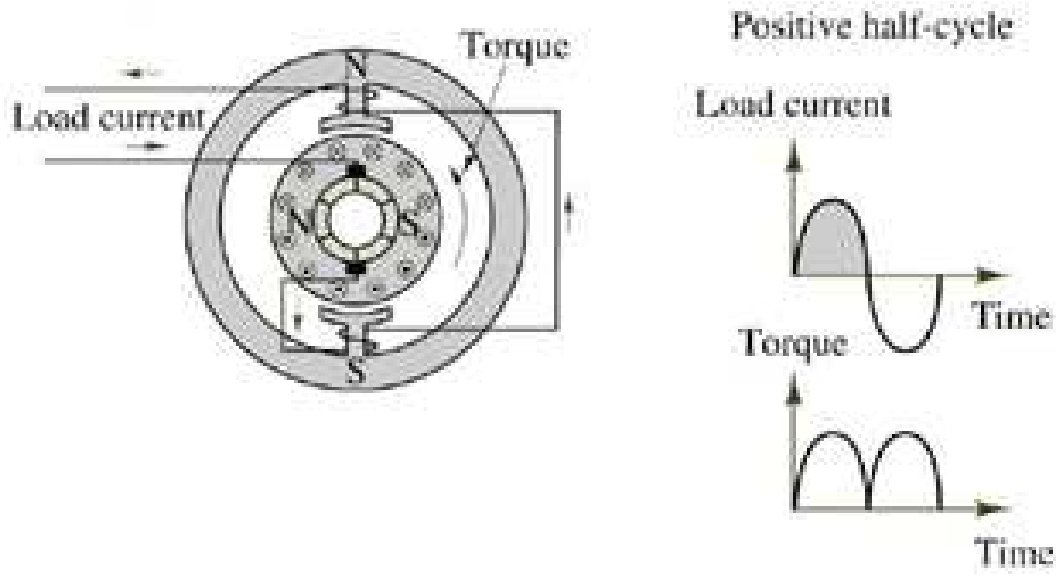

Figure 2. 24 : The frequency of the torque pulsation: twice the line frequency.

2.2.4 Linear model of universal electric motors

Electrical energy is converted to the mechanical energy by electric motors. So both electrical and mechanical principles need to be included in the model of electric motors. The machine speed and current are connecting the electrical and mechanical differential equations, which leads to an electromechanical system [46]. The equivalent circuit is presented in Figure 2.25.

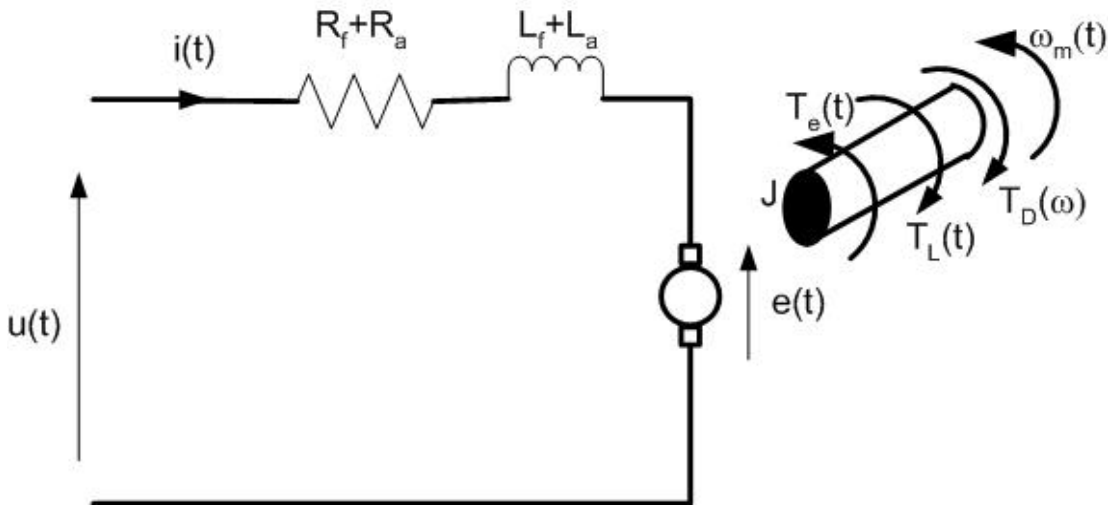

Figure 2. 25 : Equivalent circuit of the universal motor [46].

In Figure 3.28, the parameters are

$\boldsymbol{R_a}$: rotor winding resistance

$\boldsymbol{R_f}$: field winding resistance

$\boldsymbol{L_a}$: rotor winding inductance

$\boldsymbol{L_f}$: field winding inductance

$\boldsymbol{u(t)}$: terminal voltage

$\boldsymbol{e(t)}$: back emf

$\boldsymbol{i(t)}$: current in the machine

$\boldsymbol{J}$: moment of inertia of the machine and load

$\boldsymbol{D}$: viscous damping constant

$\boldsymbol{T(t)}$: electromagnetic torque

$\boldsymbol{T_L}$: load torque

$\boldsymbol{\omega_m(t)}$: angılar velocity of machine

Consequently, the behaviour of electric motor is represented by two coupled differential equations given below:

$$u(t) - (L_a + L_f)\frac{d}{dt}i(t) - K_a K_\psi i(t)\omega_m(t) = (R_a + R_f)i(t) \qquad \textbf{(2.4)}$$

$$K_a K_\psi i^2(t) = T_L + D\omega_m(t) + J\frac{d}{dt}\omega_m(t) \qquad \textbf{(2.5)}$$

2.2.5 Vibration and noise sources in electric motors

The sources of the noise and vibration of electric machines may be divided into three groups, depending on the ways in which they produce their effects. Forces of magnetic and mechanical origins produce vibrations directly in the machine structure; aerodynamic sources cause direct pressure fluctuations in the surrounding air. In this thesis, magnetic and mechanical origins of forces are considered. Aerodynamic sources are outside the scope of this study.

2.2.6 Mechanical sources of vibration and noise

The magnitude of the vibration or the sound produced at any position is primarily dependent on the magnitudes of the forces that are exerted on the system and is also dependent both on the mechanical response of the structure of the machine and its mountings and on the sound radiation characteristics of the radiating surfaces. These responses depend on the frequency and the modes of the vibration which are excited. Thus, a relatively large force may cause little vibration if the frequency of excitation is away from any of the natural frequencies of the system. Similarly, a relatively small force, exciting a particular mode of vibration of some the structure at or close to its resonant frequency, may cause large levels of noise and vibration. The noise and vibration produced by an electric machine may be reduced, either by reducing the magnitude of the original forces or by modifying the machine structure and supports and the acoustic paths. Often, more sound is radiated by surrounding objects, which are excited by machine vibrations, than is radiated directly from the machine itself. It is therefore necessary to understand the vibration and sound paths before an attempt is made to reduce the vibration/noise produced by a machine. It is usually better to reduce the vibration produced within the machine by careful design, rather than to use noise-reducing enclosures and mountings.

Mechanical sources of vibration/noise in an electric motor can be listed as;

- Unbalace
- Misalignement
- Eccentricity
- Bent Shaft
- Mechanical Looseness
- Bearing Faults

- Commutation

In what follows, a brief description for each of these sources is given.

2.2.6.1 Unbalance

Unbalance in rotating machinery is very important for high speed rotating machinery where reliability is a significant consideration. Unbalance is the most common source of vibration in the rotating components of machines, for example in turbo-machinery, electric motors, drive shafts, grinding wheels and cranckshafts [26]. Mass unbalance occurs when the geometric center and the mass center of a rotor do not coincide. Unbalance is a so-called 1X fault (Figure 2.26), that is, it occurs at the frequency of rotor speed, and is sometimes difficult to distinguish from misalignment, bent rotor or cracked shaft, and further investigation of what may cause the defect is often necessary.

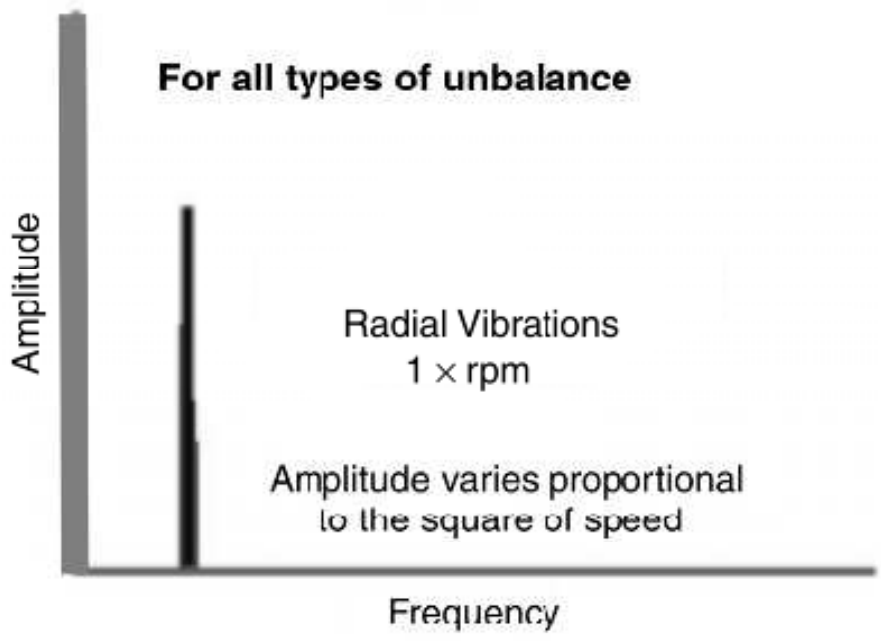

Figure 2. 26 : Typical unbalance frequency spectrum [26].

Unlike normal conditions when motions are sinusoidal, nonlinear behaviour of bearing or pedestal in the presence of excessive mass unbalance can cause truncated motions that introduce higher-order vibrations (e.g., 2X, 3X). Due to the design of the machine, the radial vibrations are usually larger than those in the axial direction. Unbalance vibration is mainly radial. For overhung rotors axial components may also be significant, but the axial component of vibration is usually small.

Generally, unbalance is clasified as:

- Static Unbalance
- Moment Unbalance
- Dynamic Unbalance

Static unbalance is defined as an eccentricity of the centre of gravity, caused by a point mass (Figure 2.27), at a certain radius from the centre of rotation of the object. Static unbalance can be corrected in one plane without running the rotor.

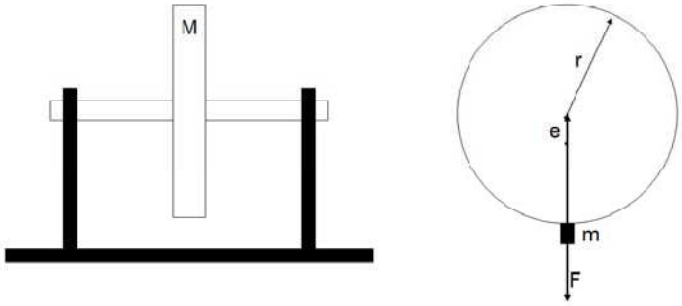

Figure 2. 27 : A static unbalance system [27].

In the case of a cylinder, as shown in Figure 2.38, it is possible to have two equal masses symmetrically placed about the center of gravity, but positioned at 180° from each other. The rotor is in static balance, i.e. there is no eccentricity of the center of gravity. However, when the rotor turns, the two masses will cause a shift in the inertia axis, so that it is no longer aligned with the rotation axis. This causes strong vibrations of the rotor. The unbalance can only be corrected by taking vibration measurements while the rotor is turning, and then making corrections in two planes [28].

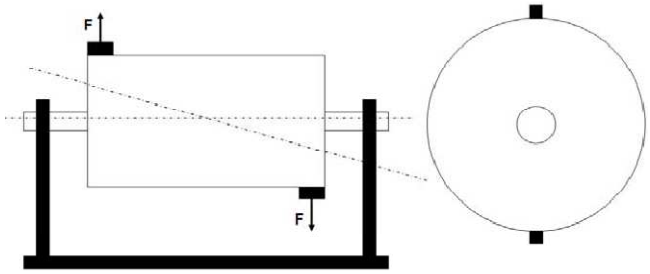

Figure 2. 28 : A moment unbalanced system [27].

In practice, generally unbalanced forces are created on the rotors due to the combinations of static and moment unbalance and this is called dynamic unbalance as depicted in Figure 2.29 Here, it is noticed that inertial axis of the rotor is changing

in every instant of rotation. To correct dynamic unbalance it is necessary to make the vibration measurements while the rotor is turning and to correct the unbalance in two planes.

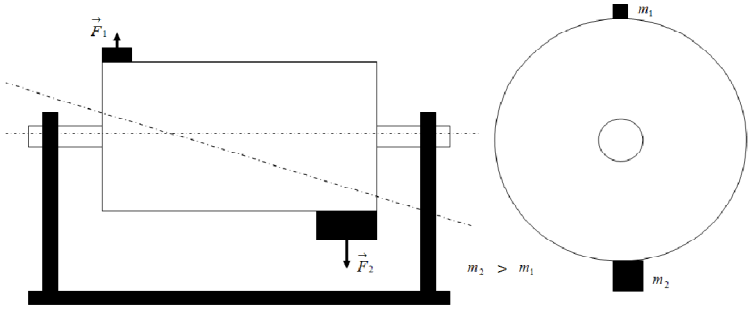

Figure 2. 29 : A dynamic unbalanced system [27].

2.2.6.2 Misalignment

Misalignment is defined as offset of radial or angular positioning tolerance of the centerlines of two shafts at the power transmission. The offset errors generate relative motion in the form of sliding and/or bending between the coupled components.

There are basically two types of misalignment [26]:

1. *Angular misalignment:* centerline of the two shafts meets at angle with each other.
2. *Parallel misalignment:* the shaft centerline of the two machine is parallel to each other and have an offset.

Depending on type of misalignment, the vibration frequencies may be predominantly 1X for angular misalignment normally causes 1X vibrations, whereas parallel misalignment causes vibrations predominaltly 2X.

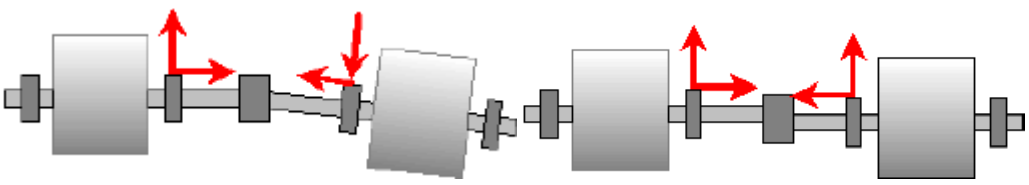

Figure 2. 30 : a) Angular misalignment, b) parallel misalignment of a system.

A misaligned rotor tend to wear in. That is after a while the bearing will get deformed after the misalignment. In the spectrum this is seen as the 2nd order component will decrease and the third order will increase as wear develops.

2.2.6.3 Eccentricity

The shaft centerline is not coincident with the rotational axis or centerline when the eccentricity condition occurs. A radial unbalance like response at 1x RPM of the eccentric rotor is produced by the eccentricity. About the false shaft centerline position, the rotating body will wobble. Since this will produce a very directional response, it will be easily distinguished with phase analysis. The reasons of eccentricity in motors are various (Figure 2.31) For example inaccurate bearing set-up, a worn bearing, bent of the rotor shaft are the frequently encountered reasons. Motors are under an excessive stress, both kinds of eccentricities can bring about worn bearing.

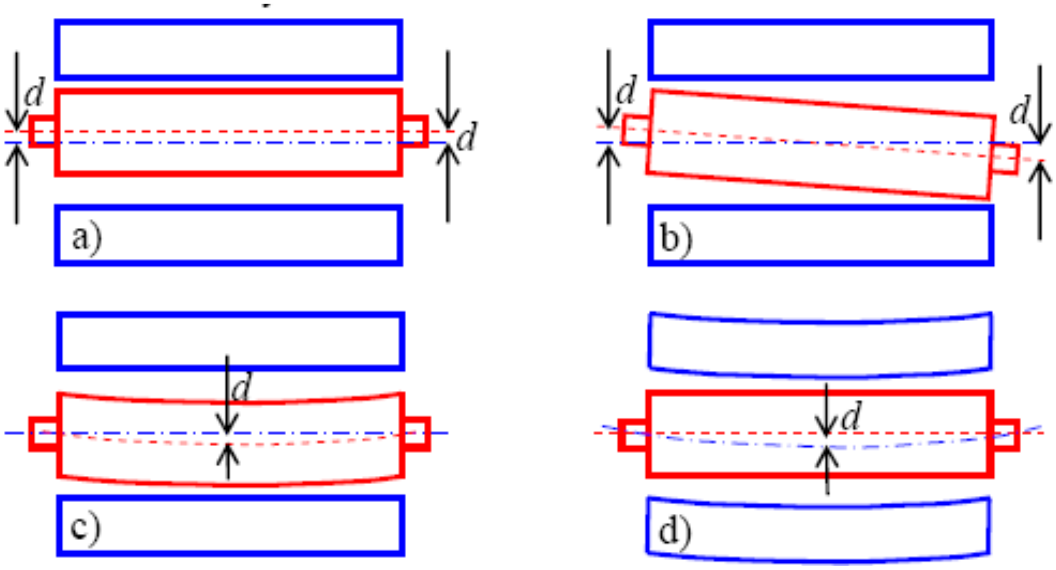

Figure 2. 31 : Eccentricity mechanism: a), b) bearing mounting defects; c), d) rotor deflection or rotor and stator lamination packing defects.

Eccentricity of a rotating mechanical component results in vibration at operating speed even though the unit is in balance. Mass unbalance must be eliminated as a cause or the eccentricity must be physically measured to diagnose the problem correctly.

2.2.6.4 Bent shaft

A bent shaft to many extents may look like a misalignment in the spectrum. A phase measurement for axial vibration across the shaft will distinguish between misalignment and bent shaft, as the bent shaft will produce a 180° phase shift**.**

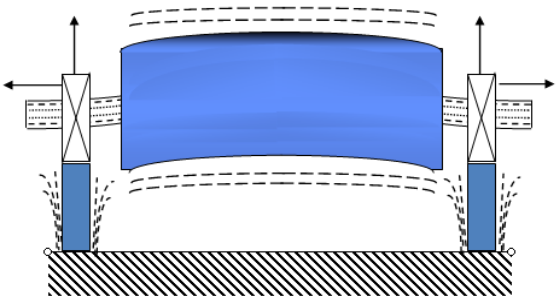

Figure 2. 32 : A bent shaft give rise to both axial and radial vibrations [29].

Rotor bow appears to be a static imbalance (Figure 2.32) since the phase at both ends of the rotor is essentially the same. Installing balance weights at the rotor end planes, however, does not solve the imbalance that results from the rotor bow. This is because an internal bending moment is created between the center of the rotor (where the bow is greatest) and the end planes.

The FFT will normally have 1X and 2X components. If the:

- Amplitude of 1X rpm is dominant then the bend is near the shaft center (Figure 2.33).
- Amplitude of 2X rpm is dominant then the bend is near the shaft end.

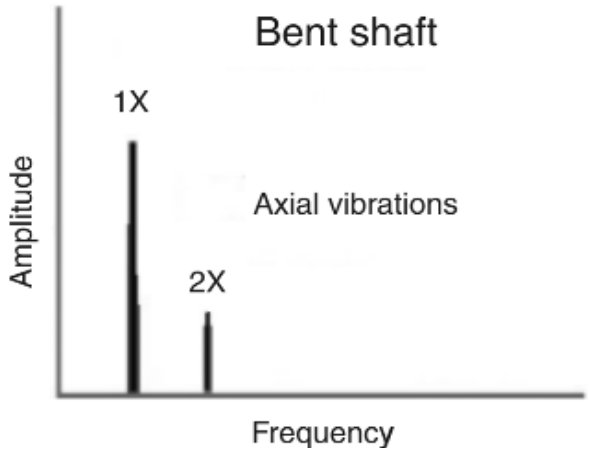

Figure 2. 33 : An FFT of a benr shaft with bend near the shaft center [26].

2.2.6.5 Mechanical looseness

Any rotating machine, mechanical looseness can occur at three locations [26]:

- Internal assembly looseness
- Looseness between machine to base plate
- Structure looseness

Mechanical looseness produce a strongly distorted signal. The inter harmonics (½, 1/3 etc.) are attributable to the fact that the loose part bounces and thus does get excited every 2nd or 3rd revolution of the shaft (Figure 2.34).

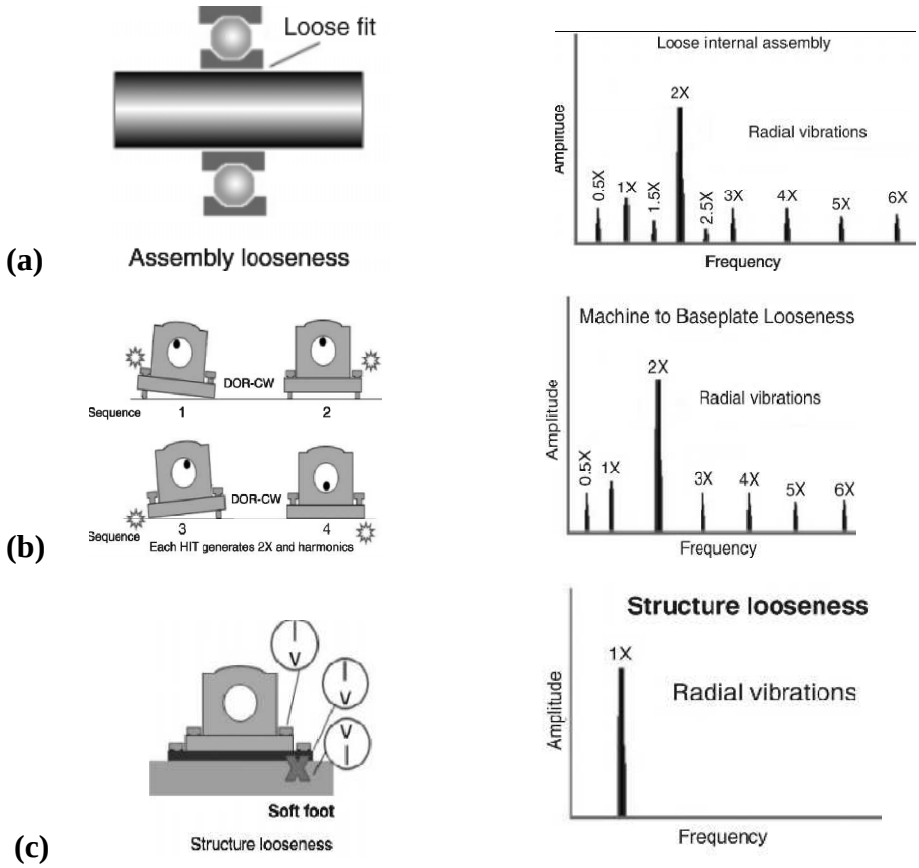

Figure 2. 34 : a) Assembly looseness and its FFT spectrum, b) baseplate looseness and its FFT spectrum, c) structure looseness and its FFT spectrum [26].

Looseness has many harmonics of 1X RPM frequency (the 2X RPM or 3X RPM frequencies may even be higher than the 1X RPM). Pure looseness has mostly odd-order frequencies (3X RPM, 5X RPM, and so on).

2.2.6.6 Ball bearing faults

There are four parts in ball bearings; cage, balls, inner and outer rings. These parts can be damaged due to over load, corrosion, improper lubrication and installation. Over load or weak lubrication causes friction. As a result of friction, temperature increases, so that oil lost its properties. Also, water and acid is dangerous for oil. Another point for damage, current flows on bearings, because of voltage difference between stator and rotor. Oil behaves as a dielectric material in condenser. These

faults produce small particles in bearing.These type of defects are repeated at frequencies which can be calculated using well known formulas. It is general experience that these frequencies show up in a FFT spectrum at a very late stage of bearing wear. With envelope analysis the bearing frequencies are seen at a very early stage of fault development. The envelope analysis can be used for accurately predicting the breakdown of a bearing. It should be noted that the balls will slip few percents in the bearings especially when lightly loaded.

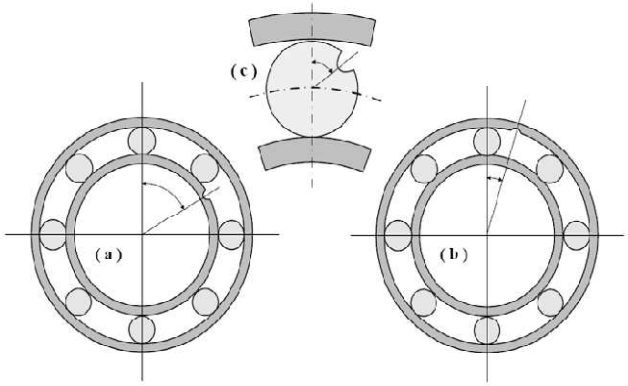

Figure 2. 35 : Different positions of localized defects affecting a ball baring. a) defect on inner race, b) defect on outer race, c) defect on ball [30].

When a rolling element passes over a bearing defect in the races, balls or cages pulse-like forces are generated that result in one or a combination of bearing frequencies (Figure 2.35).Rolling element bearings generate frequencies unique to their geometry and operating speed. Four basic frequencies can be generated by a defective bearing.

These frequencies are given as:

Ball pass frequency of the outer race (BPFO);

$$\text{BPFI} = \frac{N_b}{2}\left(1 + \frac{B_d}{P_d}\cos\theta\right)\text{xRPM} \qquad \textbf{(2.6)}$$

Ball pass frequency of the inner race (BPFI);

$$\text{BPFO} = \frac{N_b}{2}\left(1 - \frac{B_d}{P_d}\cos\theta\right)\text{xRPM} \qquad \textbf{(2.7)}$$

Ball spin frequency (BSF);

$$\text{BSF} = \frac{P_d}{2B_d}\left(1 - \left(\frac{B_d}{P_d}\cos\theta\right)^2\right)\text{xRPM} \qquad \textbf{(2.8)}$$

Fundamental train frequency (FTF);

$$FTF = \frac{1}{2}(1 - \frac{B_d}{P_d}\cos\theta)xRPM \quad \textbf{(2.9)}$$

$\boldsymbol{N_b}$: number of balls or rollers

$\boldsymbol{B_b}$: ball-roller diameter

$\boldsymbol{P_d}$: bearing pitch diameter

$\boldsymbol{\theta}$: Contact angle in degrees

The four bearing frequencies can be modulated by the speed of the rotating unit in Hz to cause sideband frequencies. In some cases the fundamental train or ball spin frequencies may modulate natural frequencies or ball pass frequencies.

2.2.6.7 Commutation

Commutation in DC motors is a source of vibration due to the mechanical contact between the brushes and the commutator segments. Since no commutator is perfectly smooth, the brushes bounce up and down as the motor spins. The bouncing of the brushes creates a vibration frequency at the number of the commutator segments times the rotational speed of the rotor, RPM. This frequency, or its harmonics, can excite other components within the system to resonance. The presence of brush vibration indicates that the brushes are still in good condition, and that the spring is still exerting tension against the commutator. When the bouncing vibration disappears, the brush is no longer being pushed against the commutator. Consequently, an air gap exists permanently between the brush and the commutator, causing excessive sparking.

2.2.7 Electromagnetic sources of vibration and noise

In this part of the thesis, electromagnetic sources of vibration/noise which are commonly seen both in practice and literature are summarised. The noise and vibration in electric motors are mostly generated by the electromagnetic sources, which can subsequently be amplified by the dynamic characteristics of the motor structure. Electromagnetic vibration and noise are associated with parasitic effects due to higher space and time harmonics, eccentricity, phase unbalance, slot openings/combinations, magnetic saturation, slip, ac rectification and magnetostrictive expansion of the core laminations. While analyzing motor vibration/noise problems, it is important to know whether the problem is mechanical

or electrical. However, there is not always clear-cut separation between the two. For example a cracked rotor bar may cause spot heating in the rotor, resulting in a thermal bow. The rotor bow will appear as rotor imbalance (mechanical), when in fact the basic problem is the rotor bar (electrical). It may be possible to detect the presence of electrical problems by acquiring data during a shutdown. The power should be cut near full load, if possible, and acquiring data during the coastdown. So, some vibration/noise related effects are disappeared in the data which is taken during the coastdown.

2.2.7.1 Slip-related vibration

The difference in frequency between the running speed of an induction motor and the synchronous magnetic frequency of the stator is known as the slip frequency, and can be expressed as:

$$S_l = (2\frac{F_l}{P}) - F_r \qquad \textbf{(2.10)}$$

where

$\boldsymbol{Sl}$ = Slip frequency in Hz

$\boldsymbol{Fl}$ = Line frequency in Hz

$\boldsymbol{P}$ = Number of poles in the motor

$\boldsymbol{Fr}$ = Rotational frequency in Hz (RPM/60)

To understand this, consider a 2-pole motor with a rotor speed of 3,420 RPM. The magnetic field in this motor's stator rotates at 3,600 RPM. The slip frequency for this motor is equal to 180 RPM. If stator magnetic field is assumed that it has zero speed, therefore rotational speed of rotor magnetic field is -180 RPM with respect to the stator's. So the direction of motion of rotor magnetic field is negative while the other one is seems to stop .

The rotor in a 2-pole motor lines up with a stator pole twice during each slip cycle during the rotor magnetic field rotation, then, vibration will occur at twice the slip frequency.

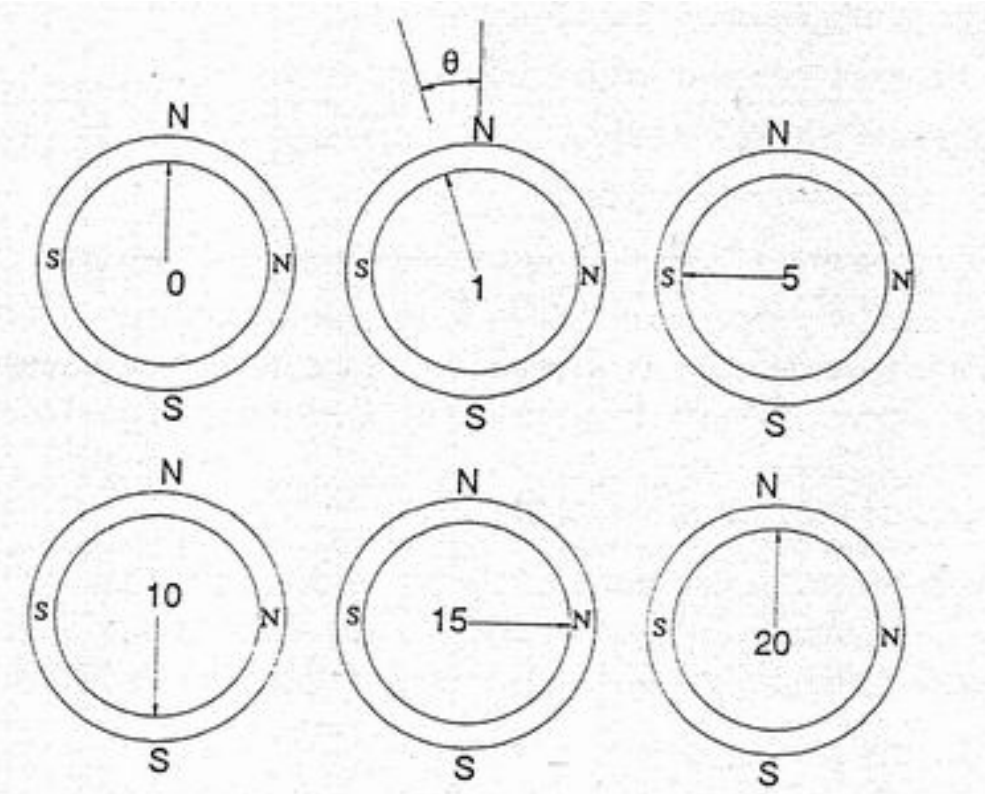

Figure 2. 36 : One slip cycle.

The previous paragraph can be rephrased to include motors with more than 2 poles: A rotor bar will line up with a magnetic pole in the stator at a frequency equal to the number of pole times the slip frequency. Therefore the maximum current flows in the rotor bar and the rotor is subject to the maximum torque at this frequency. Since the torque reaches a maximum at this frequency the rotor will speed up and slow down at a rate equal to the number of pole times the slip frequency. That is, the rotor frequency will be modulated at a rate equal to the number of pole times the slip frequency.

2.2.7.2 Rotor bar passing frequency vibration

High frequency load-related magnetic vibration at or near rotor slot passing frequency is generated in the stator when current is induced into the rotor bars under load. The magnitude of this vibration varies with load, increasing as load increases [30]. The electrical current in the bars creates a magnetic field around the bars that applies an attracting force to the stator teeth. These radial and tangential forces which are applied to the stator teeth, as seen in Figure 2.37, create vibration of the stator core and teeth.

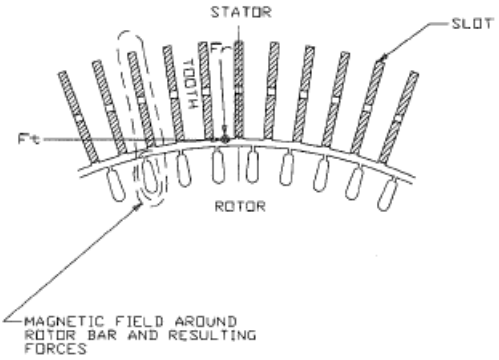

Figure 2. 37 : Radial and tangential forces which are applied to the stator teeth [12].

Figure 2. 38 : Magnetic field around a rotor bar and resulting force on stator teeth.

The rotor slot and side band frequencies are in the frequency range normally related to noise rather than vibration performance. In fact, these force components are the principal sources of high frequency noise in electrical machines. When a two or four pole motor has an even number of rotor slots, the large local forces between the stator and rotor teeth cancel each other on the opposite sides of the rotor, and the total force is zero. If the number of slots is an odd number, a net force may occur. Figure 2.39 shows the trace of the force vector generated in the four pole motor by a rotor with 33 slots [31]. In literature the forces caused by unsuitable number of rotor slots studied by Arkkio [31].

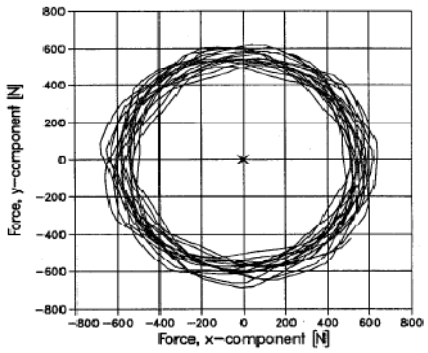

Figure 2. 39 : The trace of the magnetic pull vector when the four-pole is equipped with a rotor having 33 slots [31].

2.2.7.3 Broken rotor bar vibration

If a broken rotor bar exists, no current will flow in the rotor bar as shown in Figure 2.40 (a). As a result the field in the rotor around that particular bar will not exist. Therefore the force applied to that side of the rotor would be different from that on the other side of the rotor again creating an unbalanced magnetic force that rotates at one times rotational speed and modulates at a frequency equal to slip frequency times the number of pole (Figure 2.40 (b)). In addition, broken rotor bars or a variation in bar resistivity will cause a variation in heating around the rotor. This in turn can bow the rotor, creating an eccentric rotor, causing basic rotor unbalance and a greater unbalanced magnetic pull, thereby creating a high one times and some minimal twice line frequency vibration.

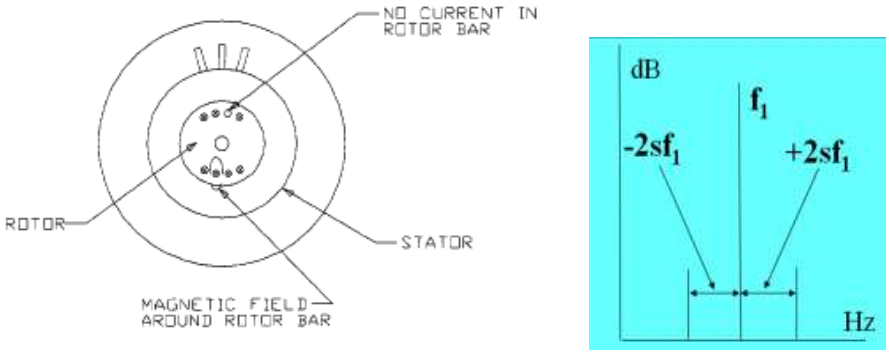

Figure 2. 40 : a) Rotor with broken bar [30] and b) signature pattern due to broken rotor bars.

2.2.7.4 Twice-line frequency vibration

A power supply produces an electromagnetic attracting force between the stator and rotor which is at a maximum when the magnetizing current flowing in the stator is at a maximum, either positive or negative at that instant in time. As a result, there will be 2 peaks of force during each cycle of the voltage or current wave reducing to zero at the point in time when the current and fundamental flux wave pass through zero as demonstrated in Figure 2.41. This will result in a frequency of vibration equal to 2 times the frequency of the power source (twice line frequency vibration). This particular vibration is extremely sensitive to the motor's foot flatness, frame and base stiffness and how consistent the air gap is between the stator and rotor, around the stator bore. It is also influenced by the eccentricity of the rotor.

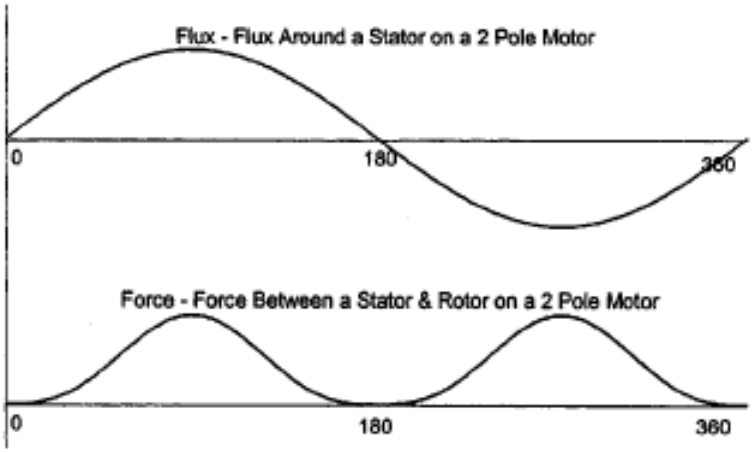

Figure 2. 41 : One period flux wave and magnetic force wave [30].

Electromagnetic forces with the frequency of twice the power supply frequency are produced on stator cores. In designing rotating electric machines, it is essential to avoid resonance of the structures caused by the 2f electromagnetic forces [32]. Twice-line frequency vibration does not vary with load. Because twice line frequency vibration excitation is not due to a magnetic field generated by the current in the stator coil which varies with load and creates a magnetic force which varies with the load current squared.

2.2.7.5 Eccentricity

For an induction machine with a uniform air gap, it is well known that the sum of the radial electromagnetic forces acting on the overall rotor periphery should be zero. However, when the axis of rotation is not concentric with the center line of the stator, the rotor is said to be eccentric. A corresponding non-uniform air gap flux density occurs due to the eccentric rotor which causes a radial force in the direction of greatest flux density (smallest air gap). This radial force has been referred to in the literature as unbalanced magnetic pull (UMP). Eccentricity of either the rotor or stator airgap surface from the centre of rotation can cause important components of the force. The larger the length of the eccentricity is, the stronger the force imbalance caused by this unbalanced magnet pull is. For this reason, the force imbalance caused by the unbalance magnetic pull can cause self-excited radial rotor vibrations. Or the unbalanced magnetic pull acts as a ‘negative’ spring and thus reduces the critical speed. An uneven air gap causes unbalanced magnetic pull, which may cause higher magnetic forces in the direction of minimum air gap, as shown in Figure 2.42. This

leads to higher structural deformation and noise. An uneven air gap not only creates higher magnetic forces but also creates additional harmonics known as eccentricity fields, hence manufacturing variation can not only create different amplitudes of magnetic forces but also different harmonics combinations. Rotor eccentricity due to the rotor unbalance, the biggest cause of vibrations in an induction motor, can be divided into two classes- static and dynamic eccentricity. As shown in Figure 2.42(a) static eccentricity occurs when the rotor rotates around the axis of rotation, but the axis of rotation is separated from the axis of the stator. On the other hand, dynamic eccentricity occurs when the rotor rotates around the axis of stator, but rotation is around the offset rotor axis [33].

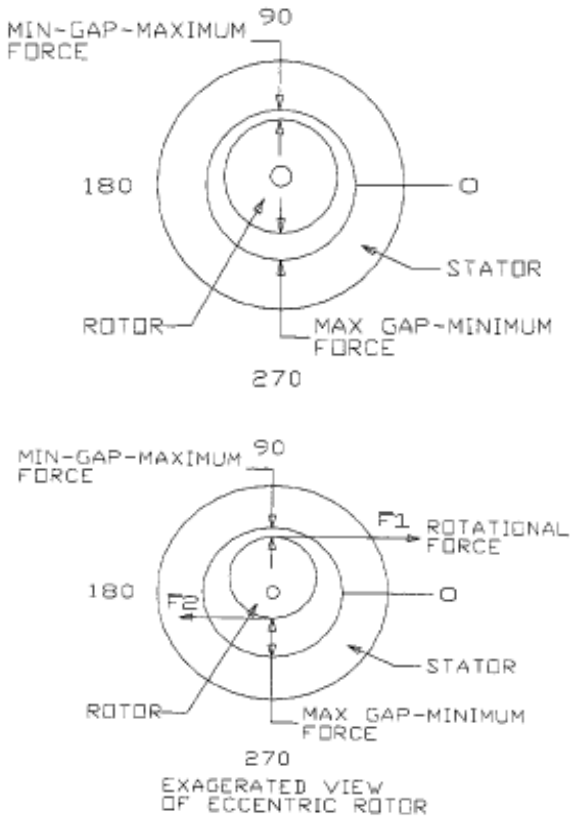

Figure 2. 42 : a) Static eccentricity, b) dynamic eccentricity [33].

If the stator has static eccentricity as in the case of Figure 2.43 (b) then it will be permanently displaced to the right. If the rotor has dynamic eccentricity then the net unbalance force will rotate at rotational frequency, with the minimum air gap, causing vibration at one time rotational frequency [34].

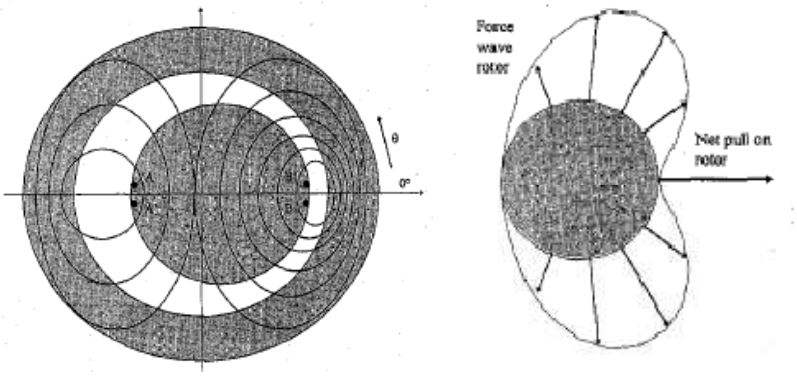

Figure 2. 43 : a) 2-Pole machine flux ditribution representation, b) force wave on rotor creating UMP [34].

Not only is the stator pulled in one direction, but also the rotor is pulled in the opposite direction to the side that has the minimum air gap (Figure 2.43). This causes higher shaft vibration, which is more damaging for bearings.

The flux causing the magnetic force is the fundamental flux wave, which rotates around the stator at the synchronous speed of the motor. The rotor attempts to keep up with the rotating flux wave of the stator, but the rotor slips behind the stator field as needed to create the necessary torque for the load. When the high point of the rotor (point of minimum air gap) aligns with the high point (maximum) of the stator flux, the force will be a maximum, and then it will decrease, becoming small under a point of minimum flux. Thus, an unbalance force is created which rotates at rotational speed and changes in magnitude with slip. The end result is a 1X RPM vibration, which modulates in amplitude with slip. The frequency of modulation in RPM will equal the slip in rpm times the number of poles.

2.2.7.6 Magnetostriction

Stator deformations are caused not only by reluctance forces, but also by magnetostriction effect of the stator iron. Magnetostriction is one of the main causes of noise in electromagnetic systems particularly when the flux density is above 1.5 T(Tesla). Magnetostriction is a property of ferrous alloys in which the material will exhibit strain in the presence of magnetic field. This strain is in addition to any other strains that might exist as a result of electrical and/or mechanical forces in devices. At low frequencies, magnetostrictive forces are undesirable. They can be large and generate acoustic noise in electromagnetic systems. Magnetostriction in magnetic materials, such as electrical silicon steel sheets, is one of the main causes of noise

and vibration in electric machinery and equipment for which there is no proven remedy. It is an important factor in governing the magnetic properties of magnetic materials. In order to achieve lower losses and noise levels in electrical machines, it is necessary to know the magnetostrictive effects in the design stage. Furthermore, it is possible that the magnetostriction or the material property changes, may be small in one direction, they can significantly vary when the domain structure changes in the magnetic flux direction.

2.2.7.7 Magnetic noise

The noise of magnetic origin in electric machines is generated by the interaction of the induction waves (fundamental and harmonics) present in the air gap. These waves are variable in space and time and exist because of the winding distribution and variation of the air gap permeance[4] due to the stator and rotor slots, saturation and eccentricity. These induction harmonics, combined themselves, genetare periodic force waves in the airgap deforming the stator core and exciting the surrounding air. This way, the acoustic noise is generated [35](Figure 2.44).

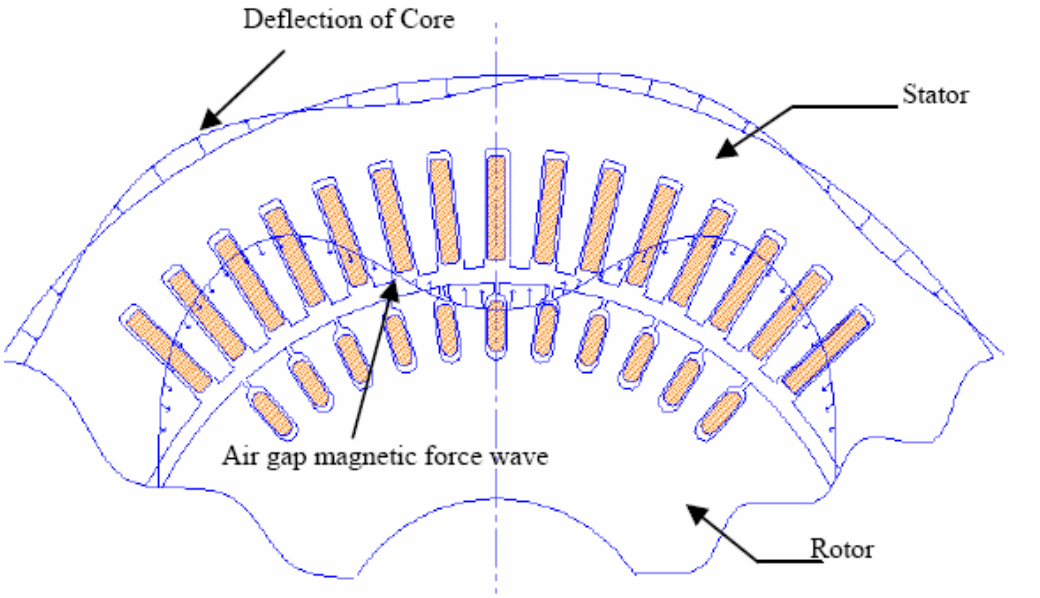

Figure 2. 44 : Deflection of stator core and teeth with magnetic forces [36].

The magnetic force acting on the stator teeth has both a tangential and a radial component. The tangential component is the reaction to the motor torque, and while it causes the tooth to bend about its base and produces localized distortions of the stator core it is only a minor sources of motor noise. The radial component produces

[4] Permeance is a measure of the ability of a magnetic circuit to conduct magnetic flux; the reciprocal of reluctance.

larger deformations of the stator core and is the principal sources of magnetic noise. Stator–rotor mechanical design, along with careful electrical coil design, can significantly cut down magnetic noise in an induction motor. It is important to know the frequencies at which radial and tangential forces are produced. If any of these forcing frequencies approaches to the natural frequencies of the stator core or stator tooth, resonance will occur and magnetic noise will be amplified. Another way is to vary the number of rotor slots, which will change the forcing frequencies and the vibration modes of the stator core. The force acting on the stator tooth is proportional to the square of the magnetic flux density in the air gap; therefore, by increasing the active magnetic core length or motor size, one can reduce the magnitude of the flux density and consequently the magnetic forces. However, when the designers make changes in regard to the slot combination, they should take into account not only the noise level, but other negative effects that these changes could impact, such as rotor standstill / crawling during motor start up.

2.2.7.8 AC rectification

In many cases, the direct current needed to drive a DC motor is not supplied from a DC generator. Since alternating current is usually available, a process called rectification is used to convert the AC to DC. When AC is rectified, the negative ‘humps’ are removed, leaving only positive current as shown in Figure 2.45. This is called half-wave rectification, since only half of the wave remains.Half-wave rectification leaves gaps in the current. Devices called full-wave rectifiers convert the negative current to positive, so that the average current flow is roughly 2/3 of the maximum current. This is shown in Figure 2.45. Rectifying three-phase AC, where each phase is offset by 90 degrees, smooths out the ripples and leaves roughly constant current (DC).

Full-wave rectification on single-phase AC, as shown in Figure 2.46, leaves 2 peaks per cycle (one for each time the SCR fires). If three-phase current is rectified, 6 peaks per cycle are now present. Since 60 Hz is normal AC line frequency in the US, 360 peaks per cycle are present in the rectified DC output of an SCR.

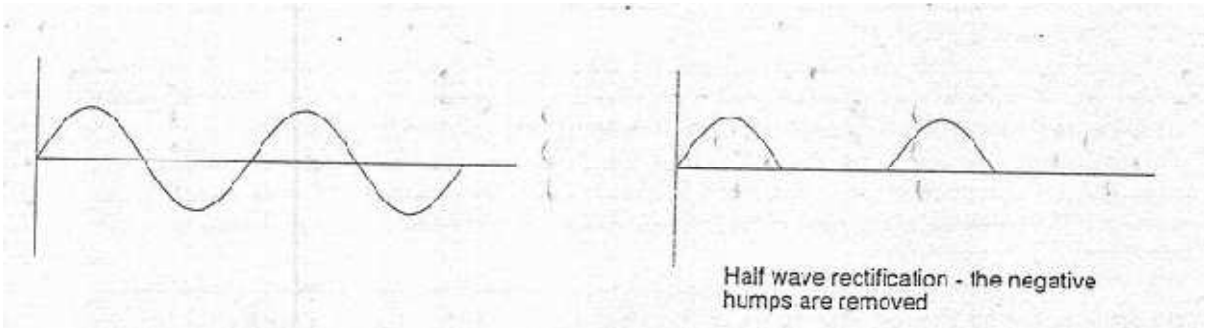

a)

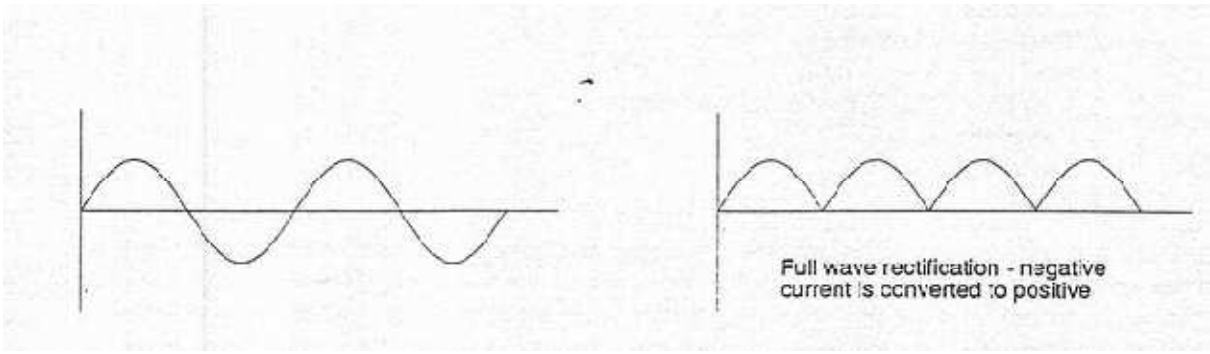

b)

Figure 2. 45 : a) Half wave and b) full wave rectification.

In countries with 50 Hz line frequency, the rectified DC output has 300 peaks per cycle.These peaks cause a pulsation in the DC that supplies the motor's main field. Consequently, the motor's speed varies by the same pulsation frequency. This SCR firing frequency is a sources of vibration, both from exciting components to resonance and from the speed variations (torsional vibration) that it introduces into the driven process.

2.2.7.9 Commutation

A direct motor utilizes a mechanical commutator to switch the supply current into its armature windings. This process involves the sliding contacts between graphite composite brushes and the commutator made up of a ring of copper segments called 'bars' connected to the armature winding. Current flow to any coil is interrupted and reversed periodically as the armature rotates and presents different bars to each brush. The natural consequences of these interruptions and reversals are voltages, current and torque disturbances. The discontinuous nature of the commutation proceduces high frequency electromagnetic disturbances [37]. To study the electromagnetic and electromechanical disturbances, a dynamic network model has

been devised to represent the changing circuit configuration due to the commutation. With this technique they could compute the instantaneous current and voltage of each of the armature coils of the motor and the instantaneous electromagnetic torque developed by the motor.The network modeling of a DC motor starts with an electrical schematic of the machine as shown in Figure 2.47. This includes the armature coils, commutator bars connecting the coils, brushes sliding on the commutator bars, and external components connecting the motor terminals to the power source.

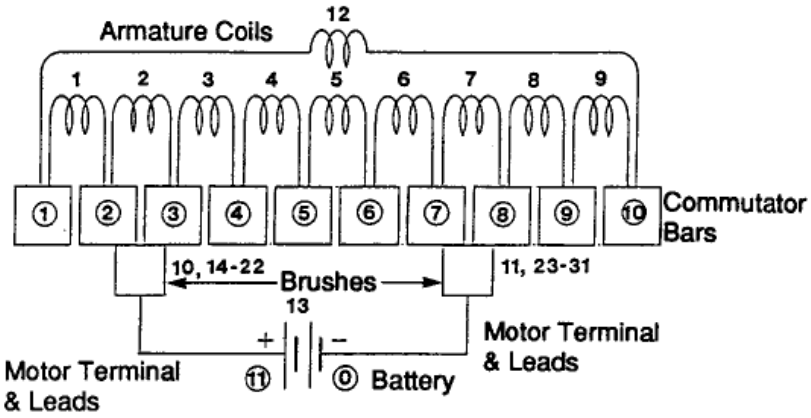

Figure 2. 46 : Electrical schematic of a DC motor [37].

The voltage between adjacent commutator bars responsible for arcing and reduction of brush life is shown Figure 2.48 (a).

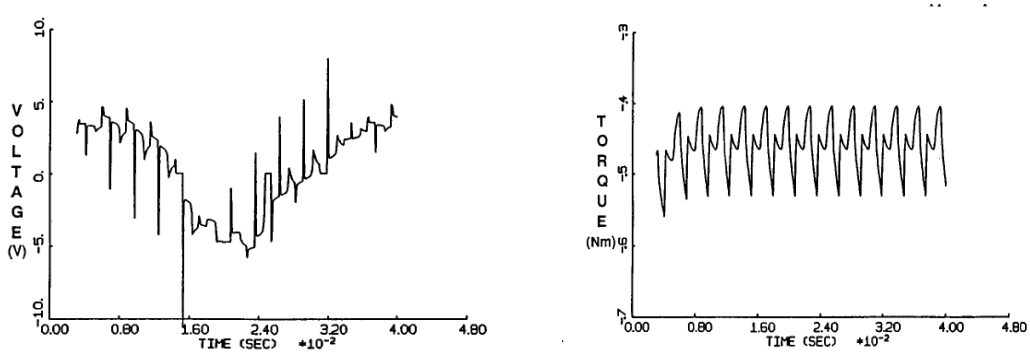

a) b)

Figure 2. 47 : a) Calculated coil voltage and b) electromagnetic torque [37].

The instantaneous electromagnetic torque in Figure 2.48 (b) can be used to identify sources of vibration and mechanical noise.

2.2.7.10 Slot combination

Electromagnetic noise is usually generated by the interaction of electromagnetic flux waves with the resonant frequencies of the stator core or teeth, and manifests itself as structure-borne noise. Magnetic field is not uniform in the air gap. The fundamental field is superimposed by various harmonics which may arise due to several reasons. Of the various causes which induce harmonics in the air gap, the field effects of stator-rotor slot combinations are the most common causes for high magnetic noise in induction motors. The electromagnetic force due to slot combination has a strong influence on acoustic noise from induction motors. When both the vibration mode and natural frequency of the stator correspond to those of the electromagnetic force, the stator causes a resonance which results in a loud noise. Therefore, it is necessary to estimate accurately the electromagnetic force before acoustic noise can be reduced. The vibration depends strongly on the slot combination which is the combination between the number of the stator slots and that of rotor slots. The slot combination is one of the most important design points for induction motors, because it determines the magnetic flux density which is the product of the magnetomotive force multiplied by the magnetic permeance. An unsuitable slot combination causes a large vibration and acoustic noise.

2.3 Order Analysis

Analysis of vibration or acoustic signals from rotating machines is often preferred in terms of order spectra rather than frequency spectra (Figure 2.49). An order spectrum gives the amplitude and/or the phase of the signal as a function of harmonic order of the rotation frequency. This means that a harmonic or sub-harmonic order component remains in the same analysis line independent of the speed of the machine. The technique is called tracking, as the rotation frequency is being tracked and used for analysis. Most of the dynamic forces exciting a machine are related to the rotation frequency so the interpretation and the diagnosis can thus be greatly simplified by the use of order analysis. The classical problem of smearing of the frequency components caused by speed variations of the machine is solved by using order analysis. In situations where the frequency components from a normal frequency analysis are smeared together, proper diagnosis will only be facilitated via order analysis. Of particular interest is the analysis of the vibrations during a run-up

or a coast-down of a machine in which case the structural resonances are excited by the fundamental or the harmonics of the rotational frequencies in the mechanical system.

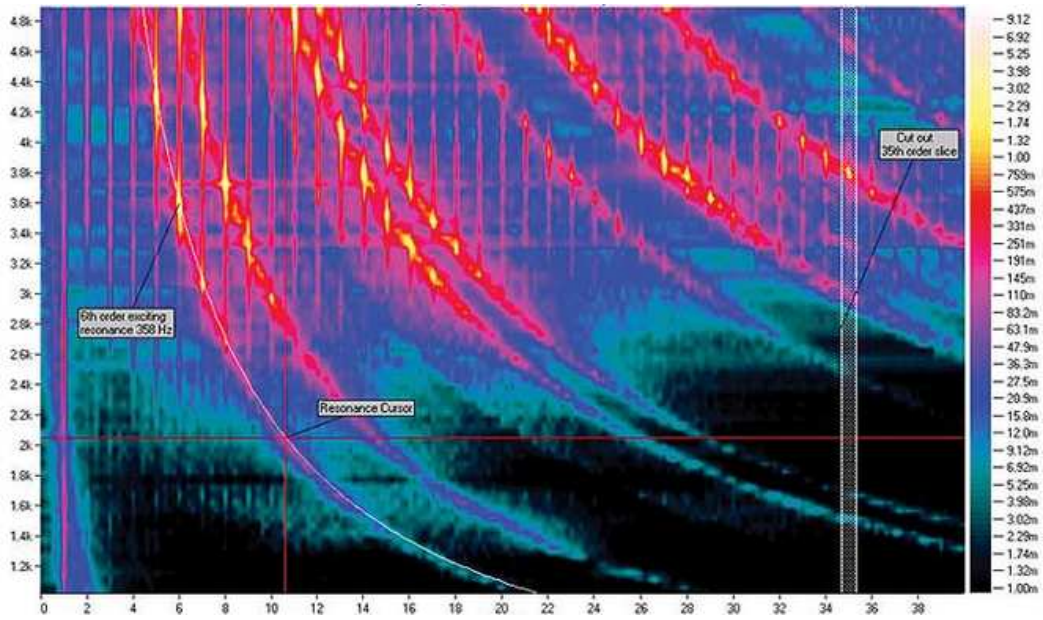

Figure 2. 48 : An order diagram

Determination of the critical speeds, where the normal modes of the rotating shaft are excited, is very important for rotating machines such as motors, turbines and generators [38]. If vibration is taken on a speed-varying machine (e.g., an electric motor), all of the forcing frequencies of the machine will vary with the shaft speed. This implies that, as a sum average is taken, each peak will 'smear' (Figure 2.50 (b)). The peaks will go into different frequency bins, with the result that the actual frequency will be indeterminate and the amplitude and motor pole frequency shifts during 8 averages taken while the speed of the machine varies.(Figure 2.50 (a)) [39]

Average No.	Pole	Shaft Speed, Hz	Mesh Freq. (100 Teeth)
1	120	30	3,000
2	120	29.5	2,950
3	120	29	2,900
4	120	28.5	2,850
5	120	28	2,800
6	120	27.5	2,750
7	120	27	2,700
8	120	26.5	2,650

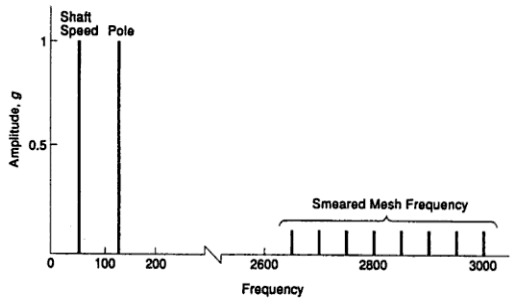

Figure 2. 49 : a) Mesh frequency and motor pole shifts during 8 averages, b)smearing due to speed variation [45].

Synchronizing the dynamic signal analyzer's data collection with the machine's rotational speed is therefore a key step in order analysis. Synchronization usually starts with a tachometer, which provides a pulse or an integral number of pulses for each revolution (Figure 2.51). Angular position, rotating speed and acceleration of rotating machine are indicated by tach pulses generated from tachometer. Using the tach pulse to trigger the dynamic signal analyzer synchronizes the machine and the measurement [40].

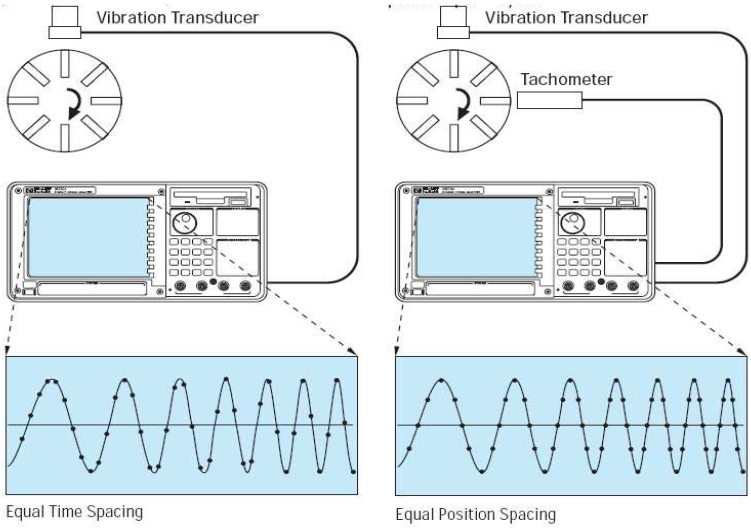

Figure 2. 50 : a) Time domain samples: If samples are gathered at equal tiem intervals, the number of samples per cycle will vary. b) Position samples [46].

Synchronizing samples to shaft position gives a constant number of points per cycle. We could then force the speed of the sampling frequency to rotate proportionally with the machine's shaft speed. As the shaft speed increased or decreased, so would sampling frequency. A peak at 1xrpm is called the first order and a peak at 100 x rpm is called the 100th order as in the Figure 2.52 [39].

Table 2.2. Mesh Speed and Motor Pole Frequency Shifts with 256 Pulses/Shaft or Revolution.

Average No.	Pole	Shaft Speed (order)	Mesh Order (100 Teeth)
1	4.00	1	100
2	4.07	1	100
3	4.14	1	100
4	4.21	1	100
5	4.29	1	100
6	4.36	1	100
7	4.44	1	100
8	4.53	1	100

a)

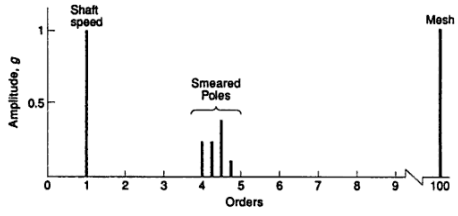

Figure 2.10. An order plot of smearing due to speed variation.

b)

Figure 2. 51 : a) Mesh speed and motor pole frequency shifts, b) order plot [45].

2.4 Modal Analysis

The objective of modal analysis is to determine the natural frequencies, damping factors and vibration mode shapes of a structure. The results from this analysis characterize the basic dynamic behavior and are an indication of how the structure will respond to dynamic loading.

2.4.1 Theoretical and experimental modal analysis

Two approaches are available to perform the Structural Dynamic Analysis (Figure 2.53). One of them is the so-called Theoretical Route and the other is the Experimental Route. Various models that are used in this processes are shown below:

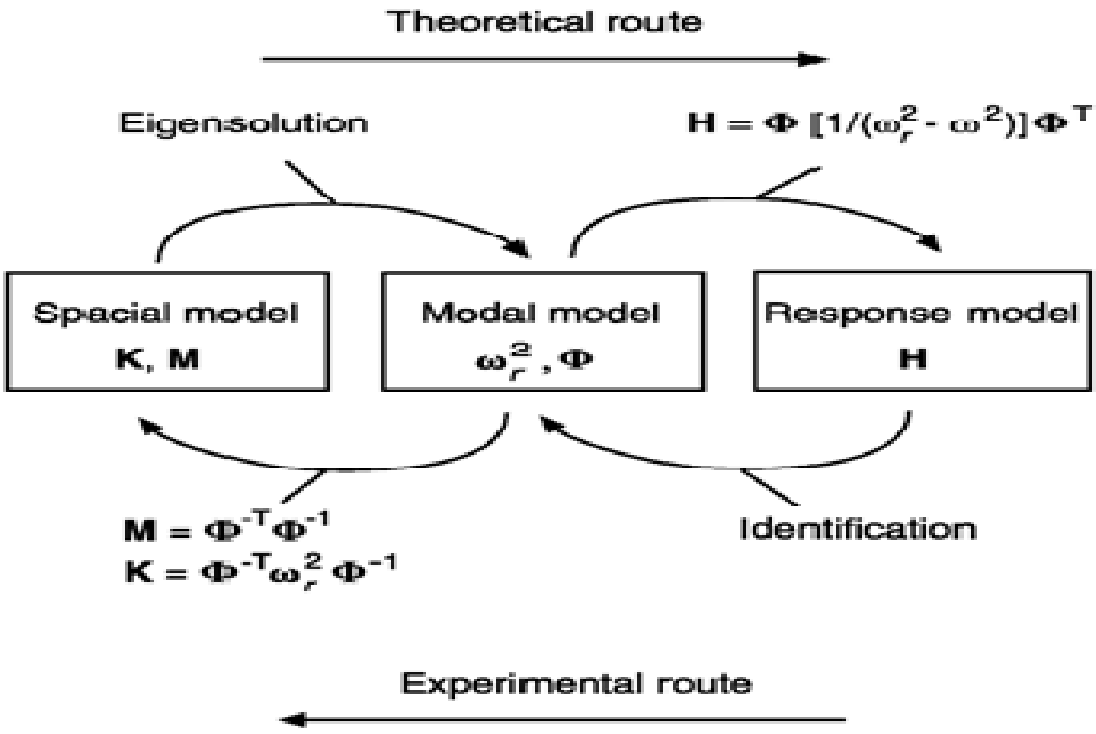

Figure 2. 52 : Interrelation among dynamic models.

2.4.1.1 Theoretical route to structural dynamic analysis

The first type of model is the spatial model which describes the distribution in space of the essential physical features of the structure - mass or inertia, stiffness and damping properties. In simple terms, the spatial model is the set of mass, stiffness and damping elements which are used in describing the equations of motions for the system.

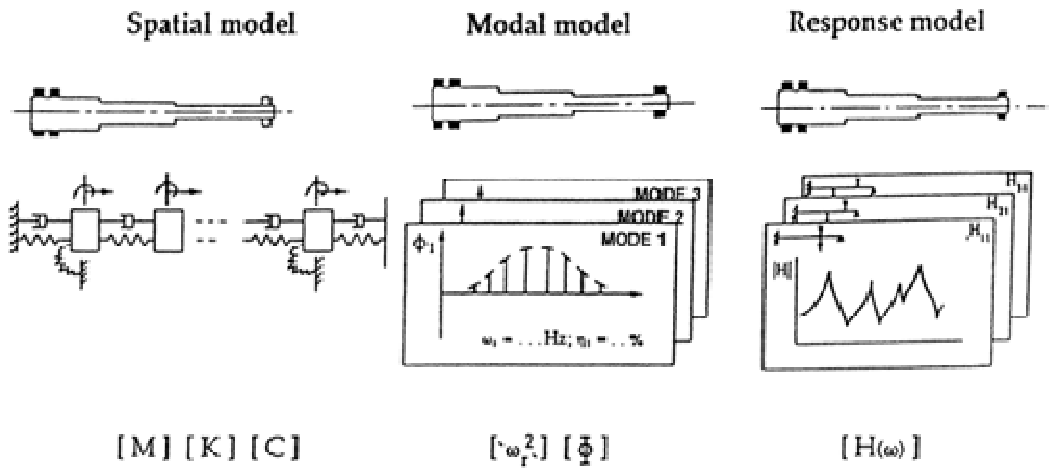

Figure 2. 53 : Dynamic analysis models [49].

Then it is customary to perform a theoretical modal analysis of spatial model which leads to a description of the structures behavior as a set of vibration modes; the Modal Model. This model is defined as a set of natural frequencies with corresponding modal damping factors and vibration mode shapes. It is important to remember that this solution always describes the various ways in which the structure is capable of vibrating naturally, i.e. without any external forcing or excitation, and so these are called the 'natural' or 'normal' modes of the structure. The third stages is generally that in which we have the greatest interest; namely, the analysis of exactly how the structure will respond under given excitation conditions and, especially, with what amplitudes. Clearly this will depend not only upon the structure's inherent properties but also on the nature and magnitude of the imposed excitation and so there will be innumerable solutions of this type. However, it is convenient to present an analysis of the structure's response to a 'standard' excitation and to describe this as the Response Model.

2.4.1.2 Experimental route to structural dynamic analysis

The experimental modal analysis is usually perforfmed for the purpose of verification/correction of the results of the analytical approach.If an analytical model does not exist, the modal parameters determined experimentally serve as the model for future evaluations such as structural modifications. A response model is simply the set of frequency response measurements acquired during the modal test (Figure 2.55). These measurements contain all the dynamics of the structure needed for subsequent analyses. A modal model is derived from the response model by using

one of various modal analyses techniques. It not only includes frequencies, damping factors, and mode shapes, but also modal mass and modal stiffness.

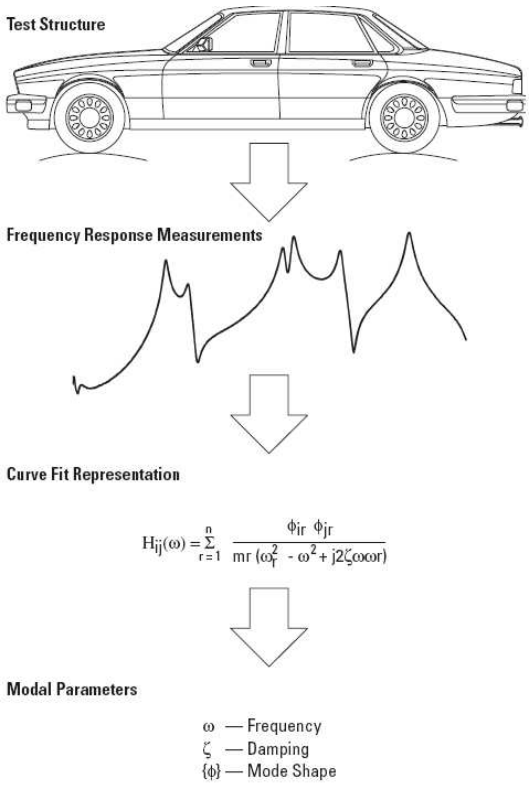

Figure 2. 54 : Phases of an experimental modal analysis [50].

The frequency response functions can be measured by acquiring the input excitation and output response simultaneously and then processing the acquired data.

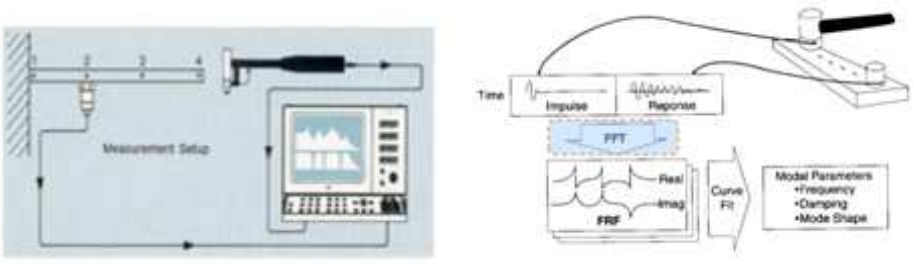

a) b)

Figure 2. 55 : a) Measurement setup of an experimental modal analysis and b) types of signals that we obtain in a measurement.

Generally, the choice of the excitation function dictates the choice of the excitation system, a true random or burst random function requires a shaker system for implementation. In general, the reverse is also true. Choosing a hammer for the

excitation system dictates an impulsive type excitation function. The best choice of excitation function depends on several factors: available signal processing equipment, characteristics of the structure, general measurement considerations and, of course, the excitation system.

Figure 2. 56 : Hammers and shakers.

For making measurements on simple structures, the exciter mechanism can be as basic as an instrumented hammer. The convenience of this technique is attractive because it requires very little hardware and provides shorter measurement times. An electrodynamic shaker may be needed for exciting more complicated structures.

Figure 2. 57 : Force sensor and accelerometer.

After excitation system is set up to force the structure into motion, the transducers for sensing force and motion need to be selected. The piezoelectric types, which measure force and acceleration, are the most widely used for modal testing. It has wide frequency and dynamic ranges, good linearity and is relatively durable

2.5 Finite Element Correlation

Finite element analysis is a numerical procedure useful for solving structural mechanics problems. More specifically, it is an analytical method for determining the modal properties of a structure. It is often necessary to validate the results from this theoretical prediction with measured data from a modal test. This correlation method is generally an iterative process and involves two major steps. First, the modal parameters, both frequencies/FRFs and mode shapes, are compared and the

differences quantified. Second, adjustments and modifications are made, usually to the finite element model, to achieve more comparable results. The finite element model can then be used to simulate responses to actual operating environments.

3. TEST RIG DEVELOPMENT FOR LOADED ELECTRICAL MOTOR AND MEASUREMENTS

3.1 Frequency Response Functions (FRF) Analysis

Various FRF measurements are carried out in order to validate and improve the numerical model For the static case (non rotating situation), frequency response functions of the whole system and some individual components are measured. The equipments used during this experimental process are shown in Figure 3.1.

Figure 3. 1 : Hardware used during FRF measurements.

The structure is excited using a modal impact hammer and CCLD 4394 type accelerometers are used to measure the responses. An analyzer (B&K 3560) with proper signal conditioning hardware is used. Thus, an experimental set up is prepared for measuring frequency response functions of individual components of an electric motor. The components of the electric motor used for FRF testing are front cover, rear cover, stator and rotor. Individual components of the electrical motor are hanged by using flexible string (fishing line). The main purpose of the FRF measurements presented here is to validate the first few natural frequencies of individual

components. Accordingly, based on experience gained in these components, there was no need for extensive FRF testing or full modal testing. Therefore, it was decided to measure a few FRFs for each component so as to validate the first few modes. Some typical measurements are presented here for each component. The excitation and response locations for typical FRFs are also included here for possible use in the future. Figure 3.2 shows a typical measurement for the front cover, depicting the force and response measurement locations. A *hammer* is used to excite the structure and an *accelerometer* is used to measure the response at certain locations and directions. Thus, frequency response functions for individual parts of the electrical motor are obtained and they are used for validating numerical models. Generally, frequency range is set to 0 to 1600 Hz as this range appears to be sufficient for evaluations of vibrations. However, if the first mode of a component is greater than 1600 Hz, a new appropriate frequency range is chosen.

Figure 3. 2 : Locations of impact force and acceleration response for the front cover.

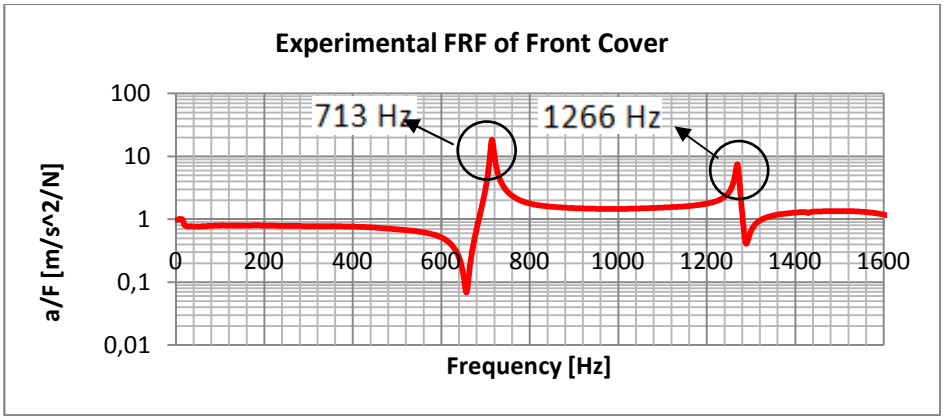

Figure 3. 3 : Frequency Response Function of the front cover corresponding to excitation and response locations shown in Figure 3.2.

The experimental FRF in Figure 3.3 shows a few peaks indicating natural frequencies of the front cover. The first natural frequency of the front cover is identified as 713 Hz and the second one is 1266 Hz.

Figure 3. 4 : Locations of impact force and acceleration response of rear cover.

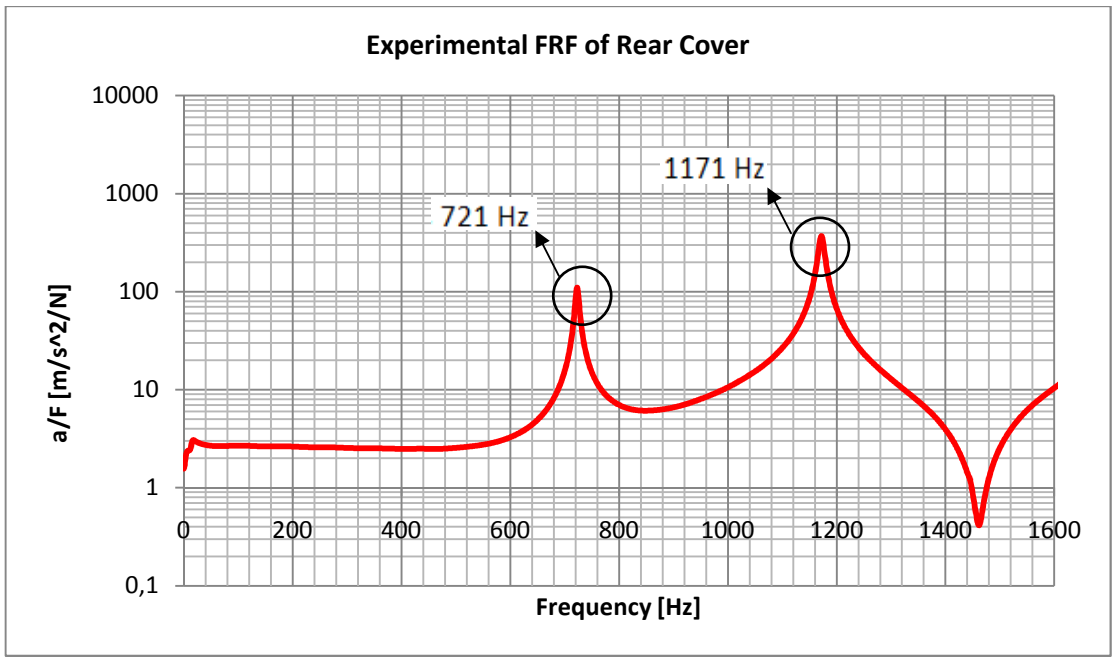

Figure 3. 5 : Frequency response function of rear cover corresponding to excitation and response locations shown in Figure 3.4.

The measured FRF in Figure 3.5 shows a few peaks again within the frequency range of interest indicating natural frequencies of the rear cover. The first natural frequency of rear cover is 721 Hz and the second one is 1171 Hz.

Figure 3. 6 : Locations of impact force and acceleration response of stator.

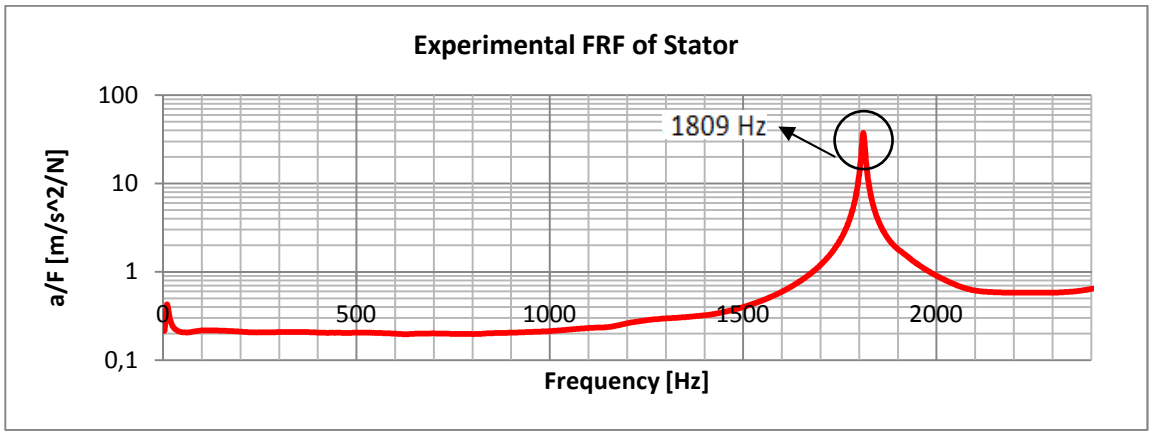

Figure 3. 7 : Frequency resposne fuction of stator corensponding to exciitation and response locations shown in Figure 3.6.

The measured FRF in Figure 3.7 shows only one mode up to 2.4 kHz. The first natural frequency of the stator is determined to be 1809 Hz.

Figure 3. 8 : Locations of impact force and acceleration rsposne of rotor.

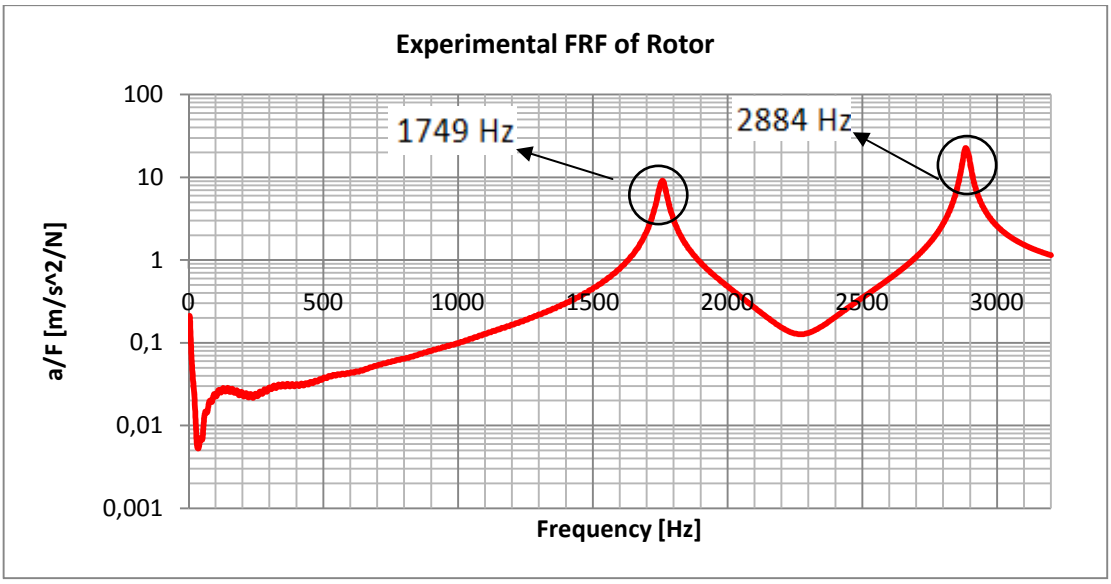

Figure 3. 9 : Frequency response funciton of rotor corresponfing to excitation and response locations shown in Figure 3.8.

The experimental FRF in Figure 3.9 shows two natural frequencies of the rotor. The first natural frequency of the rotor is 1749 Hz and the second one is 2884 Hz. So far FRF results of individual components of electric motor are presented. After these results FRF of electric motor assembly is measured while it is placed on a flex part in order to provide free-free condition. As it is seen in Figure 3.10 accelerometer is placed on the stator and excitation force is applied to the rear cover.

Figure 3. 10 : Locations of impact force and acceleration response of motor.

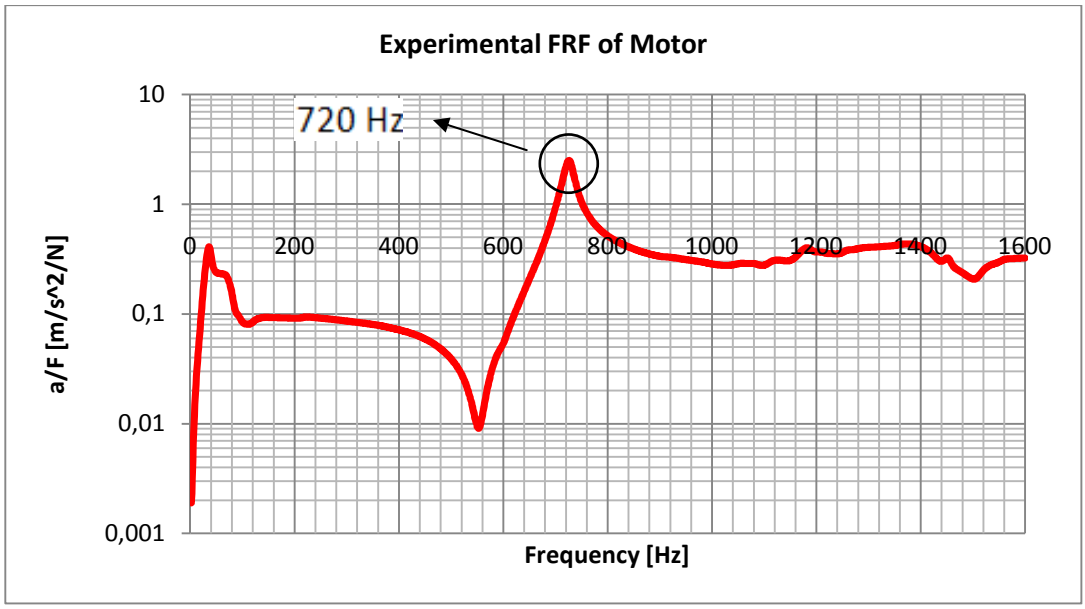

Figure 3. 11 : Frequency Response Function of the motor corresponsing to excitation and response locations shown in Figure 3.20.

The FRFs of the electric motor is also measured within a frequency range 0-1600 Hz. A typical FRF is presented in Figure 3.11. It is seen that the motor has one mode in this frequency range its first natural frequency is 720 Hz. As it previously mentioned, a cylindrical mass is assembled in front of the motor so as to provide load conditions. But this time, motor is not able to performed on a flex part with this cylindirical mass because it is very difficult and dangerous. So a test rig is designed and FRFs are measured for this case (Figure 3.12).

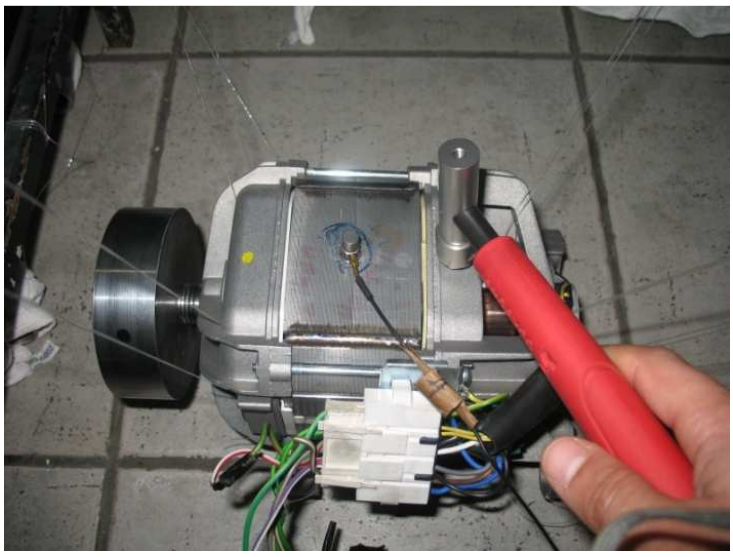

Figure 3. 12 : Locations of impact force and acceleration response of hanged motor.

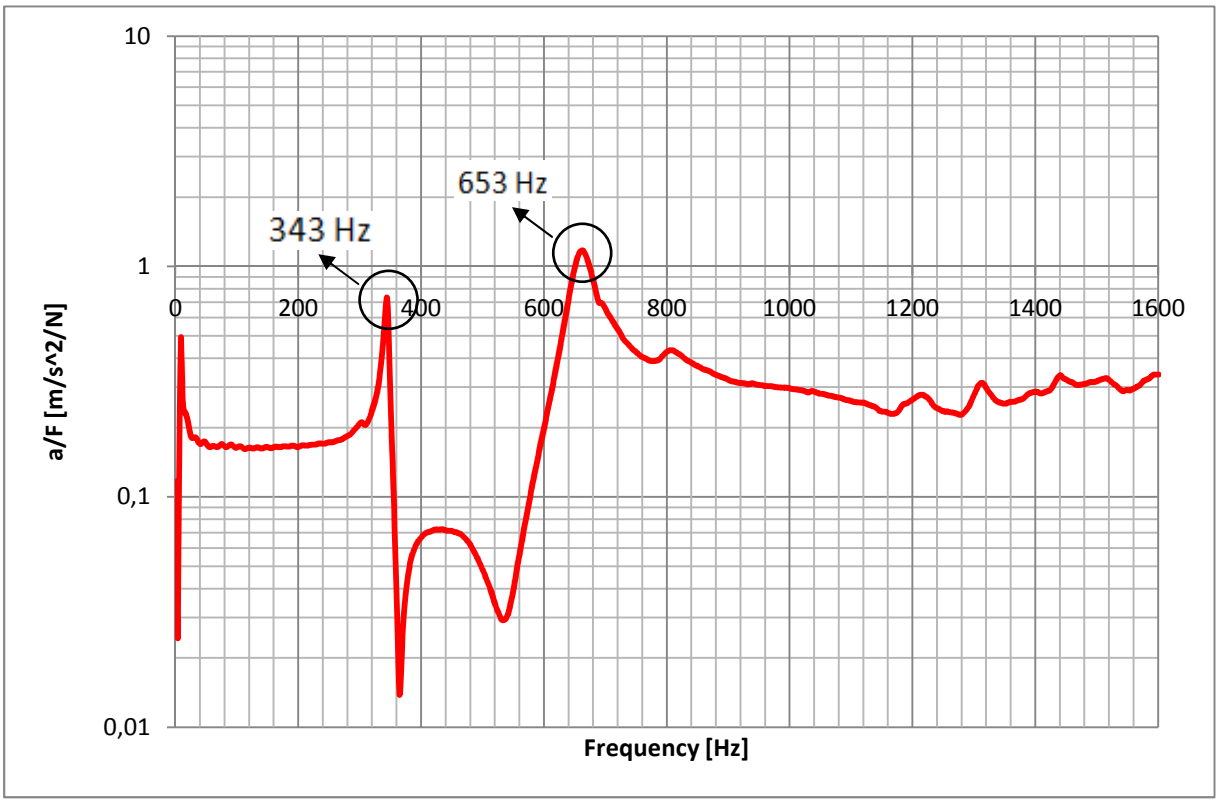

Figure 3. 13 : Frequency Response Funtion of hanged motor corresponding to excitation and response locations shown in Figure 3.12.

The experimental FRF in Figure 3.13 shows peak indicating resonance frequency of the motor. First resonance frequency of the motor is 343 Hz and the second one is 653 Hz.

3.2 Test Rig

In order to compare and validate the numerical model of the electrical motor, a test rig is designed and developed for acquiring experimental data. Experimental results are also used for further improvements of the numerical model. Some pictures of the set-up are presented in Figure 3.14.

Figure 3. 14 : Test rig

The main objective of this test rig is to measure the forced response behaviour of the electric motor itself without the effect of the structure it may be attached to. Accordingly, it is decided to perform the tests in free-free conditions. The electric motor is suspended by using flexible strings again from four points. A cylindrical steel part, whose mass moment of inertia is equal to the rotating parts of the washing machine including the wash load, is assembled in front of the rotor in order to simulate operating load conditions. A cage is is also designed for the test rig for safety considerations.

3.3 Measurement Set-ups

Basically two different kinds of measurements are made on the electrical motor. One of them is used for vibration measurements while the other one is used for electrical current measurements. Vibration measurements in terms of acceleration are made by using two different measurement set-ups in order to observe the effects of different operating conditions of the electric motor. The main differences between these two measurement set-ups are about the way of controlling the speed and applying types of electric current (AC or DC). Speed of the electric motor is controlled by variac and controller.

3.3.1 Variac-controlled measurement set-up

The input voltage to the electric motor is adjusted by variac in order to control the speed of the motor in a variac-controlled measurement set-up. The Campbell and order diagrams are obtained by controlling the speed and the angular acceleration of the motor. Schematic view of the measurement set-up is depicted in figure 3.15.

The variac, number 2 in Fig.3.15, is used to adjust the speed of the system and it is connected to the motor (3). The tachometer, available in the motor, is used for tracking the rotational speed. Accelerometer (6) is positioned on the stator of the motor and vibration data are collected. CCLD type accelerometer shown in Figure 3.15 Analyzer (4) and accelerometer types are Bruel & Kaejer 3560D and 4394 respectively. Electrical current probe is placed between the variac and the motor in order to measure the current feeding the motor. An amplifier (8) is also used for current probe. The collected rotational speed of the motor and the acceleration data are collected by the analyzer and then transferred to the computer (7). B&K PULSE

platform is used during these measurements in order to display the results and manage the measurements.

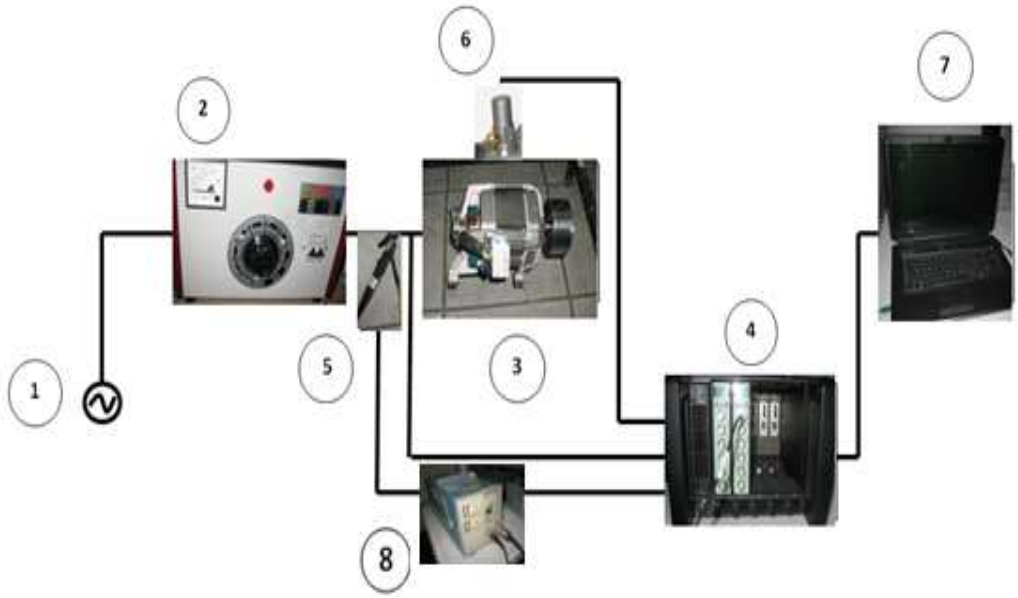

Figure 3. 15 : Variac-controlled measurement set-ups.

3.3.2 Controller-controlled measurement set-up

In this set-up, the rotational speed of the motor is controlled by a controller (3), of the washing machine. Also, instead of the internal tachometer of the electric motor, an external laser tachoprobe (2) is used for sensing the rotational speed of the motor(4). Laser tachoprobe type is Bruel & Kaejer 360M. Schematic view of this measurement set-up shown below;

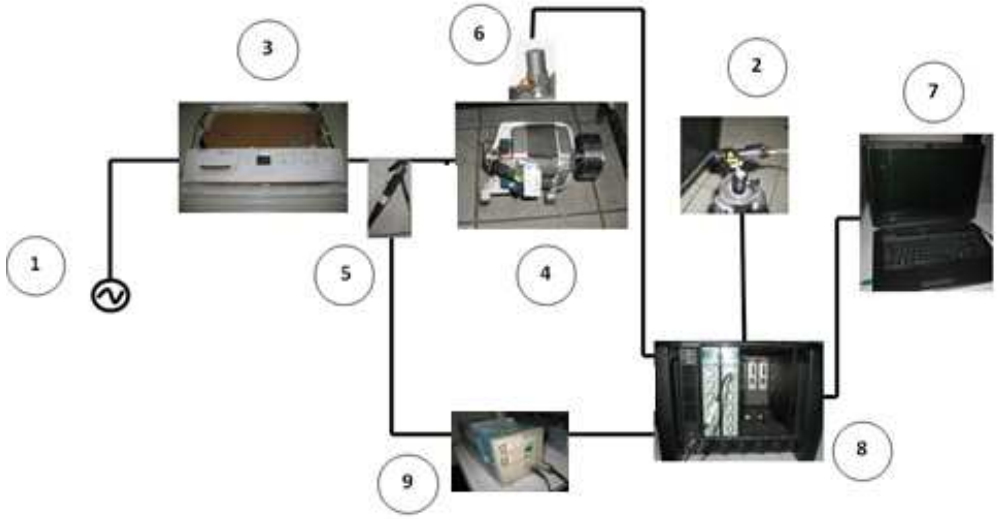

Figure 3. 16 : Controller-controlled experimental set-up.

3.3.3 Current measurement set-up

Variations of electric current flow are investigated by using a current probe attached to the current carrying cable of the electrical motor. The measured current results are used to correlate vibrations of the motor and the current. The type of electric current probe used in these test is Tektronix A6302. An amplifier (Tektronix TM502A) is also for the amplification of the signal from the current probe before the signal is passed to the analyser. Current measurement set-up of electric motor is seen below;

Figure 3. 17 : Current measurement set-up.

3.4 Measurements and Discussions

Current and acceleration are the main output data from the measurements described above. The associated measurement set-ups are presented in the previous sections. Measurements are conducted by using both 50 Hz and 60 Hz electrical network in order to determine the effects of the frequency of the electrical network. As mentioned before, to investigate the effects of the load, a cylindrical part is designed and assembled in front of the rotor. The order tracking analysis can be done for run-up and run-down situations. In this study, both run-up and run-down analyses are performed. The Pulse platform enables the adjustments of the order span, the rpm interval and the order resolution of the diagrams. The analyzer has some limits about the resolution, order and frequency span. For instance, when more resolution in the rpm axis is desired, the order span or the rpm range should be reduced. During the experimental studies various span and resolutions are used for different cases.

3.4.1 Identifying electric network harmonics with current measurements of lamp

Although it is thought that the frequency of electrical network is purely 50 Hz, it is decided here to test the frequency content of the AC electric signal. Lamp test illustrated in Figure 3.18 is used for this purpose.

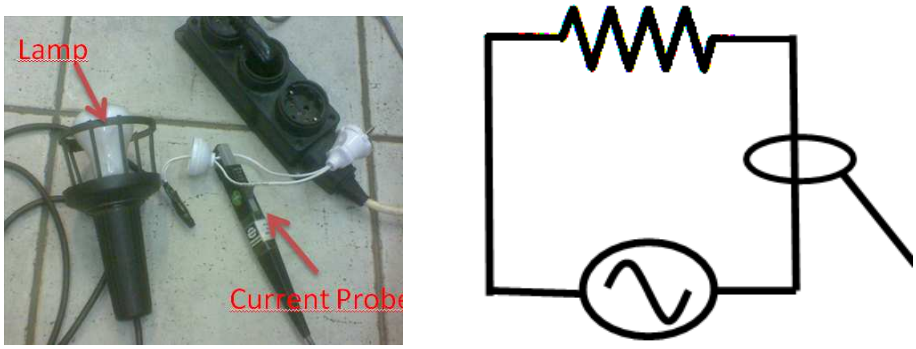

Figure 3. 18 : a) Picture, b) schematic view of the test set-up.

Ordinary lamp has only resistance effects, so it is not expected to cause any unpredictable effects in term of frequency content of the current. First, the noise level of the current probe is determined by free measurement without electricity in the lamp (Figure 3.19a-red curve). Then, it is compared with measurement taken while lamp is in action in order to see the differences between them(Figure 3.19a-blue curve). Odd harmonics of 50 Hz are clearly observed in the spectrum of the current. At the same time, time history of the current is also investigated. Comparison and time data of current can be seen in the following figure;

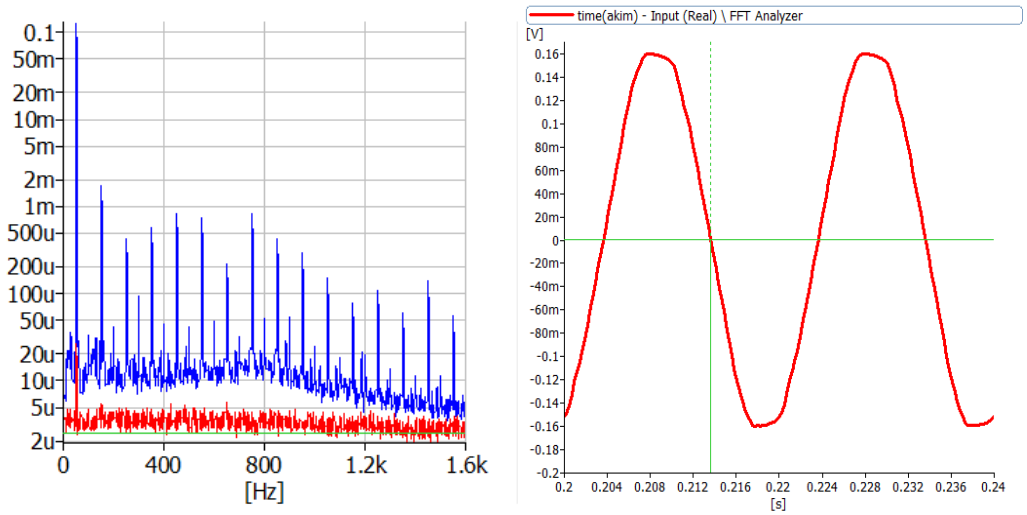

Figure 3. 19 : a) FFT diagrams of open and close lamp, b) time data of current.

Results of curruptions in the time data of current produce strong odd harmonics and also weak even harmonics are seen in the FFT spectrum of the current due to the curruptions in the time data of the current (Figure 3.19b). These harnonics cause additional electromagnetic-based vibrations in the electrical motor.

3.4.2 Current measurements and discussions

Applied current to the electric motor is measured for the purpose of determining the changes of current relative to the rotational speed of the motor (Figure 3.20). First point that needs to be noticed is the variations of current vibrations proportional to the rotational speed of the motor in terms of frequency content. And also constant frequencies such as 50 Hz, 150 Hz are available in the waterfall FFT diagram of the current. The results show that the spectrum of the electrical current has certain pattern. Within the frequency range of interest, the speed dependent spectrum of the electrical current can be easily noticed from the results. The electrical current measurements are also made by using main electric power with 60 Hz main frequency in order to understand the relationship between the main line frequency and the mechanism of the current variations. The regions marked in these plots (Figure 3.20) show some important characteristics of the system. As discussed before, the parabolic curves in the order diagrams correspond to constant frequencies, whereas these frequencies are shown as straight lines in the Campbell diagrams. The frequency content of the 50Hz main line frequency consists of 50 Hz, 150 Hz, and 250 Hz… as odd harmonics of 50 Hz. In the case of 60 Hz main line frequency, 60 Hz, 120 Hz, 180 Hz... are seen as the dominant frequencies in the spectrumas in 50 Hz main line frequency case.

In Figure 3.21 waterfall diagrams of the current is seen but this time it is started to measure from very low frequency. So certain pattern of the current variations related with rotational speed of the motor can be understand better. Careful inspections of these results reveal that the sidebands of the main frequency contents are related to the rotational speed of the motor (Figure 3.21). Another interesting detail is about the behaviour of these sidebands especially when the frequency is close to 0 Hz. When operating frequency is equal to the main power line frequency, left sidebands of 50 Hz and 60 Hz reach to the 0 Hz. Immediately after this, frequency of these sidebands continue to increase proportional to the rotational speed of the motor.

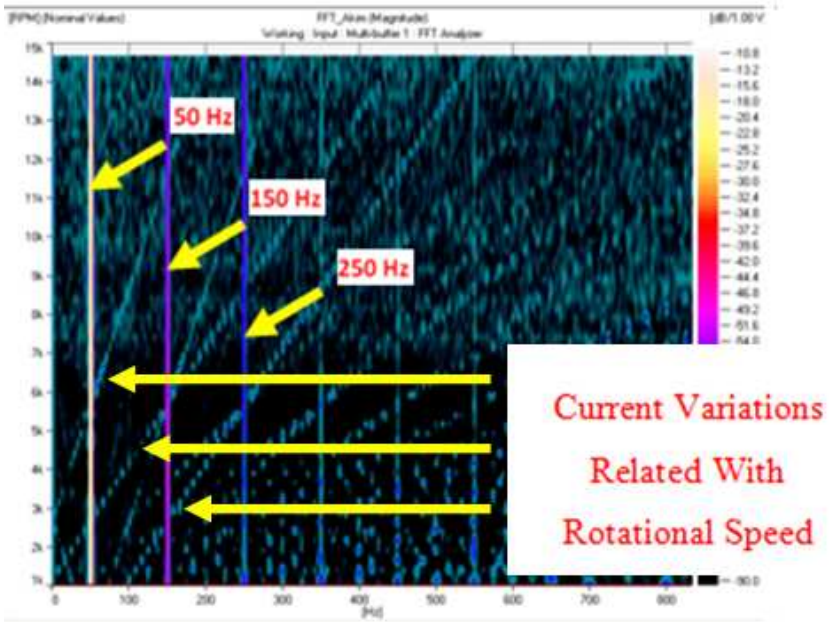

Figure 3. 20 : a) Waterfall FFT diagram of current (with 50 Hz electricity source).

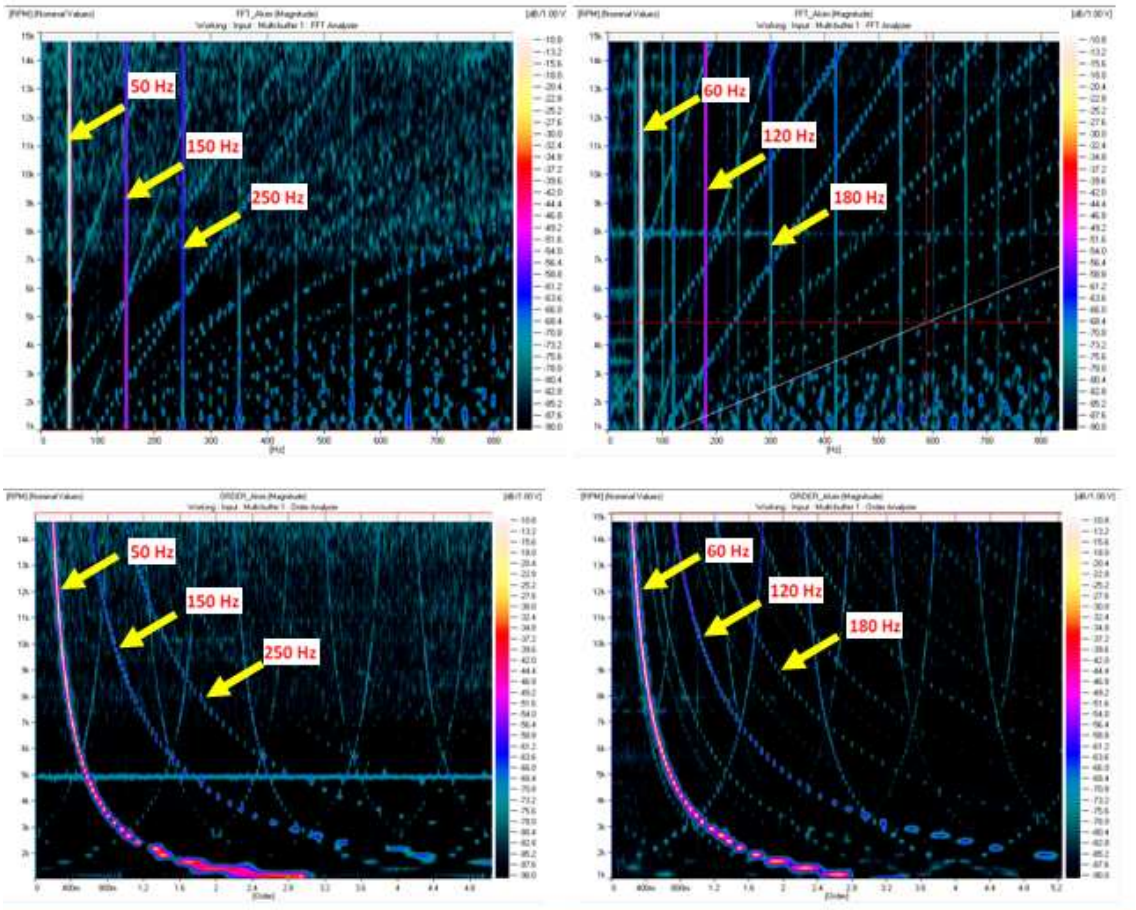

Figure 3. 21 : a) FFT diagram of current (with 50 Hz elctricity source), b) Order diagram of current (with 50 Hz electricity source), c) FFT diagram of current (with 60 Hz electricity source), d) Order diagram od current (with 50 Hz electricity source).

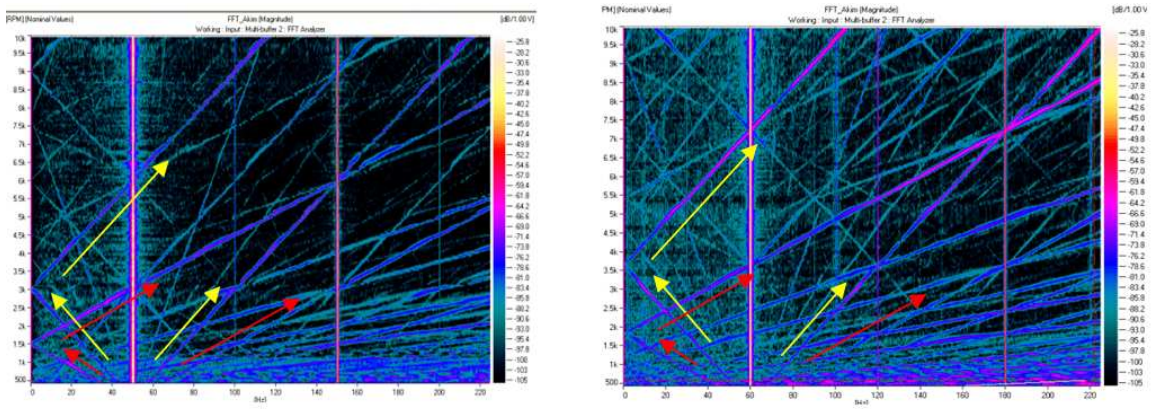

Figure 3. 22 : a) 0-200 Hz FFT diagram of current (with 50 Hz electricity source), b) 0-200 Hz FFT diagram of current (with 60 Hz electricity source).

3.4.3 Acceleration measurements and discussions

Acceleration measurements are made with a frequency range of 0-1600 Hz. The speed of the motor is varied between 0 and 15000 RPM. Loaded and unloaded run-up acceleration are presented in Figure 3.22 where resonance regions are noticed at a first glance. First and second resonance frequencies of the unloaded motor are approximately 420 Hz and 670 Hz but loaded motor resonance frequencies are 340 Hz and 650 Hz. Furthermore, first three orders of the electrical motor are immediately noticed. Also crossing of various orders with the resonance region can be seen.

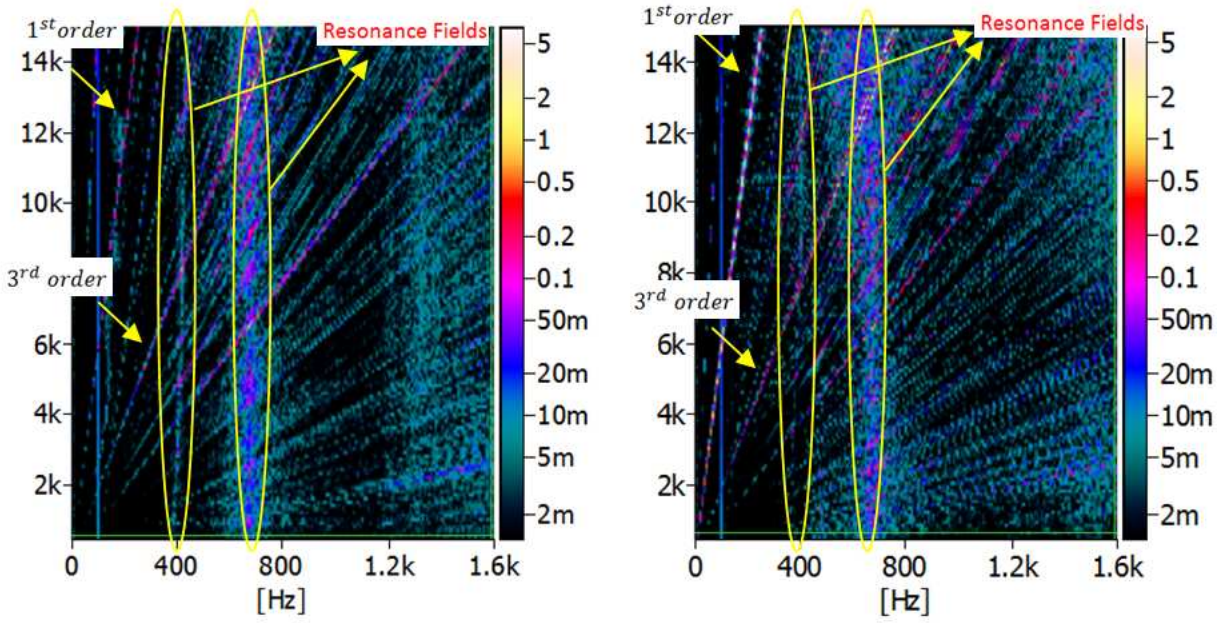

Figure 3. 23 : Run-up FFT diagrams a) unloaded, b) loaded.

A close inspection of the results shows that there are significant vibrations at 100 Hz and its harmonics as well as at sidebands of 100 Hz. At the same time 50 Hz and its harmonics are also observed but they are less dominant than 100 Hz and its harmonics. Yellow marks indicate 100 Hz and its harmonics and red mark indicate sideband of 100 Hz shown in Figure 3.23

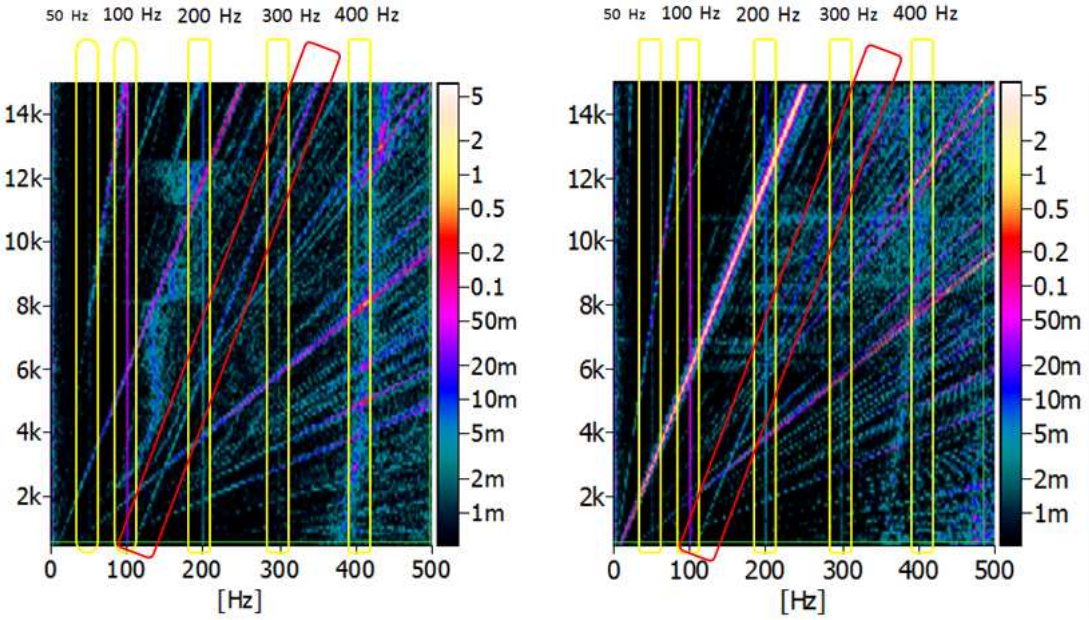

Figure 3. 24 : (0-500 Hz) Run up FFT diagrams a) unloaded, b) loaded.

Run down measurements are presented in Figure 3.24. These measurements are recorded when the electrical power to the motor is cut-off, allowing the observations of mechanical vibrations only. By comparing the run-up and run-down (coast down) measurements, it is then possible to identify electromagnetic based vibrations.

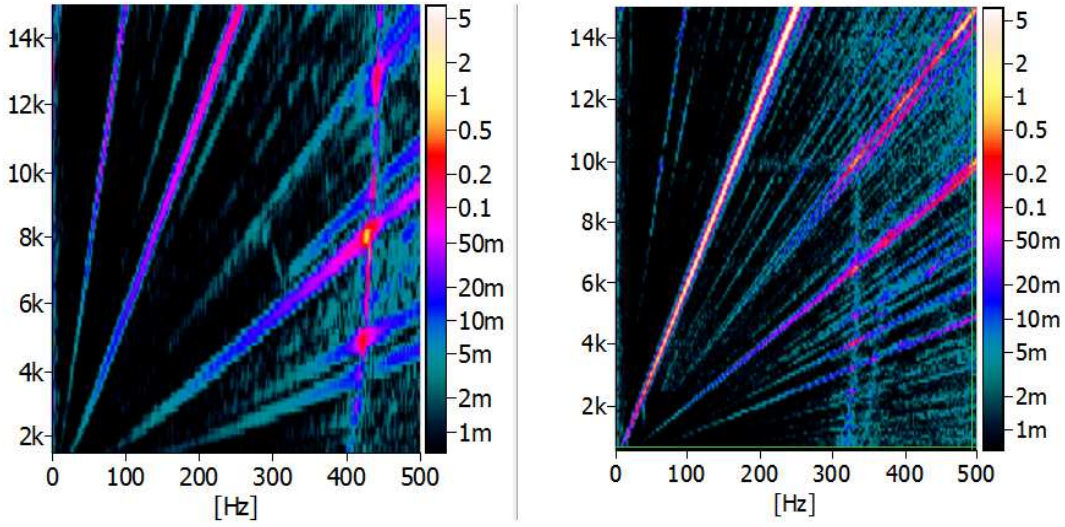

Figure 3. 25 : a) Unloaded, b) loaded run-down FFT measurements.

Comparisons of run and run down diagrams reveal the difference which is due to the electromagnetic vibrations. As a matter of fact, differences between these diagrams are very noticeable. As can be seen, 50 Hz, 100 Hz, 200 Hz ... and also sidebands are not seen in run-down measurements. These results show that, electromagnetic vibrations can be determined via vibration and current measurements.

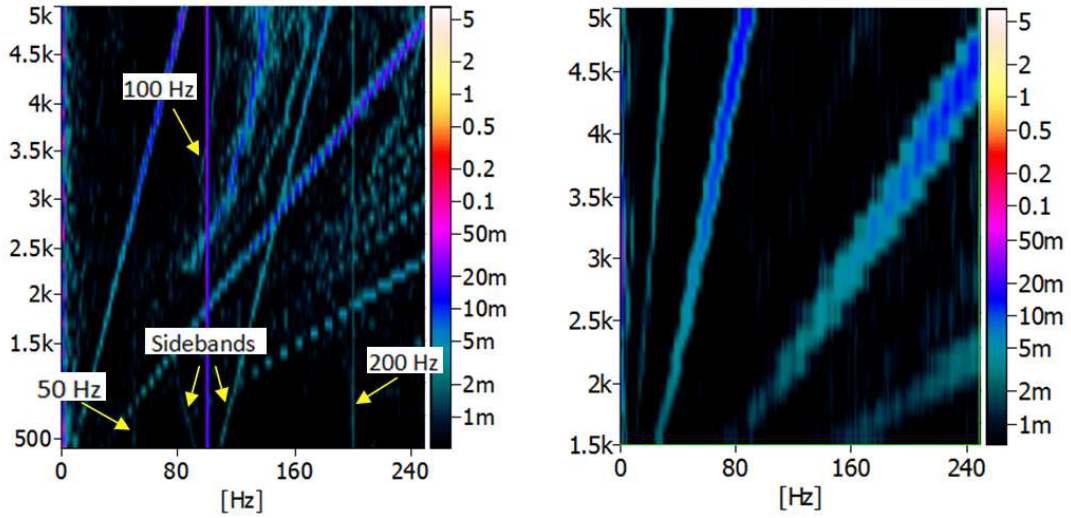

Figure 3. 26 : a) Unloaded, b) loaded run-down FFT measurements.

Acceleration measurements discussed up to now, are all performed using the 50 Hz main power line. 60 Hz main power line is also used in order to determine the effects of the main power line frequency on the acceleration and current vibrations of the motor. Requirement of electrical current is increased due to the increase of the load, so sidebands and 50 Hz data can be observed more clearly in Figure 3.26.

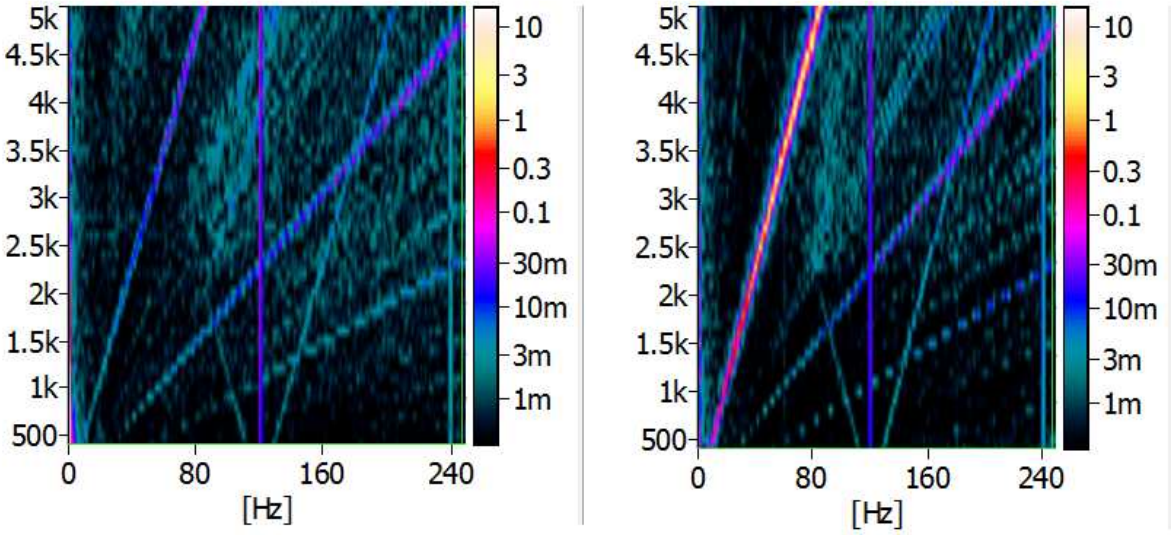

Figure 3. 27 : a) Unloaded, b)loaded run-down FFT measurements (with 60 Hz electricity source).

Since the electrical motor is normally driven by a controller in typical applications, some measurements are also made using a motor controller (Figure 3.27). As in the previous cases, loaded and unloaded measurements are performed. When FFT diagram is carefully investigated, not only 100 Hz and its harmonics but also sidebands of these harmonics are clearly seen in the comparison of the run-up and run-down diagrams given below (Figure 3.27).

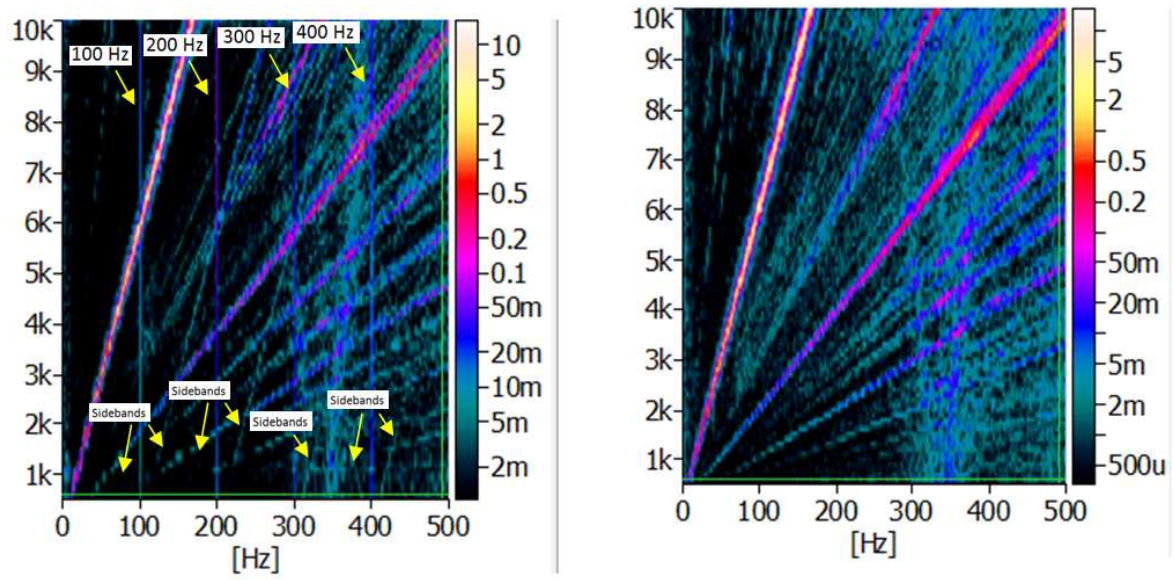

Figure 3. 28 : FFT a) run-up and b) run down measurements taken from controller-controlled measurement set-up.

4. DEVELOPING A FORCED VIBRATION MODEL FOR UNIVERSAL MOTOR

In order to perform dynamic analyses and also to optimize the performances of machines, numerical models validated by experimental data are necessary. In this chapter, numerical models for ball bearings and motor parts are developed separately. Then, these models are assembled so as to predict the dynamic behaviour of the complete electrical motor.

First of all, a numerical model for the ball bearings are developed. Then, individual parts (stator, rotor, front cover, rear cover) of an electrical motor are modelled based on FE approach. The individual models of the electrical motor and the ball bearing model are assembled and thus free vibration model is obtained. Finally, in order to build forced vibration model of an electrical motor, approximate forces that are caused by electromagnetism and ball bearings are included in the model and acceleration-based Campbell diagrams are obtained from simulations in MSC ADAMs platform.

4.1 Developing The Ball Bearing Model

During this study, a single row deep groove ball bearing is used. The model number for the specific ball bearing studied here is 6202-2Z. In Figure.4.1 and Table.4.1 the sectional view and some properties of the ball bearing with important dimensions are shown.

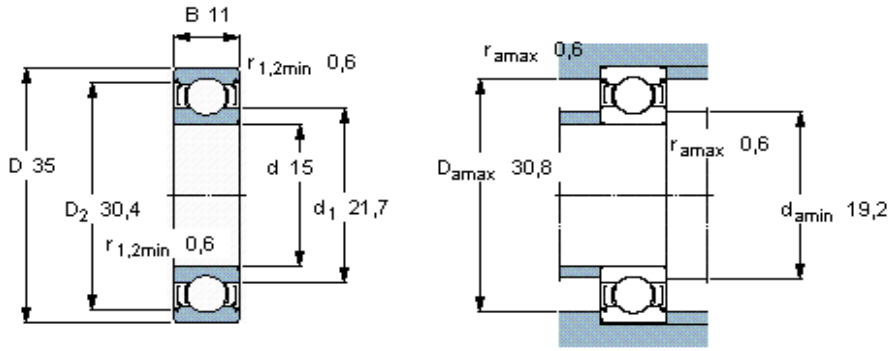

Figure 4. 1 : Section view of the 6202-2Z ball bearings

,

Table 4.1: SKF 6202 ZZ ball bearing critical physical property values

SKF 6202 ZZ Bearing				
Ball Diameter	**Pitch Diameter**	**Contact Angle**	**Number of Balls**	**Clearance**
BD [mm]	PD [mm]	b [rad]	n [unit]	Cd [μm]
6	24,60	0,3	8	11-25

Individual elements of the ball bearing are modelled as rigid bodies because of their high stiffness and low mass properties. Their natural frequencies are out of our interested frequency range. Besides, this type of assumption also leads to effective use of computer CPU time. However, the rigidity assumption of the ball bearing components can limit the observation of high frequency vibrations. On the other hand, a flexibility assumption of these components can lead to very severe increase in CPU requirements. The vibrations associated with the modes of individual bearing components are beyond the scope of this thesis. A ball bearing consists of inner and outer rings, rolling elements, and cage and for some types shield or sealing. Shields or sealings are not included in the model.

a) b)

Figure 4. 2 : Bearings used in a) electrical motor and b) its numerical model.

Some assumptions are made during the development of ball bearing model using MSC ADAMS software. In accordance with the rigidity assumption, the inner and outer rings and the rolling elements are assumed to be rigid. However, the contact stiffness between the rings and the balls (Figure.4.3) are included and can be determined based on the Hertzian Theory. The cage, connecting the balls to each other, is modelled using rigid links. The balls are positioned equi-pitched around the inner ring and there is no interaction between them. The process of building up the ball bearing model using ADAMS software is described in detail in reference [30].

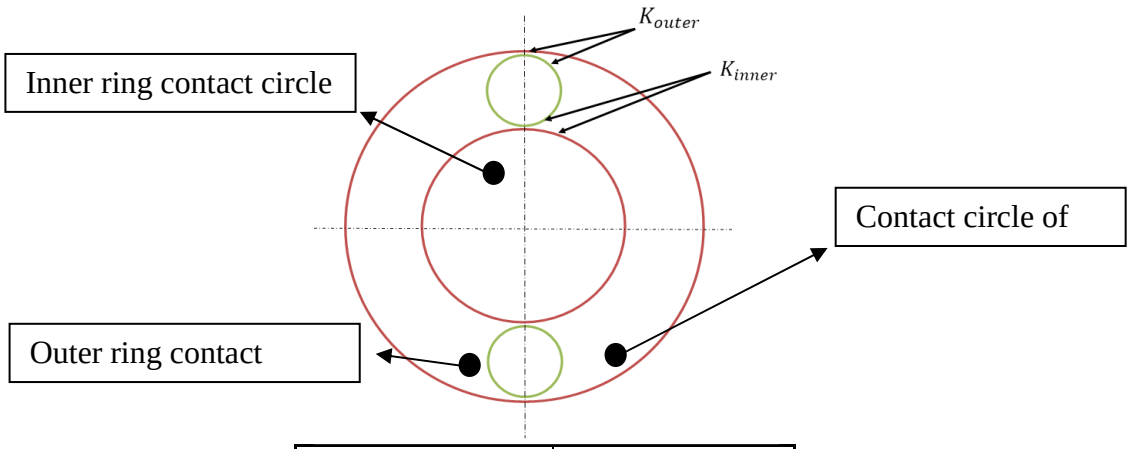

Kinner [N/mm]	**K**outer [N/mm]
9,03E+05	9,45E+05

Figure 4. 3 : The contact stiffness between contacting components and their values.

Bearing model is analysed and it is seen that bearing model can be produce its particular excitation forces. Outer ring is fixed but bearing model is free during analyses. The acceleration of the point A shown in Figure 4.4 on the inner ring along the vertical direction is obtained from MSC ADAMS simulations. A Fast Fourier Transform (FFT) is applied to the time-domain data and the amplitude spectrum is obtained when the system is at steady state and the rotational speed is 1200 rpm. As seen in Figure 4.5, the rotational speed at 20 Hz, Ball Passing Frequency (BPF) at 61 Hz and its harmonics at 122, 183.... Hz are all visible. Also, there are significant peaks at sidebands of the BPF and its harmonics. The Fundamental Train Frequency (FTF) of this system is 7.68 Hz. The sidebands of the BPF are BPF ±nxFTF.

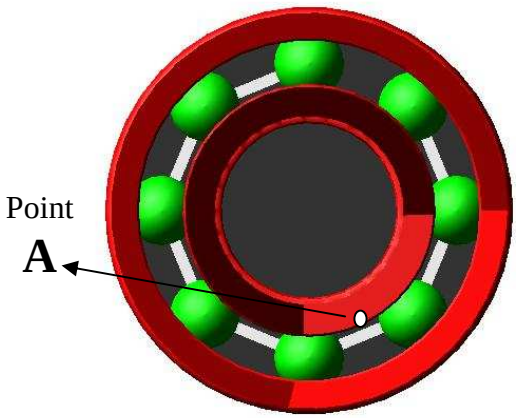

Figure 4. 4 : Measurement point of acceleration of the ball bearing.

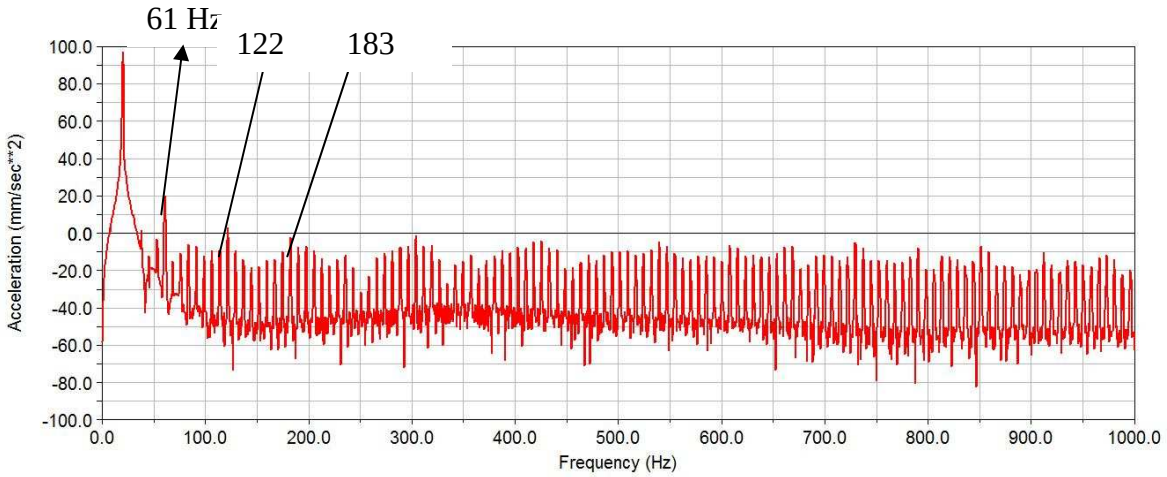

Figure 4. 5 : The amplitude spectrum of the standalone ball bearing model.

4.2 Developing Individual Parts of Electic Motor Model

Basically, individual parts of a universal motor such as stator, rotor, front cover, rear cover are modelled via numerical approach by using NX I-DEAS package software. In order to reduce CPU time, front and rear covers are modelled by shell elements rather than solid elements. But first, solid models of front and rear covers are transformed to shell models and after this process these shell models are built as a shell FE models. FE model of front cover, rear cover, rotor and stator are shown in Figure 4.6-9, respectively.

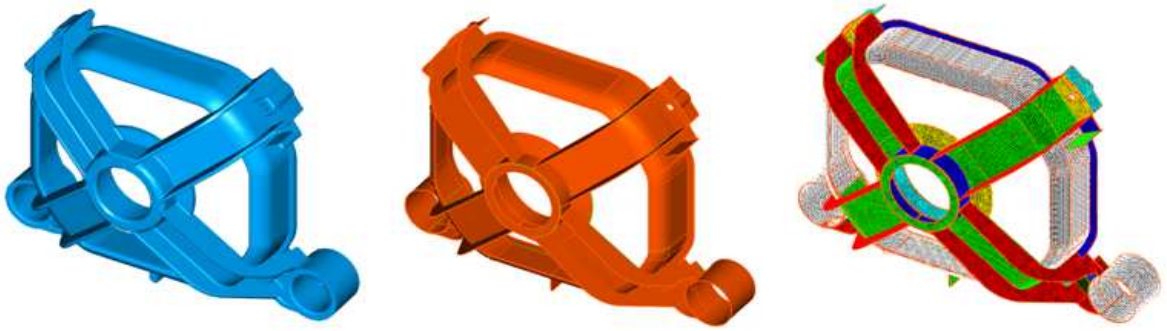

a) b) c)

Figure 4. 6 : Front cover a) solid model, b) surface model, c) FE model

Approximately 30000 thin shell linear quadrilateral elements for front cover and 50000 thin shell linear quadrilateral elements for rear cover numerical model are used.

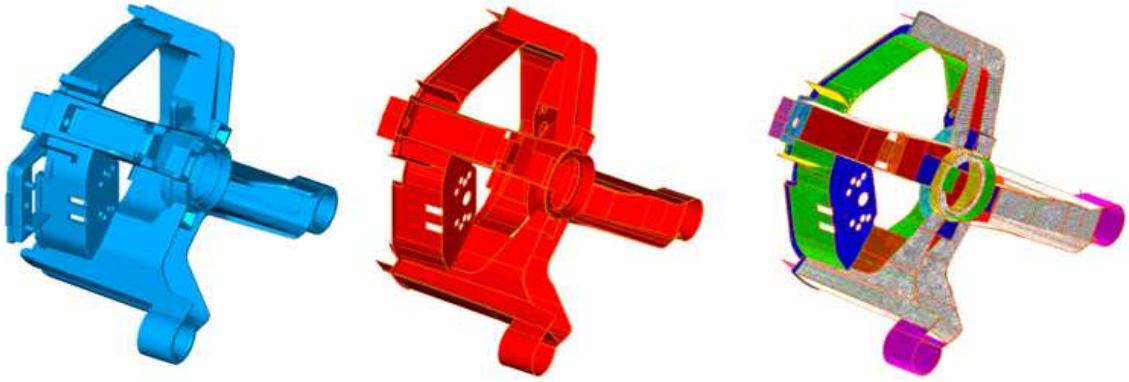

a) b) c)

Figure 4. 7 : Rear cover of electric motor, a) solid model, b) surface model, c) FE model.

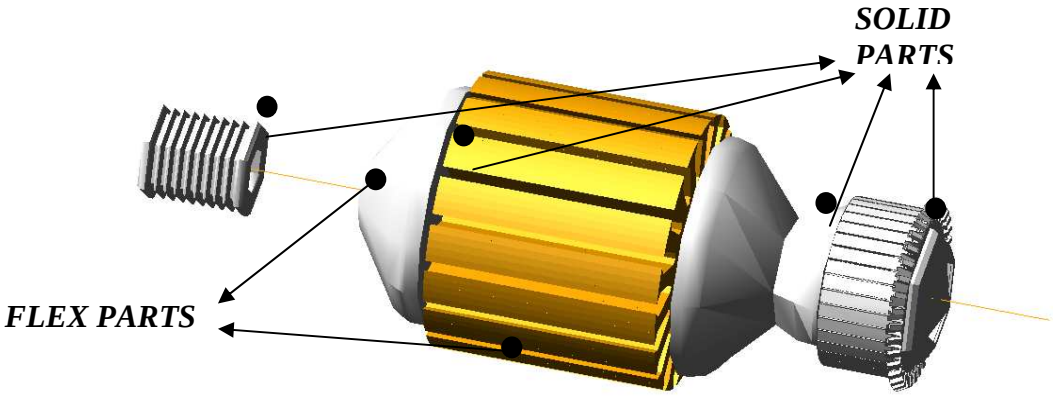

Figure 4. 8 : Rotor model of electric motor

FE model of the rotor (Figure 4.8) consists of a flexible shaft, a flexible armature and other rigid parts including commutator, windings, pulley. During the modelling process, it is aimed to limit the the number of flexible parts as much as possible in order to save CPU time.

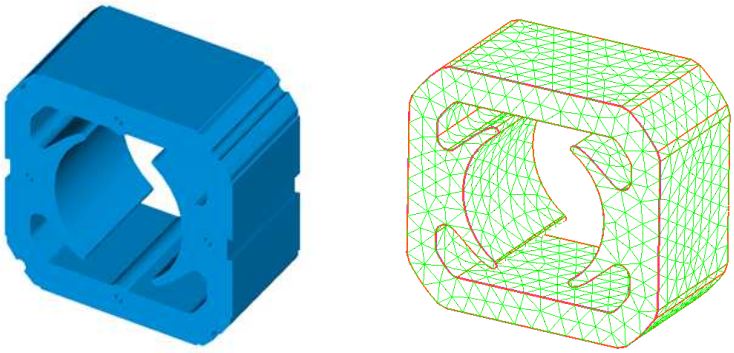

a) b)

Figure 4. 9 : Stator, a) solid model, b) FE model.

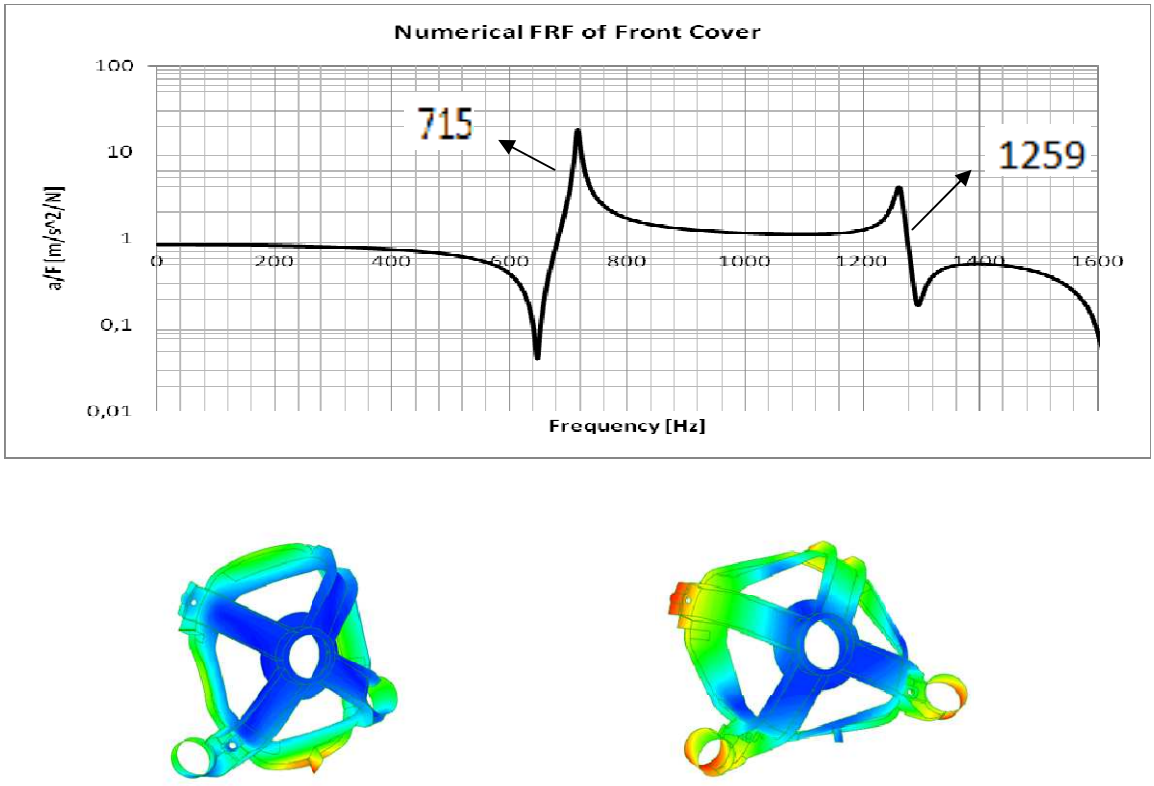

Figure 4. 10 : Numerical FRF and mode shapes of front cover.

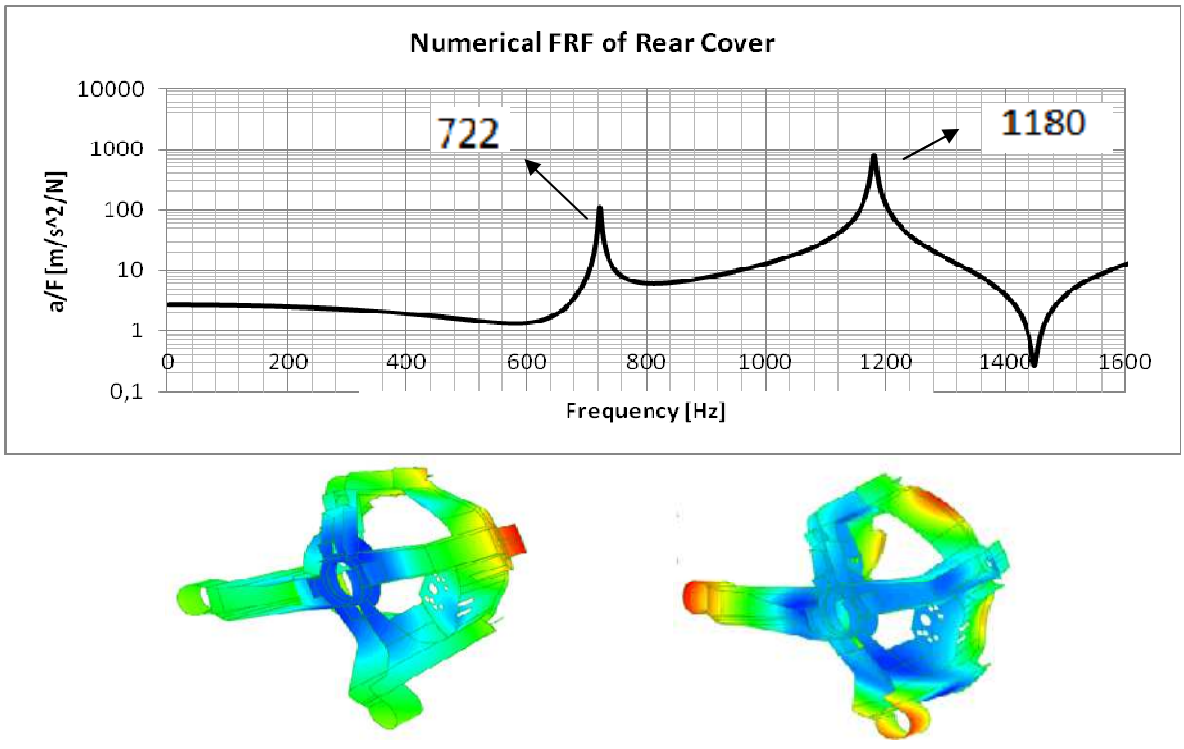

Figure 4. 11 : Numerical FRF and mode shapes of front cover.

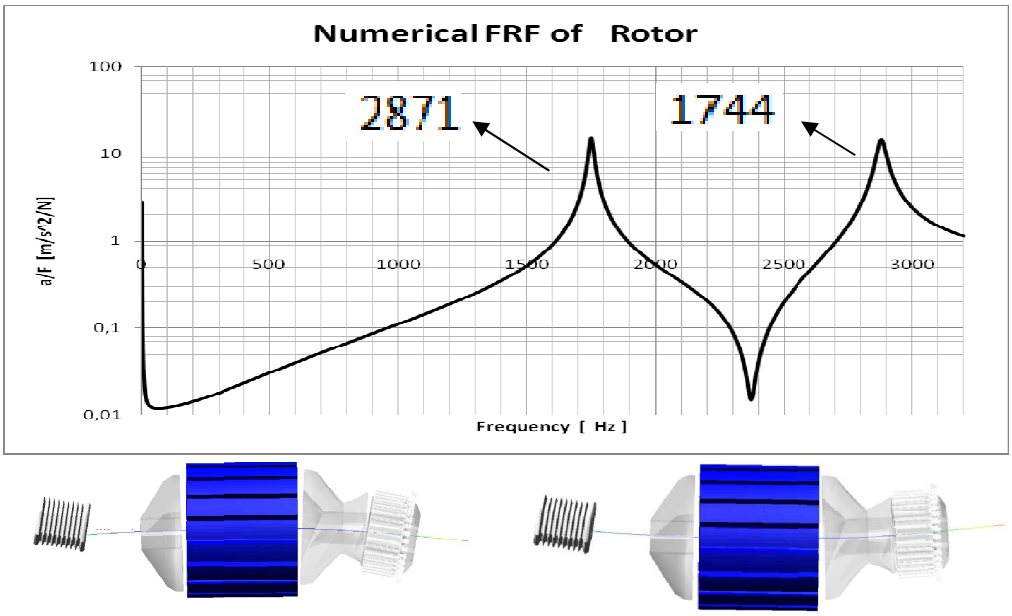

Figure 4. 12 : Numerical FRF and mode shapes of rotor.

Approximately 4000 solid parabolic tetrahedron elements are used in numerical model of the stator. Some holes and radii are ignored before creating FE model in order to minimise the number of degrees of freedoms in the model. Once the models are built, numerical modal analyses are carried out; also numerical FRFs are obtained from I-DEAS commercial software. Fopr each part, the response and excitation co-ordinates for the calculated FRFs are the same as those in measured FRFs. The first few natural frequencies and corresponding mode shapes are given in Figures 4.10-13.

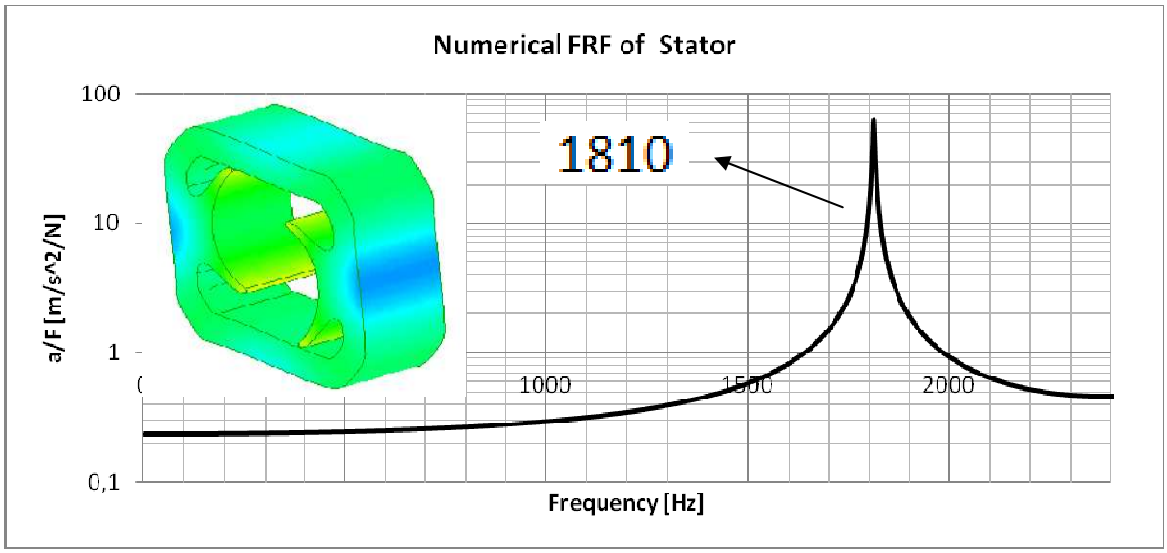

Figure 4. 13 : Numerical FRF and mode shapes of stator.

4.3 Developing Free Vibration Model Of The Electric Motor

Experimentally verified vibration models of individual parts are assembled in MSC ADAMS platform in order to obtain the free vibration model of the motor assembly in this step. Ball bearing model is also added to the assembly of the motor. Finally, all numerical models including bearings are assembled and in the light of the experimental data, motor model is refined and improved. The numerical motor model illustrated in Figure 4.14 is built using MSC. ADAMS software.

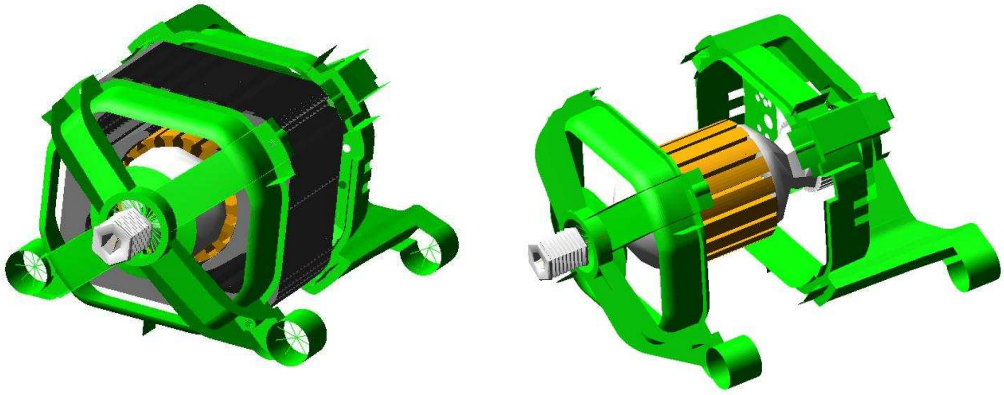

Figure 4. 14 : Numerical model of electrical motor

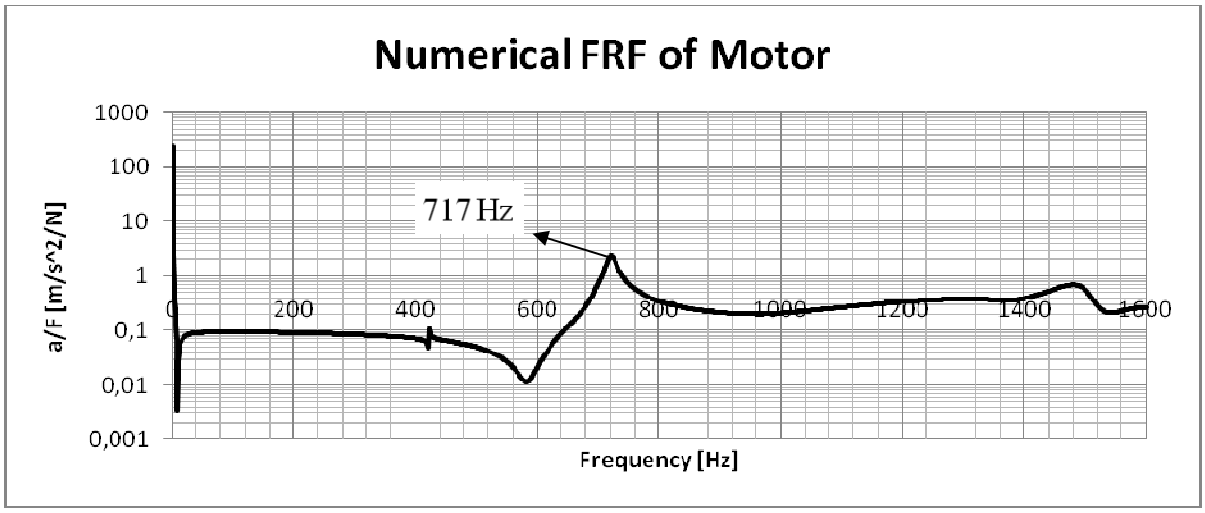

Figure 4. 15 : Numerical FRF of obtained from motor model.

Numerical frf of the motor assembly is obtained(Figure 4.15). The mode shape of the electrical motor corresponding to natural frequency at 717 Hz is obtained from numerical modal analysis is presented in Figure 4.16. The next step after modelling the free vibration model of the motor is to built forced vibration model. In this step, a flywheel (a cylinder) which is used during forced response measurements is also added to the numerical model (Figure 4.17) So-called bushings elements are also

included in the model so as to represent the suspension system used during the forced response measurements of the motor. An estimated FRF of the motor including the flywheel and the suspension strings is is given in Figure 4.18.

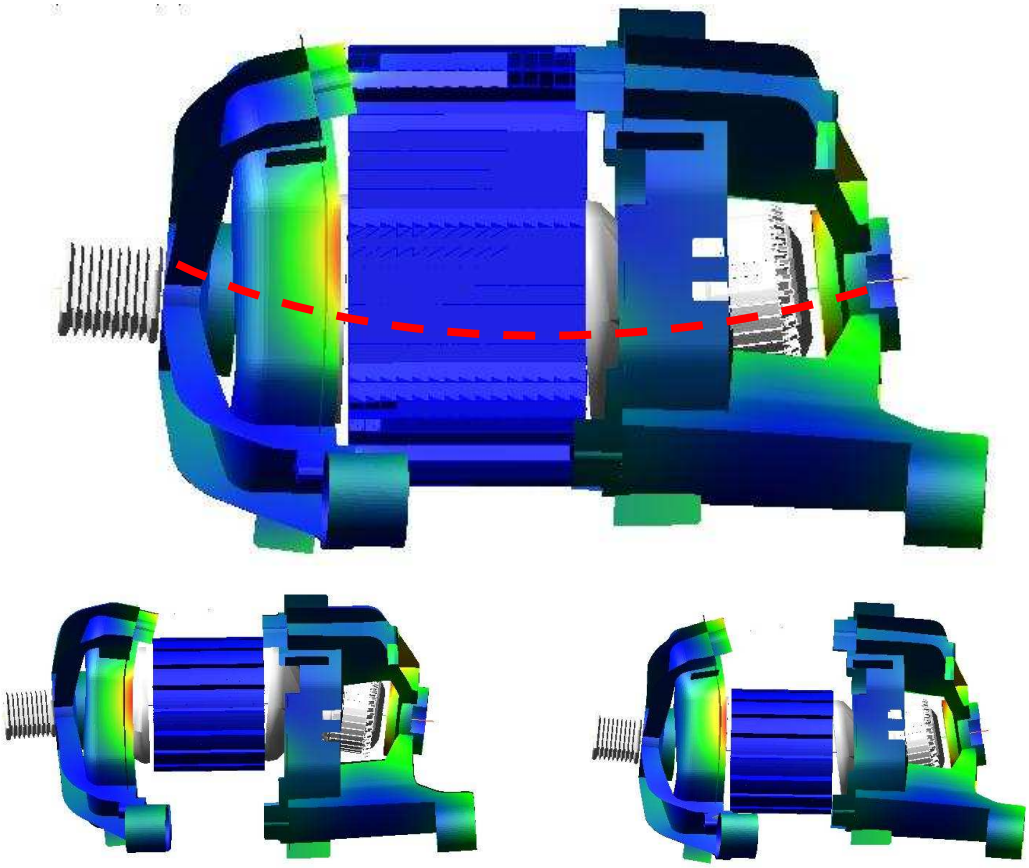

Figure 4. 16 : First bending mode shape of the electrical motor.

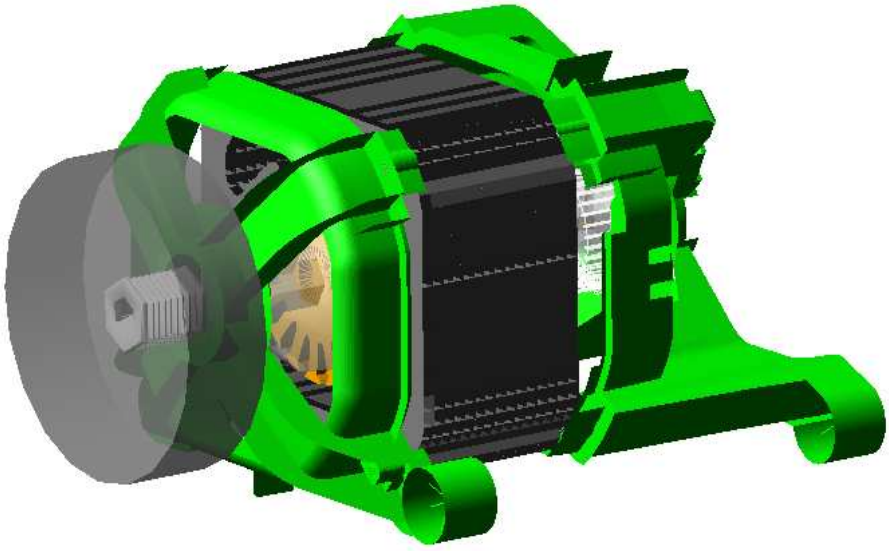

Figure 4. 17 : Numerical model of suspended motor.

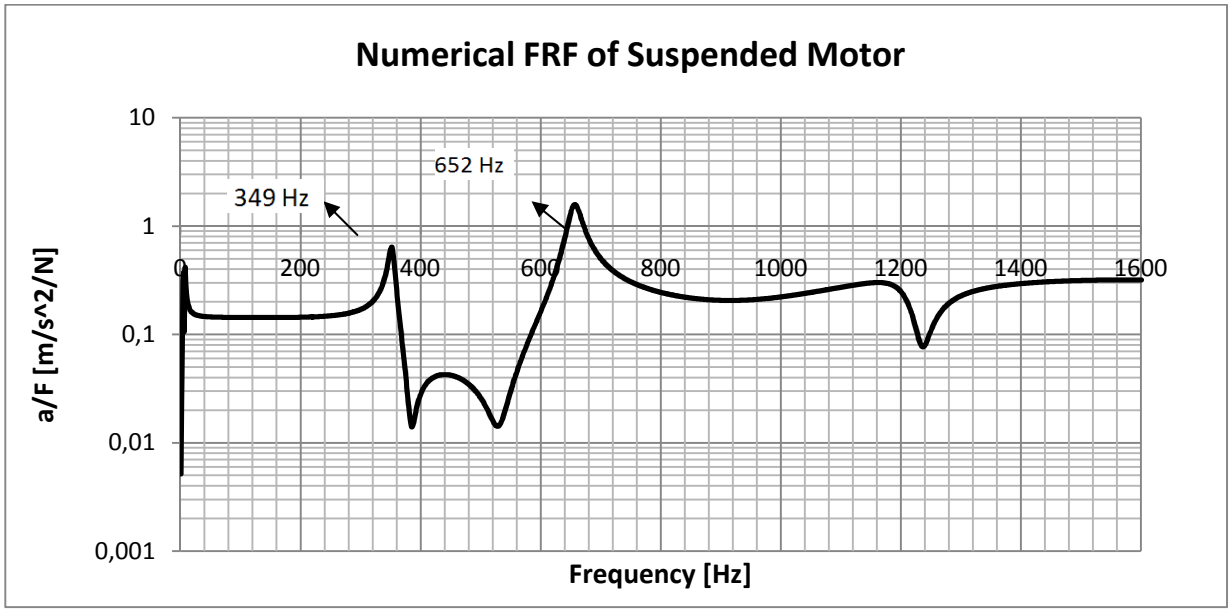

Figure 4. 18 : Numerical FRF of the suspended motor with a flywheel .

4.4 Developing A Model for Electromagnetic-Based Vibrations

Principle of operation of electric motors is based on electromagnetic excitation. In this section, it is aimed to develop a model for electromagnetic excitation mechanism in order to improve the understanding of electromagnetic-based vibrations in electric motors. A simple model of electromagnetic excitation is presented in Figure 4.19 which shows a simplifiedrotor, comprising four arms. The tips of these arms are assumed as points where electromagnetic forces act. Blue circular element represent bearings, which is connected to the ground by spring. So, electomagnetic forces acting on the rotor are balanced by the spring force.

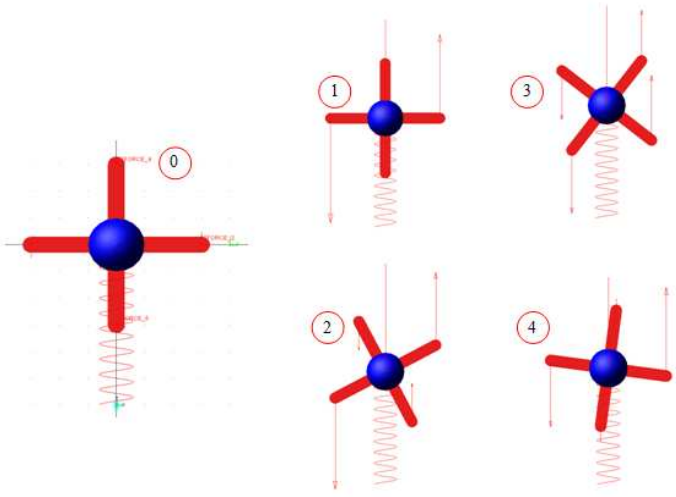

Figure 4. 19 : Simple electromagnetic excitation model of a rotor.

Different positions of simple model while it is rotating are depicted in the Figure 4.19. Forces applied to the vertical arms' tip are minimum (zero) but horizontal ones are maximum for the first state. After a little while horizontal forces are decreasing but vertical ones increasing gradually in the second step. Third position of the illustration shows just the same state but forces are bigger than the second state. One period of the motion is completed in the fourth step of the illustration. Functions of applied forces are shown below;

$$\cos(\theta)\,|10\sin\,(50(2\pi)time)| \qquad \textbf{(4. 1)}$$

Main electric power with 50 Hz is used for running the electrical motor and as a result, electromagnetic forces are acting at 100 Hz to the rotor slots of the electric motor. Equation for this rectification is implemented by using ABSOLUTE (ABS) operator in ADAMS software. The amplitudes of these forces are chosen as appropriate levels. However, at any given instant, theamplitude of the electromagnetic forces around the circumference of the rotor are not equal due to the operating principle of the electric motor in this study. So, electromagnetic force amplitudes are also multiplied by cosine function in order to represent this condition. The resulting electromagnetic force is evaluated by observing the spring force. The force that is developed on the spring is given in time domain in Figure 4.20. It is clear that applied force on the spring is a static force, because all forces are balanced around the rotor. So these forces induce only torque.

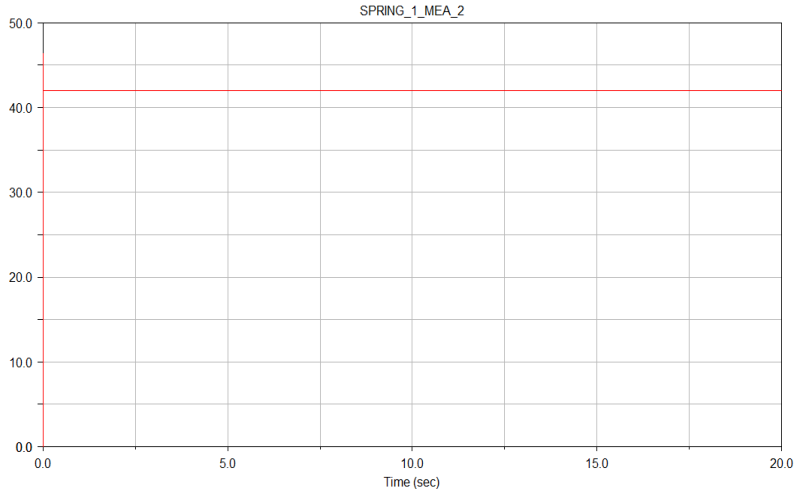

Figure 4. 20 : The spring force for the first case, each counter forcesin the horizantal and vertical arms are equal around the rotor.

Counter forces on the rotor are not equal in practice because of inequality of copper windings' cross section areas in slots and also inequality of permeance of all the points of on the rotor. In this case, counter forces of rotor arms are applied as unequal from each other so as to model this imperfection. Implemented equations are shown below;

$$\cos(\theta)\,|8\sin\,(50(2\pi)time)| \quad \textbf{(4. 2)}$$

$$\cos(\theta)\,|6\sin\,(50(2\pi)time)| \quad \textbf{(4. 3)}$$

$$\cos(\theta)\,|10\sin\,(50(2\pi)time)| \quad \textbf{(4. 4)}$$

$$\cos(\theta)\,|8\sin\,(50(2\pi)time)| \quad \textbf{(4. 5)}$$

The estimated spring force in time domain of this new model is given in Figure 4.23. It is seen that both the static and the dynamic forces on the spring are available this time.

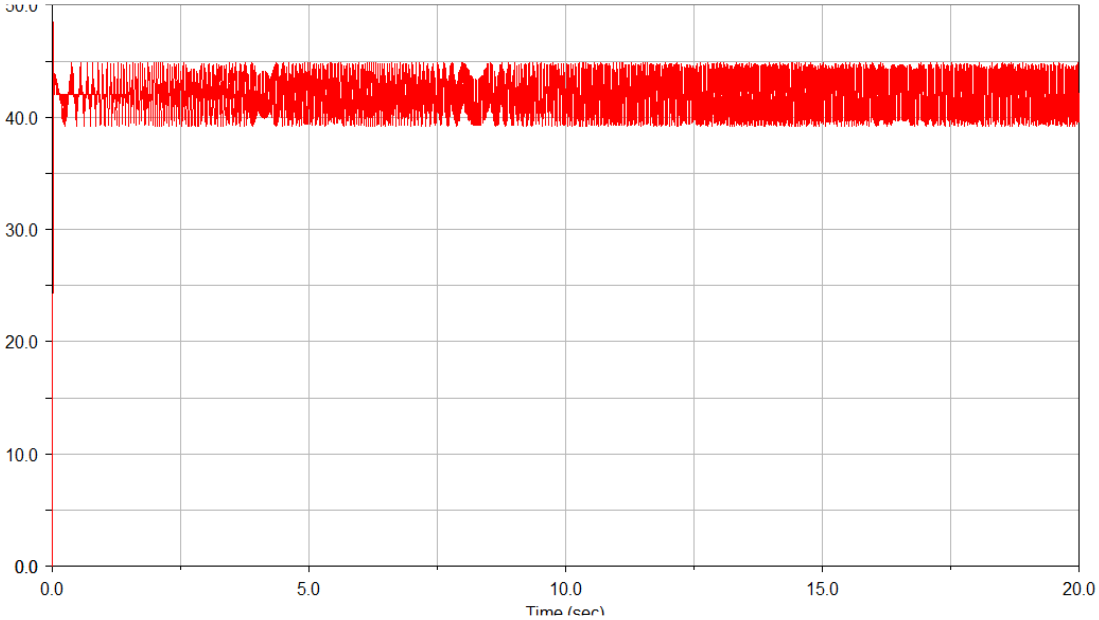

Figure 4. 21 : Time domain data for the dynamic spring force

Forward and backward sidebands of 100 Hz and its hormonics are clearly seen when spring force STFT is investigated. Reflections of 100 Hz and 200 Hz can be observed as in the experimental measurements.1X RPM forces are resulted in the spring. This observation is important because it can not observed in the experimental studies due to the unbalance forces. Unbalance forces are shadowed these 1X electromagnetic forces. STFT diagram of spring force is given in Figure 4.22.

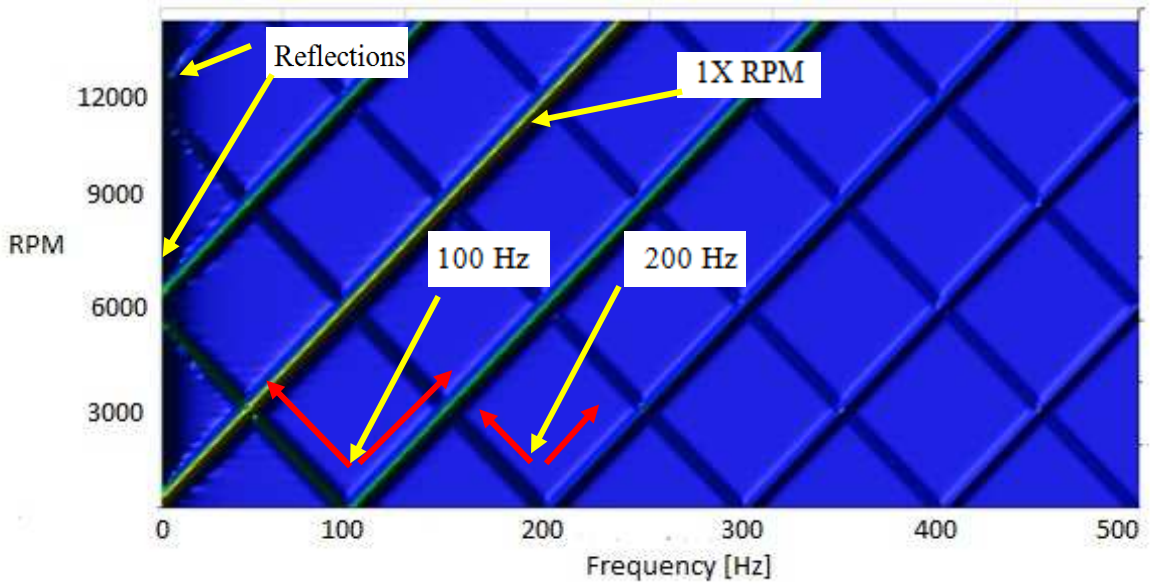

Figure 4. 22 : STFT diagram of the spring force.

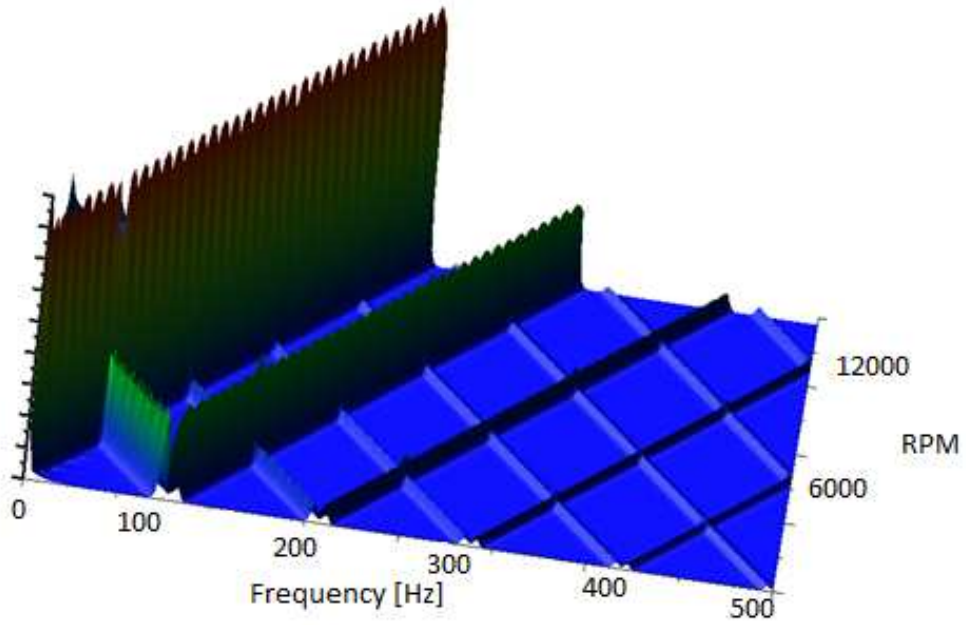

Figure 4. 23 : Amplitudes of the spring force do not change in time.

The electrical current applied to the electrical motor is evaluated in terms of its frequency spectrum in previous chapter. 50 Hz was observed as a dominant frequency and also hormanics of 50 Hz were also apparent. From this point of view, other main power current components (100 Hz and 150 Hz) are also included in the numerical model. These current flow components caused some changes in the vibration spectrum of the model. In this case, sideband forces of 50 Hz and its odd

harmonics are also observed. The results of these induced forces (Figure 4.24) are shown below;

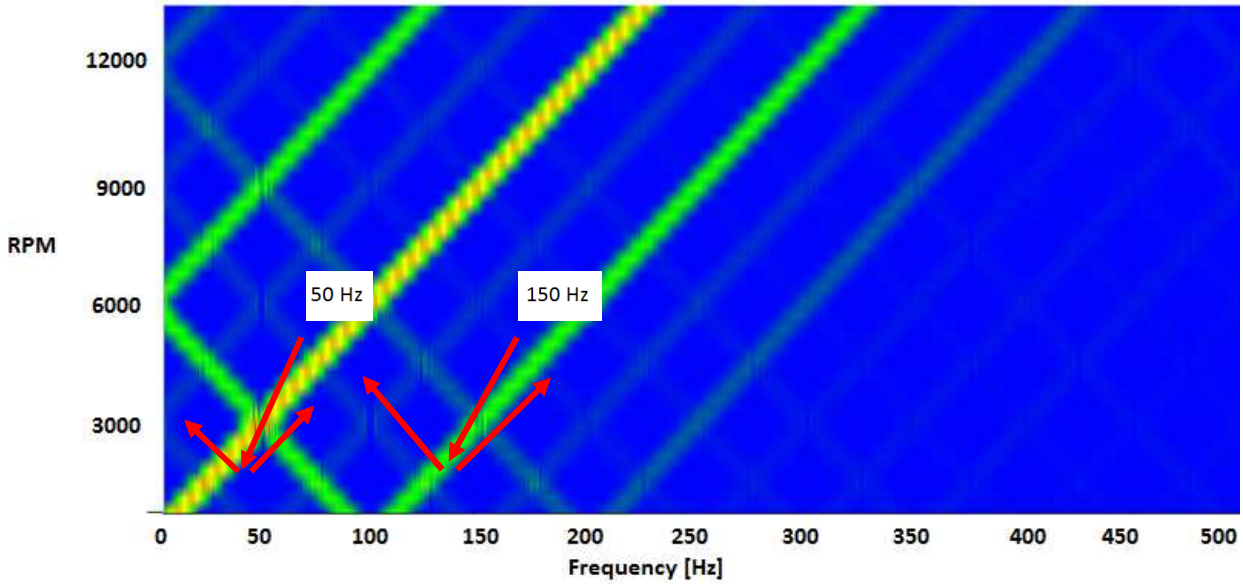

Figure 4. 24 : STFT diagram of the spring force when the main electric power consists of additional frequency components (100 Hz and 150 Hz)

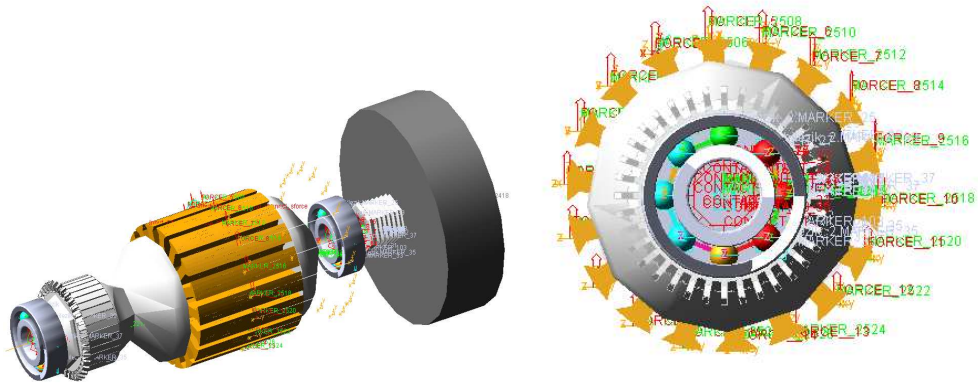

Figure 4. 25 : Numerical model of the rotor and applied electromagnetic forces.

Previously presented simple electromagnetic model is adopted in to the rotor model (see Figure 4.27). This rotor has 18 slots, so the electromagnetic forces are implemented all of these slots as a perpendicular direction. Functions of applied forces are the same as in the simple electromagnetic Model and each counter forces in slots has different amplitudes.

5. COMPARISONS OF NUMERICAL AND EXPERIMENTAL RESULTS

5.1 FRF Compasisons For Individual Parts Of The Motor

Results of the experimental modal analysis are used for validating and improving the numerical models. Experimental results are compared with numerical results and studies for model improvement are performed by using iterative approach. After this improvement process, the degree of correlation achieved between the measured and the predicted FRFs are illustrated in Figures 5.1 to 5.6 for various parts as well as for the assembled motor in two diferent configurations. The good correlation between the numerical and experimental results is clearly seen. Especially for the first two natural frequencies, the predictions are in very good agreement with the measurements.

a. Front Cover

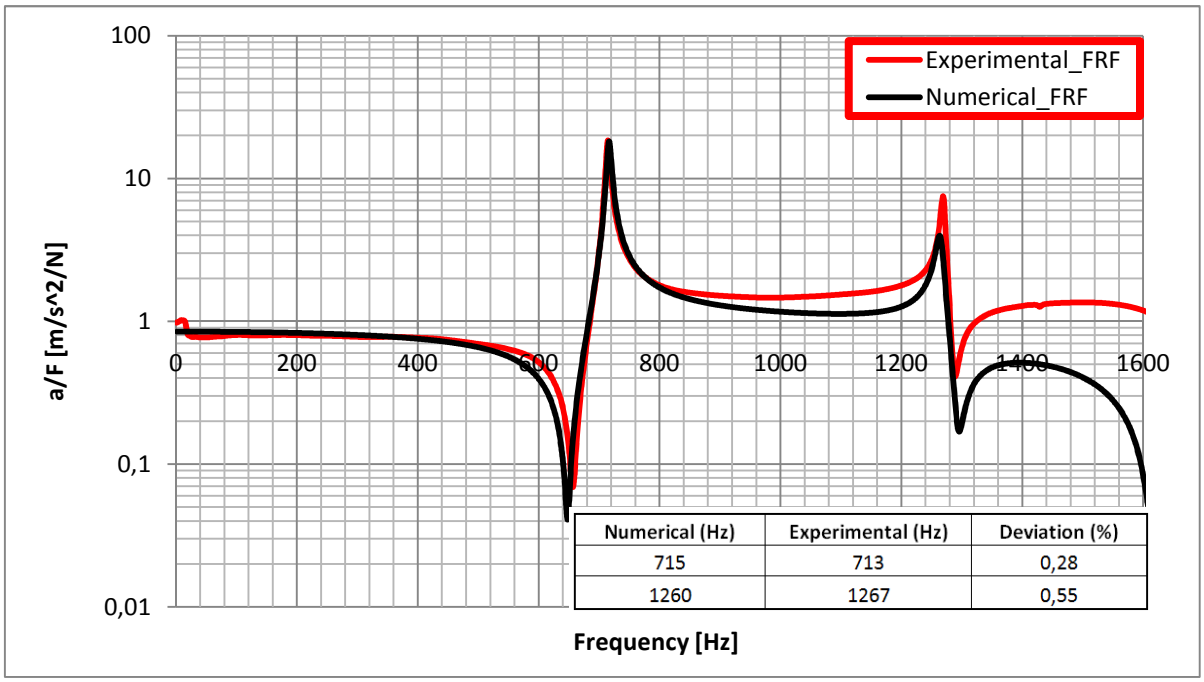

Figure 5. 1 : Comparison of predicted and measured FRF of front cover.

b. **Rear Cover**

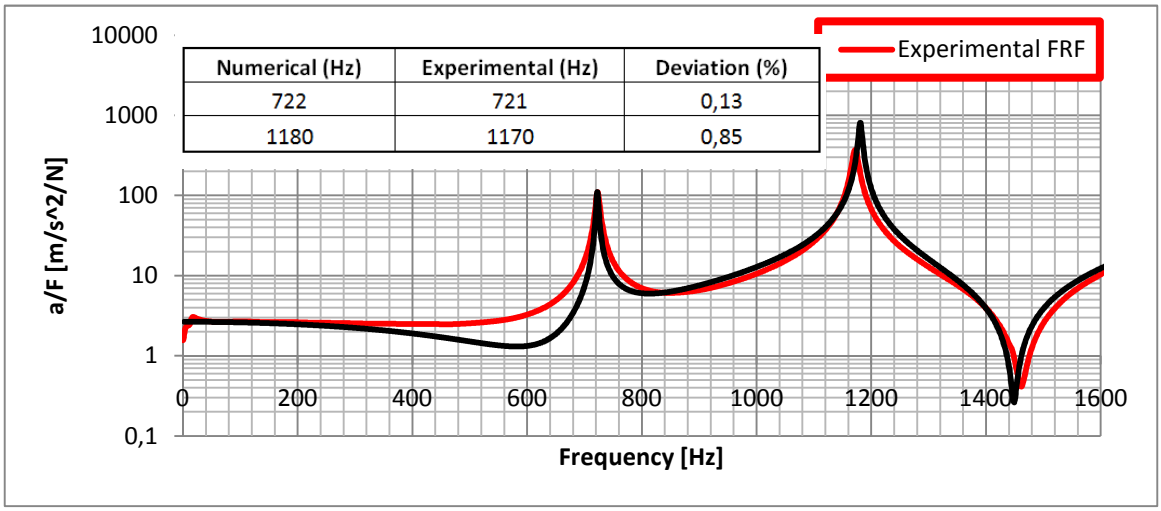

Figure 5. 2 : Comparison of predicted and measured FRF of rear cover.

c. Rotor

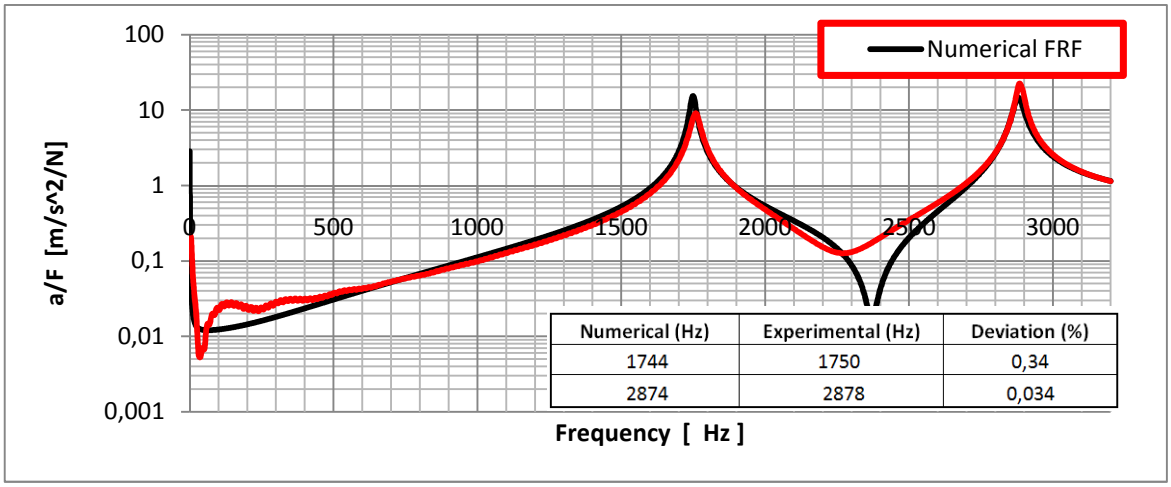

Figure 5. 3 : Comparison of predicted and measured FRF of rotor.

d. Stator

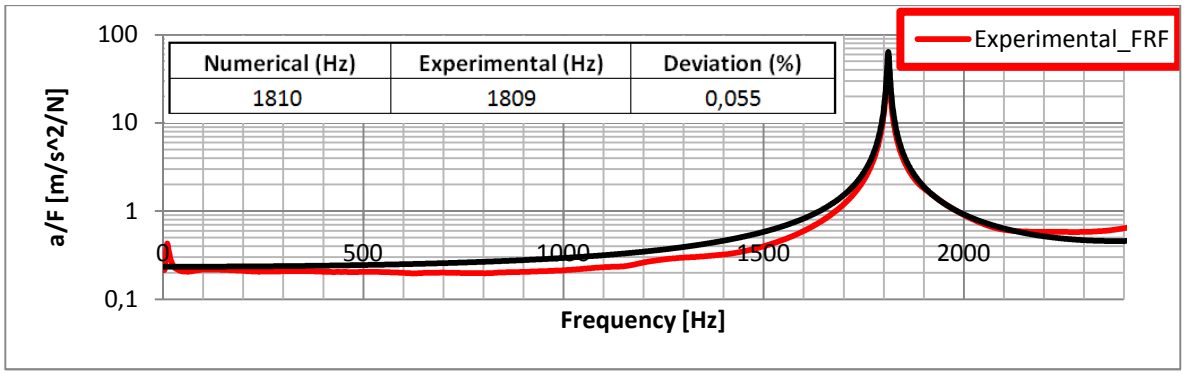

Figure 5. 4 : Comparison of predicted and measured FRF of stator.

e. Motor

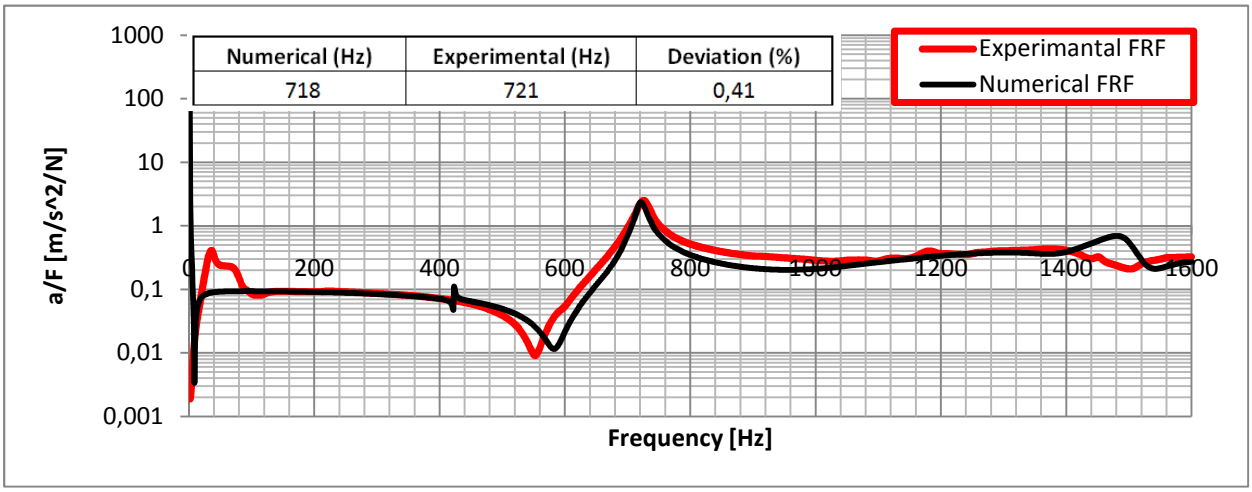

Figure 5. 5 : Comparison of predicted and measured FRF of motor.

f. Motor with flywheel

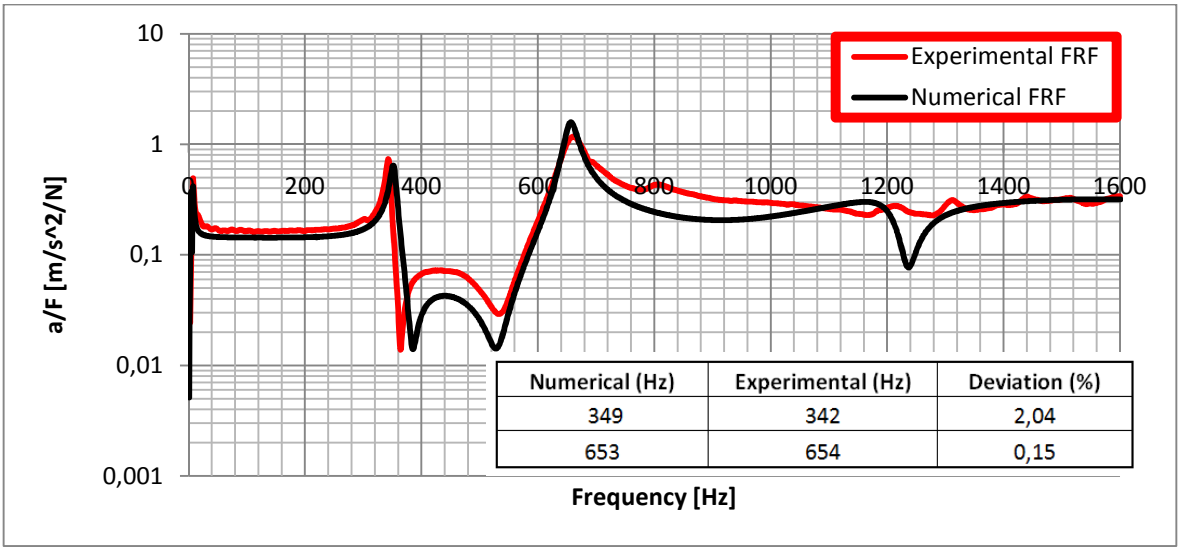

Figure 5. 6 : Comparison of predicted and measured FRF of suspended motor.

5.2 Compasisons Of The Dynamic Results

A simple model for electromagnetic vibrations is presented in previous chapter. Experimental and numerical results are compared in this section. Observations in terms of similarities and differences between these models are discussed.

As can be seen in the Figure 5.7, the sidebands of 100 Hz and its harmonics can be detected quite easily from measured Campbell diagrams. Vibrations mechanism predicted using the simple electromagnetic model is the same as seen in the experimental measurements.

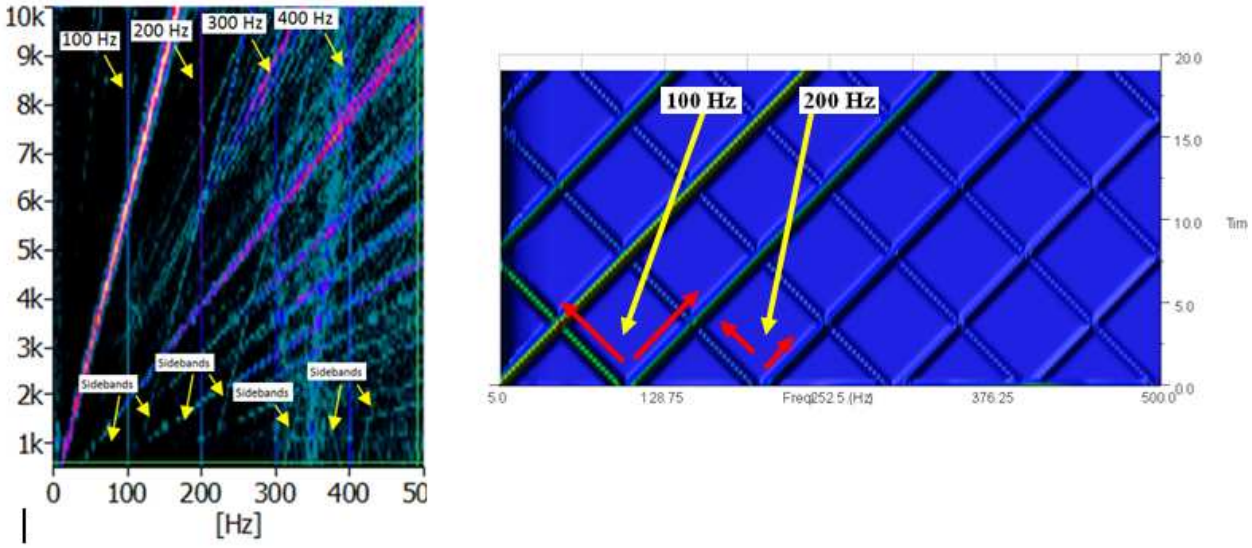

a) b)

Figure 5. 7 : Comparisons of electromagnetic based sidebands of 100 Hz and its harmonics, a) Experimental measurements b) simple electromagnetic vibration model STFT data

When the rotational speed of the motor is reached to the main power line frequency, left sideband of the 100 Hz goes to the 0 Hz. This circumstance is the same in both experimental and numerical diagrams. But as one can see in the model, vibrations of 100 Hz and its harmonics are not available in the numerical model. These forces are felt only by the stator; that is why we cannot see these effects in this simple model.

6. CONCLUSIONS AND SUGGESTIONS FOR FUTURE WORKS

6.1 Conclusions

In this study, a forced response model of a universal electric motor is developed using MSC ADAMS software platform. During this process individual parts of the electrical motor are modelled using FE approach and their dynamic properties such as natural frequencies and damping levels are verified via experimental modal analyses. After this verification process, first, the models for individual parts including bearings are assembled so as to obtain free vibration model of the electric motor. Approriate interface and other boundary conditions are imposed during this assembly process and FRF verification is made for this free vibration model.

Bearings are included the forced vibration model in order to monitor excitation frequencies associated with bearings. Also, a mathematical expression is established which has the ability of simulating electromagnetic excitation. Substantial amount of vibrations measurements are made during run-up and coast-down of the electric motor in order to understand the dynamic characteristics of the electromagnetic excitation and the resulting vibrations. The collected data are processed to obtain Campbell and Order diagrams which are used to characterise the vibrations due to electromagnetic effects in electric motors.

In order to compare and validate the numerical model of the electrical motor, a test rig is also designed and developed for acquiring experimental data. The main objective of this test rig is to measure the forced response behaviour of the electric motor itself without the effect of the structure it may be attached to. Accordingly, it is decided to perform the tests in free-free conditions. A flywheel (cylindrical part), whose mass moment of inertia is equal to the rotating parts of the washing machine including the washing load, is assembled in front of the electric motor in order to simulate the operating conditions.

Electormagnetic excitation mechanism is modelled using approximate mathematical expressions and this model is first applied to a simple rotor model in order to check

whether the model for eceltromagnetic excitation mechanism can reproduce the associated vibrations. After obtaining satisfactory results from simple rotor model, the electromagnetic excitation mechanism is also applied to the numerical model of the electric motor itself.

6.2 Suggestions For Future Works

In forced vibration model of the electric motor, a ball bearing model is used to see the excitation frequencies. The ball bearing model can be improved. However, an improved ball bearing model may substantially increase the computing effort. Definition of the interfaces between individual parts of the electric motor can be improved further in order to obtain better correlation between measured and predicted vibration levels. So as to decrease computing time for forced vibration model, optimum mesh density for individual components of the motor can be studied. Finally, the test rig can be improved so as to better simulate the operating conditions in terms of load and boundary conditions.

REFERENCES

[1] **M. Furlan, and M. Boltezar,** 2003: The magnetic noise of a DC electric motor-modeling of three-time-coupled electromagnetic, mechanical and acoustic phenomena, *ISEF 2003-11th International Symposium on Electromagnetic Fields in Electrical Engineering*, September 18-20, Slovenia.

[2] **C. Schlensok et al.,** 2007: Electromagnetically excited audible noise – evaluation and optimization of electrical machines by numerical simulation, *The International Journal for Computation and Mathematics in Electrical and Electronic Engineering*, **26,** 3,727,742.

[3] **P. Zhou et al.,** 1999: Dynamic Modeling of Universal Motors, *IEEE Trans.*, 419,421.

[4] **T.S. Low, C.Bi and Z.J. Liu,** 1997: A hybrid technique for electromagnetic torque and force analysis of electric machines, *The International Journal for Computation and Mathematics in Electrical and Electronic Engineering*, **16**, 3, 191,205.

[5] **F. Ishibashi et al.,** 1998: Numerical simulation of electromagnetic vibration of small induction motors, IEE Proc.-Electr. Power Appl.,**145**, 6, November, 528,533.

[6] **M. Furlan et al.,** 2003: A coupled electromagnetic-mechanical-acoustic model of a DC electric motor, *The International for Computation and Mathematic in Electrical and Electronic Engineering*, **22,** 4, 1155,1167.

[7] **C. G. C. Neves et al.,** 1998: A Study on Magnetic Vibration Sources Identification in Introduction Motors by FEM Simulation and Experimental Procedures", *IEEE trans.,* 237,242.

[8] **Michael van der Giet et al,** 2008: Comparison of 2D and 3D Coupled Electromagnetic and Structure-Dynamic Simulation of electrical Machines, *IEEE Transactions on Magnetics*, **44**, 6, June, 1594,1597.

[9] **F. Ishibashi et al.,** 2010: Change of Mechanical Natural Frequencies of Induction Motor, *IEEE Trans.*

[10] **Shigeru SAKAMOTO et al,** 1999: "Vibration Analysis Considering Higher Harmonics of Electromagnatic Forces for Rotating Electric Machines", *IEEE Transactions on Magnetics*, **35**, 3, May,1662-1665.

[11] **B. Liang et al.,** 2002: Simulation and fault detection of three-phase induction motors ,Elsevier Science B. V., *Mathematics and Computers in Simulation,* 61, 1,15.

[12] **P. Zaskalicky, J. Dupej,** 2006: Modeling of an Universal Motor Supplied by a Harmonic Voltage, *IEEE Trans*., 100,1072, Technical University of Kosice and BSH Drives and Pumps, Slovakia.

[13] **N. TANDON and A. Choudhury,** 1997: An Analytical Model for the Prediction of the Vibration Response of Rolling Element Bearing Due to a Localized Defect, *Journal of Sound and Vibration*, **205**, 3, August, 275,292.

[14] **ÇAKMAK, Onur and ŞANLITÜRK, Kenan,** 2010: Modelling and Validation of a Rotor System with Ball Bearings, *Proceedings of the 10th Biennial Conference on Engineering Systems Design and Analysis*, July

[15] **O. A. Mohammed et al,** 2002: Computation of Transient Magneto-Mechanical Problems in electrical Machines, *Proceedings IEEE SoutheastCon*, 187,191.

[16] **Hwang, Don-Ha et al,** 2006: A Method for Dynamic Simulation and detection of air-gap Eccentricity in Induction Motors by Measuring Flux Density, *Electromagnetic Field Computation, 12th Biennial IEEE Conference*, 69,69.

[17] **Besnerais, Jean Le et al,** 2009: Characterization and Reduction of Magnetic Noise Due to Saturation in Induction Machines, *IEEE Transactions on Magnetics*, **45**, 4, April.

[18] **CURIAC, Radu S. and SINGHAL, Sumit,** 2009: Causes and Reduction Techniques of electromagnetic Noise In Induction Motors, *Pulup and Paper Industry Technical Conference*, June, 39,44.

[19] **J. L. Besnerais,** 2009: Optimal Slot Opening Width for Magnetic Noise Reduction in Induction Motors, *IEEE Trans. on Energy Conversion*, **24**, 4, December, 869,874.

[20] **KOBAYASHI, Takashi et al,** 2007: Effects of Slot Combination on Acoustic Noise from Induction Motors, *IEEE Transactions on Magnetics*, **33**, 2, March, 2101,2104.

[21] **Li, Y.B. et al,** 2009: Analysis and Solution on Squeak Noise of Small Permanent-Magnet DC Brush Motors in Variable Speed Applications, *IEEE Transactions on Magnetics*, **45**, 10, October, 4752,4755.

[22] **DORRELL, D. G.,** 1996: "Calculation of Unbalanced Magnetic Pull in Small Cage Induction Motors with Skewed Rotors and Dynamic Rotor Eccentricity", *IEEE Transactions on Energy Conversion*, **11**, 3, September, 483,488.

[23] **H. T.BELEK,** 'Elektrik motorlarında kalkış duruş esnasında yapılan titreşim ölçümleri ile arızaların tanımlanması'.

[24] **P. J. Tsivitse and P. R. Weihsmann,** 1971: "Polyphase Induction Motor Noise", *IEEE Trans. on Industry and General Appl.*, **IGA-7**, 3, May/June, 339,358.

[25] **William, H. Yeadon,** 2001, Handbook of Small Electric Motors, P.E.,Mc-Graw Hill.

[26] **D. H. Cho, and K. J. Kim,** 1998: Modeling of electromagnetic excitation forces of small induction motor for vibration and noise analysis, *IEE Proc. - Electr. Power Appl.*, ***145***, 3, May, 199,205

[27] **F. Kako et al.,** 1983: Experimental Study on Magnetic Noise of Large Induction Motors, *IEEE Trans. on Power Apparatus and Systems*, **PAS-102**, 8, August, 2805,2810.

[28] **Z. Glowacz, and W. Glowacz,** 2007: Mathematical Model of DC Motor for Analysis of Commutation Processes, *Electrical Power Quality and Utilisation*, **XIII**, 2, 65,68.

[29] **E.W. Summers,** 1955: Vibration in 2-Pole Induction Motors Related to Slip Frequency, *AIEE Trans.*, April 1955, 69,72.

[30] **W. R. Finley et al.,** 1999: An Analytical Approach to Solving Motor Vibration Problems, *IEEE Trans.*, **PCIC-99-20**, 1999, 1,16.

[31] **A. Arkkio,** 1997: "Unbalanced Magnetic Pull in Cage Induction Motors with Asymmetry in Rotor Structures", *IEEE Conference Publication*, No. 444 EMD 1-3 September, 36,40.

[32] **S. C. Chang, and B. Hansen,** 1997: "Electrical Noise in Small Electrical Motors", IEEE Conference Publication No. 444 EMD 1-3 September, 391,395.

[33] **D. H. Hwang et al.,** 2005: "Analysis of a Three Phase Induction Motor under Eccentricity Condition", *IEEE Trans.*, 2609,2613.

[34] **D. G. Dorrell,** 1999: Experimental Behaviour of Unbalanced Magnetic Pull in 3-Phase Indution Motors with Eccentric Rotors and the Relationship with tooth Saturation, *IEEE Trans. on Energy Conversion*, **14**, 3, September, 304,309.

[35] **S. L. Nau, and H. G. G. Mello,** 2000: Acoustic Noise in Induction Motors: Causes and Solutions, IEEE Paper No. PCIC-2000-26, 2000, 253,263.

[36] **R. S. Curiac, and S. Singhal,** 2008: Magnetic Noise in Introduction Motors , *Proceeding of NCAD2008 NoiseCon2008-ASME NCAD*, July, 28,30, Dearborn, Michigan, USA.

[37] **J. Suriano, and C. M. Ong,** 1989: Modeling of Electromechanical and Electromagnetic Disturbances in DC Motors, *IEEE Trans.*, 258-262.

[38] Rotating Vibration Analysis - Order Tracking Techniques, ADM Messtechnik GmbH & Co.

[39] Order Tracking Analysis, Technical Review of Brüel & Kjaer, Denmark, 1995

[40] Rotating Machinery Analysis – Outline, Brüel & Kjaer, Denmark

[41] **Irwing Gottlieb**, 1997, Practical Electric Motor Handbook, Newnes

[42] STEP 2000 AC Motors, Siemens

[43] Elektrik elektronik Teknolojisi, Elektrikli Ev Aletlerinde D.C. Motorlar, Ankara, 2007, MEGEP

[44] Grundfos Motor Book, 2004, GRUNDFOS Management A/S.

[45] **Steve Goldman**, 1999, Vibration Spectrum Analysis, P.E., Industrial Press Inc, New York

[46] Order Analysis, Fall 1996 – Winter 1997, Realtime Update, Hawlett-Packard

[47] **Austin Hughes,** 2006, Electric Motors aDrives; Fundamentals, Types and Applications, Newnes

[48] **Url-1** *http://hyperphysics.phy-astr.gsu.edu/hbase/electric/farlaw.html#c1* alındığı tarih 28.06.2010.

[49] **D J Ewins**, 2000, Basics and state-of-the-art of modal testing, *Sadhana Academy Proceedings in Engineering Sciences*, **25**, June, 207,220.

[50] The Fundamentals of Modal Testing, Application note 243-3, Agilent Technologies

CIRRICULUM VITAE

Candidate's full name: Cihan ORHAN

Place and date of birth: Babaeski/KIRKLARELİ 02/02/1985

Permanent Address: Üsküdar/İstanbul

Universities and Colleges attended: Yıldız Teknik Üniversitesi Makina Mühendisliği Bölümü
(İ.Ö.-Bölüm İkincisi)

Companies: 2009-2011 ARÇELİK A.Ş. Vibration & Acoustics Lab.

2011- Now Ford-OTOSAN Engine NVH Department

Scholarships: 2008-2010 TÜBİTAK-Bideb Master Scholarship